

RICE UNIVERSITY

**Constraints on Ocean Acidification Associated with Rapid and
Massive Carbon Injections of the Early Paleogene: The
Geological Record at Ocean Drilling Program Site 1215,
Equatorial Pacific Ocean**

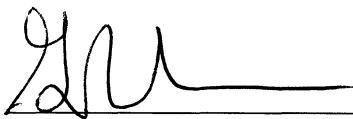
by

Lizette Leon-Rodriguez

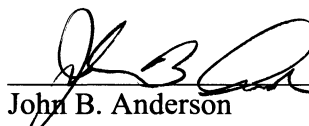
A THESIS SUBMITTED
IN PARTIAL FULFILLMENT OF THE
REQUIREMENTS FOR THE DEGREE

Doctor of Philosophy

APPROVED, THESIS COMMITTEE



Gerald R. Dickens, Chair
Professor of Earth Science



John B. Anderson
W. Maurice Ewing Professor in
Oceanography



Caroline A. Masiello
Assistant Professor of Earth Science



Volker H. W. Rudolf
Assistant Professor of Ecology &
Evolutionary Biology



R. Mark Leckie
Professor Department Head, Department
of Geosciences, University of
Massachusetts, Amherst

HOUSTON, TEXAS
August 2011

Abstract

Constraints on Ocean Acidification Associated with Rapid and Massive Carbon Injections of the Early Paleogene: The Geological Record at Ocean Drilling Program Site 1215, Equatorial Pacific Ocean

by

Lizette Leon-Rodriguez

Massive amounts of ^{13}C -depleted carbon rapidly entered the ocean more than once during the early Paleogene, providing a geological framework for understanding future perturbations in carbon cycling, including ocean acidification. To assess the number of events and their impact on deep-sea carbonate accumulation, I have studied carbonate ooze units of the upper Paleocene–lower Eocene, which were deposited on a subsiding flank of the East Pacific Rise (ODP Site 1215). From this record several proxies were used to ascertain changes in carbonate dissolution: carbonate content, foraminiferal test fragmentation, and planktic/benthic foraminiferal ratio. Based on these analyses, I observe that carbonate preservation generally increased from the late Paleocene (56 Ma) through the early Eocene (51.5 Ma), after which it became poor to negligible. This trend was punctuated by four short-term intervals characterized by carbonate dissolution and pronounced negative $\delta^{18}\text{O}$ and $\delta^{13}\text{C}$ excursions. It is inferred that these were anomalously warm periods (hyperthermals) caused by massive and relative fast ^{13}C -depleted carbon injections. These correspond to the PETM (~55.5 Ma), H1/ETM-2 (~53.7 Ma), I1 (~53.2 Ma), and K/X (~52.5 Ma) events.

I also calculated carbonate, planktic, and benthic foraminiferal mass accumulation rates for the Site 1215. These were used to comprehensively examine the history of carbonate accumulation in the equatorial Pacific Ocean throughout the early Paleogene. I deduce that in the long-term ($>10^5$ yr) the lysocline and calcite compensation depth (CCD) generally deepened between 55.4 and 51.5 Ma; but rapidly ($\leq 10^5$ yr) shoaled and subsequently overcompensated during and after the four intervals of massive carbon injection.

Planktic foraminiferal assemblages found in the record of Site 1215 follow a predicted pattern for selective dissolution. Species of *Acarinina* are preferentially preserved over *Morozovella*, which are preferentially preserved over *Subbotina*, *Igorina* and *Globanomalina*. A tiny and previously overlooked species, *Praetenuitella antica* n.sp, is formally described in this manuscript. This species is also resistant to dissolution.

The findings of this study provide firm constraints to model the short and long-term carbon cycle dynamics during the early Paleogene

Acknowledgments

I would like to thank my advisor Dr. Jerry Dickens for his support and guidance during my time at Rice. His insight and advice has made me a better scientist and has helped prepare me for my future endeavors.

I also especially thank Dr. Mark Leckie, for his scientific support and encouragement. The short meetings we had resulted in insightful conversations. I want to thank those who served on my thesis and proposal committees, including Dr. Carrie Massiello, Dr. John Anderson, and Dr. Volker Rudolf.

During these years at Rice, I have met many people that opened their hearts to me. They are excellent co-workers but foremost they are friends. Many thanks to: Rodrigo Fernandez, Glenn Snyder, Karem Lopez, Kevin Davis, Becky Minzoni, Jeniffer Masy, Maria Guedez, Maximiliano Bezada, Sookie Sanchez, Mary Ann Lebar and all the members of my "Gente Querida". Your conversations, your help, and your kindness have made me feel a very fortunate person.

The best experience that I have ever had as a scientist was to be able to participate in the Expedition 320 and sail on the Joides Resolution. The two months I spent in the sea made me grow as a researcher. I learned from every single of my shipmates. I specially want to express my appreciation to the biostratigraphers Kirsty Edgar, Tom Dunkley-Jones, Paul Bown, and Ted Moore.

I also want to express my gratitude to the Stratigraphy Skill Area and the Biostratigraphy Core Group at ExxonMobil. They have been always tremendously considerate and accommodating.

I will be ever thankful to my mother. Her support, her strength, her advice, and her love were essential for me throughout this process. It is worthwhile to mention that she helped with the sample preparation. The time we spent at the laboratory was productive and always fun.

Ultimately, this would not have been possible without the most supportive and caring man, my husband, Fermin. Through him, I have found the complete meaning of the word family.

*This work is dedicated to Fernando Etayo-Serna and Hermann Duque-Caro,
My first educators, indeed they showed me the path.*

Contents

Acknowledgments	iv
Contents	vii
List of Figures	xi
List of Tables	xiv
Chapter 1: Introduction	1
1.1. Objectives	5
1.2. Organization of this Dissertation	6
Chapter 2: Constraints on Ocean Acidification Associated with Rapid and Massive Carbon Injections: the Early Paleogene Record at Ocean Drilling Program Site 1215, Equatorial Pacific Ocean	11
2.1. Introduction	13
2.2. Site and Samples	16
2.3. Methods	18
2.3.1. Sample Processing	18
2.3.2. Nannofossil Biostratigraphy	18
2.3.3. Planktonic Foraminifer Biostratigraphy	18
2.3.4. Geochemistry	19
2.3.5. Fragmentation and Planktonic/Benthic Foraminiferal Ratio	19
2.4. Results	21
2.4.1. Age Model	21
2.4.2. Stable Isotopes	23
2.4.3. Carbonate Content	24
2.4.4. Fragmentation of Foraminiferal Tests	25
2.4.5. Planktonic/Benthic Foraminiferal Ratio	26
2.5. Discussion	27
2.5.1. The Overall Carbonate Unit at Site 1215	27

2.5.2. Early Eocene Carbon Isotope Excursions and Multiple Carbon Injection Events	30
2.5.3. Complications and Highlights of Lower Eocene Records at Site 1215	33
2.5.4. Evidence for Multiple Hyperthermals	37
2.6. Conclusions	38
2.7. Acknowledgements	39
2.8. Appendix 1	40
Chapter 3: Lower Paleogene Carbonate and Planktic Foraminiferal Accumulation at ODP Site 1215, Eastern Equatorial Pacific Ocean	52
3.1. Introduction	54
3.2. Background	57
3.2.1. Site and Samples	57
3.2.2. Age Model and Isotope Stratigraphy	58
3.3. Methods	59
3.3.1. Sample Processing	59
3.3.2. Abundance of Foraminifers	59
3.3.3. Mass and Component Accumulation Rates	60
3.4. Results	61
3.4.1. Relative Abundance of Planktic Foraminifera	61
3.4.2. Mass and Component Accumulation Rates	63
3.5. Discussion	67
3.5.1. Carbonate Accumulation at ODP Site 1215	67
3.5.2. Planktic Foraminiferal Preservation	69
3.5.3. Evidence for Paleoenvironmental Changes?	72
3.5.4. A Cooling Trend with Global Warming Episodes?	75
3.6. Summary and Conclusions	76
3.7. Acknowledgments	78
3.8. Appendix 1: Taxonomic List	79
Chapter 4: <i>Praetenuitella antica</i> n. sp.: A Macro to Microperforate Planktic Foraminifer from the Lower to Middle Eocene of the Equatorial Pacific Ocean	97

4.1. Introduction	99
4.2. Materials and Methods	102
4.2.1. SEM Imaging and Morphometrics	104
4.2.2. Stable Isotopes	104
4.2.3. Cross-plots	104
4.3. Results	106
4.3.1. Systematic Taxonomy	106
4.3.2. Morphometrics	112
4.3.3. Stable Isotope Composition (Inferred Paleobiology)	113
4.3.4. Stratigraphic Distribution	114
4.3.5. Geographic Distribution	114
4.3.6. Abundance	114
4.3.7. Solution Susceptibility and Temperature Control	116
4.4. Discussion	117
4.4.1. Phylogenetic Importance	117
4.5.2. Inferred Paleobiology	118
4.5.3. Susceptibility to Dissolution	120
4.6. Conclusions	120
4.7. Acknowledgements	121
Chapter 5: Conclusions	136
References	139
Appendix A: Data Report: Stable Isotope and Carbonate Content Analyses of the Middle to Upper Eocene Sediments at IODP Sites U1332 and U1333	154
A.1. Introduction	155
A.2. Sites and Samples	159
A.3. Methodology	160
A.3.1. Sample Processing	160
A.3.2. Geochemistry	161

A.3.3. Composite Depths and Age Models	162
A.4. Results	162
A.4.1. Bulk Oxygen Isotope Record	162
A.4.2. Bulk Carbon Isotope Record	163
A.4.3. Carbonate Content	164
A.5. Summary and Future Work	166
A.6. Acknowledgments	167
A.7. References	168
Appendix B: Data Repository	185

List of Figures and Plates

Chapter 2

Figure 2.1 – Location of Site 1215 and other sites drilled by ODP Leg 199	41
Figure 2.2 – Lithology and stratigraphy at ODP Site 1215	42
Figure 2.3 – Late Paleocene and early Eocene planktonic foraminifers at IODP Hole 1215A	44
Figure 2.4 – Stable isotope records of bulk carbonate and various carbonate records at ODP Site 1215	46
Figure 2.5 – Hypothetical evolution of the CCD and the lysocline in the Equatorial Pacific during the early Eocene	48
Figure 2.6 – Age correlation of 4 early Eocene Hyperthermals at different locations	50

Chapter 3

Figure 3.1 – Location of Site 1215 and other sites drilled by ODP Leg 199	82
Figure 3.2 – ODP Site 1215 lithological record and splice using magnetic susceptibility from Holes A and B	83
Figure 3.3 - Age model for ODP Site 1215	84
Figure 3.4 – Isotope stratigraphy, Linear Sedimentation Rate (LSR), Smooth Sedimentation Rate (SSR), and relative abundances of planktic foraminifers at ODP Site 1215	85
Figure 3.5 - Carbonate Mass Accumulation Rate (carbonate MAR), Fish Debris Accumulation Rate (FDAR), Benthic Foraminiferal Accumulation Rate (BFAR), Planktic Foraminiferal Accumulation Rate (PFAR), and accumulation rates for selected planktic foraminiferal genera at the ODP Site 1215	86

Figure 3.6 - Crossplots of (a) Carbonate content vs. absolute abundance of planktic foraminifera, and (b) Carbonate content vs. relative abundance of planktic foraminifera	88
Figure 3.7 - Comparison of $\delta^{13}\text{C}_{\text{bulk}}$ and $\delta^{18}\text{O}_{\text{bulk}}$ records from the eastern equatorial Pacific Ocean, ODP Site 1215 and the South Atlantic Ocean, ODP Site 1262 Walvis Ridge.....	89
Plate 3.1 - Selected early Eocene acarininids from ODP Site 1215	90
Plate 3.2 - Selected early Eocene morozovellids from ODP Site 1215	92
Plate 3.3 - Selected late Paleocene and early Eocene subbotinids, igorinids, chiloguembelinids, and tenuitellids from ODP Site 1215	94
 Chapter 4	
Figure 4.1 – Location of ODP Site 1215 and IODP Site U1333 in the eastern Pacific	122
Figure 4.2 – General morphology of <i>Praetenuitella antica</i> n. sp.	123
Figure 4.3 – Morphometrics and descriptive statistics of <i>P. antica</i> n. sp.....	124
Figure 4.4 – Multispecies isotope data from selected samples of ODP Site 1215 and IODP Site U1333	125
Figure 4.5 – Stratigraphic distribution of <i>Praetenuitella antica</i> n.sp. and other tenuitellids of the Eocene	126
Figure 4.6 – Relative and absolute abundance of <i>Praetenuitella antica</i> n. sp. at ODP Site 1215	127
Figure 4.7 – Tridimensional crossplots showing the abundance of <i>Praetenuitella antica</i> n. sp., carbonate content, and bulk carbonate oxygen isotope values from samples at ODP Site 1215	128
PLATE 4.1 - <i>Praetenuitella antica</i> n.sp. Holotype.....	129
PLATE 4.2 - <i>Praetenuitella antica</i> n.sp. Paratypes	131
PLATE 4.3 - <i>Praetenuitella antica</i> n.sp. Wall structure	133

Appendix A

Figure A.1 – IODP Sites U1332 and 1333 location map	171
Figure A.2 – IODP Site U1332 (hole A and B) stable isotopes and carbonate content profiles	172
Figure A.3 – IODP Site U1333A stable isotopes and carbonate content profiles ...	173

List of Tables

Chapter 3

Table 3.1 - CIE events at the ODP Site 1215	96
---	----

Chapter 4

Table 4.1 – Stable isotope analysis on <i>Praetenuitella antica</i> n. sp. and other Eocene foraminifera from samples at ODP Site 1215 and IODP Site U1333	135
--	-----

Appendix A

Table A.1 – IODP Site U1332A stable isotope and carbonate content data	174
Table A.2 – IODP Site U1332B stable isotope and carbonate content data	177
Table A.3 – IODP Site U1333A stable isotope and carbonate content data	180

Appendix B

Table B.1 – Carbon and oxygen isotopes carbonate content, sample dry weight, and foraminifera counts at ODP Site 1215A	186
Table B.2 – Counts of other microfossils and mineral grains at ODP Site 1215A ..	189
Table B.3 - Counts of planktic foraminifera fragments and whole test, and fragmentation percentage at ODP Site 1215A	192
Table B.4 – Relative abundances of selected planktic foraminiferal genera at ODP Site 1215A	195
Table B.5 – Species counts at ODP Site 1215A	199
Table B.6 – Accumulation rates using a LSR approach	203
Table B.7 – Accumulation rates using a SSR approach	207

Chapter 1

Introduction

Much of the scientific research of the last decades and the near future have and will be focused on the detailed prediction of the climatic, biotic and chemical responses that the Earth will suffer as a result of the fast and massive CO₂ release into atmosphere/ocean systems. It is almost certain that human activities are responsible for this process, as shown by proxy measurements that indicate that during the pre-industrial era CO_{2 atm} concentrations were between about 180 and 280 ppmv while at the present time are higher than 390 ppmv and will probably reach 700 ppmv by the end of this century (Forster et al., 2007; Zeebe, 2011). This will have at least two direct consequences: (1) a rise on global temperatures, and (2) a significant drop in seawater pH (Caldeira and Wickett, 2003; Demicco et al., 2003; Denman et al., 2007; Zeebe, 2011). However, the timing and amount of these temperature and pH changes is yet to be addressed

Ocean/atmosphere dynamics are extremely difficult to model because the lack of constraints for the number of variables involved. For instance, it is expected that carbonate

ion concentration and the solubility of calcium carbonate minerals in the ocean will decrease (Caldeira and Wickett, 2003). For that, we should fully understand the carbonate chemistry of the oceans, and how it might change as carbon uptake from the atmosphere increases. How much will the pH decrease? Is this a fast or slow process? Is this going to be roughly equal in all the ocean basins? How might ocean circulation affect this process? How will fauna and flora calcifiers respond? How rapidly can oceans recover from this process?

“Ocean acidification” has therefore become a focal point of research because of the impact on marine organisms and carbonate pelagic sedimentation (Kleypas et al., 1999; Kleypas and Yates, 2009; Ries et al., 2009; Zeebe, 2011; Zeebe et al., 2008). Ultimately, to accurately model the changes in ocean carbonate chemistry and carbon cycle dynamics, modelers need data, observations, and analyses of analogs to realistically set a framework to make predictions (e.g. Caldeira and Wickett, 2003; Demicco et al., 2003; Zachos et al., 2008; Zeebe et al., 2008; Zeebe et al., 2009).

The Paleocene Eocene Thermal Maximum (PETM) ca. 55 million years ago is probably one of the best past analogs to understand ocean acidification. This was an event of ca. 120 kyr (Farley and Eltgroth, 2003) in which global temperatures, including in the deep ocean, increased by 5 to 9 °C (Bowen et al., 2001; Sluijs et al., 2007; Wing et al., 2005; Zachos et al., 2001; Zachos et al., 2005). This thermal perturbation is recorded by a negative excursion in the $\delta^{18}\text{O}$ of carbonate (Kennett and Stott, 1991; Zachos et al., 2001), as well as by other geochemical and biological tracers (Bowen and others, 2006; Sluijs et al., 2007). Somehow associated with the rise in temperatures, there were numerous biotic changes (e.g. Bralower et al., 1995; Kelly, 2002; Kelly et al., 1998; Sluijs et al., 2007;

Thomas, 2007; Thomas and Shackleton, 1996; Wing et al., 2005), especially affecting calcifying marine organisms (Kelly, 2002; Raffi et al., 2005). It is widely accepted that the PETM is related to a “sudden” and a massive addition of ^{13}C -depleted carbon into the atmosphere/ocean system (Dickens et al., 1997; Koch et al., 1992; Zachos et al., 2005), although its source and amount remain debatable (Cramer and Kent, 2005; Dickens, 2011; Svensen et al., 2004; Zeebe et al., 2009). The carbon input of the PETM left direct impacts on the geological records, i.e. a negative Carbon Isotopic Excursion (CIE) has been globally documented in both marine and terrestrial deposits (Bowen and others, 2006; Kennett and Stott, 1991; Koch et al., 1992; Pagani et al., 2006; Zachos et al., 2003). There is also evidence that the pH of the oceans lowered at global scale causing dissolution of pelagic carbonate sediment (Dickens, 2000; Dickens et al., 1997; Zachos et al., 2005), which is reflected on an abrupt shoaling of the lysocline and the CCD within a few thousand years (Murphy et al., 2010; Sluijs et al., 2007; Zachos et al., 2005).

Two intriguing and open issues have emerged in recent discussions of the PETM and the associated ocean acidification: How does carbonate dissolution vary from one deep-sea sediment section to another? Was the PETM unique or instead it was one of several similar events or “hyperthermals” in the Early Paleogene?

To answer the first question we can refer to carbon input models and field observations. Based on these models and several observations in the deep ocean, it is suggested that the gradient of carbonate ion was inverse to what is observed today (Zeebe and Zachos, 2007; Zeebe et al., 2009), meaning that deep-ocean waters were more corrosive in the Atlantic than in the Pacific Ocean. Most of these models need to be refined and supported by additional data. Our best approximation to understand the preservation of

pelagic carbonate through time is based on lysocline and CCD (Calcite Compensation Depth) reconstructions for the Pacific Ocean in the Cenozoic (Lyle, 2003; Rea and Lyle, 2005; Van Andel, 1975). These are “depth horizons” in the ocean related to calcite accumulation (Bramlette, 1961; Broecker and Broecker, 1974; Peterson, 1966; Takahashi and Broecker, 1977): the lysocline is the depth where calcite dissolution begins to increase significantly, such that carbonate accumulation decreases markedly; the CCD is where calcite dissolution balances calcite rain, such that accumulation effectively drops to zero (Boudreau et al., 2010). However, the lack of resolution of the paleoreconstructions of these curves makes it very difficult to fully capture small-term fluctuations (hundred of thousands of years) that may have occurred as consequence of short-life events. Therefore, there is need for high-resolution studies of the marine geological records to elucidate the behavior of the CCD and the lysocline during and after the “hyperthermals”, such data can ultimately feed into carbon input used in numerical simulations.

More controversial in nature is the second question. There are a number of suggested explanations (e.g., a comet impact, explosive volcanism, intrusion-forced injection of thermogenic methane, tectonic-forced methane hydrate release) implicitly consider the PETM as an isolated event (Cramer and Kent, 2005; Jones and Maclennan, 2006; Kent et al., 2003; Svensen et al., 2004). On the other hand, other studies have suggested instead that the PETM was the most pronounced of a series of “hyperthermal” events in the Early Paleogene (Agnini et al., 2009; Cramer et al., 2003; Lourens et al., 2005; Nicolo et al., 2007; Röhl et al., 2006; Stap et al., 2009). These include short intervals centered at ~53.7 Ma (H1 or ETM2), ~53.2 Ma (I1), and ~52.5 Ma (K or X). At multiple locations, each of these events is characterized by a significant negative $\delta^{13}\text{C}$ excursion and

lithological expressions similar to the PETM (Lourens et al., 2005; Nicolo et al., 2007; Röhl et al., 2006; Stap et al., 2010; Stap et al., 2009). Nevertheless, with the current information, we are not able to discern whether all of these hyperthermals are related to the same causal mechanism and/or whether they all have the same kind of chemical and biotic responses.

1.1. Objectives

The present work aims to study under high-resolution the lysocline and CCD fluctuations occurred in the Equatorial Pacific Ocean during the Late Paleocene and Early Eocene and the relationship between these fluctuations and the short and long-term variations of ^{13}C -depleted carbon input during that time. We use for that purpose the sedimentary record from Ocean Drilling Program (ODP) Site 1215 in the Eastern Equatorial Pacific Ocean. This site was chosen because it should have been located near or below the lysocline between 58 and 50 Ma, which would allow a better understanding of the pelagic carbonate accumulation records and its relationship to inputs of ^{13}C -depleted carbon in the oceans. Different paleoceanographic techniques and analyses (e.g., stable isotope and carbonate dissolution records) are combined here to more completely understand suspected carbon injection events of the early Paleogene..

Specific objectives include,

- I. To generate geochemical and dissolution records from ODP Site 1215, particularly: $\delta^{18}\text{O}_{\text{bulk}}$ and $\delta^{13}\text{C}_{\text{bulk}}$, carbonate content, Carbonate Mass Accumulation Rates (MAR), fragmentation of planktic foraminifera, planktic/benthic foraminiferal ratio, and component MARs of planktic foraminiferal genera and benthic foraminifers.

- II. To establish the short-term ($<10^5$ years) and long-term ($>10^5$ years) behavior of the lysocline and CCD in the Eastern Equatorial Pacific Ocean during the Late Paleocene to Early Eocene.
- III. To analyze the planktic foraminiferal assemblages from ODP Site 1215 to identify their patterns of fragmentation and dissolution
- IV. To investigate the possible paleoenvironmental impact of the “hyperthermals” in the Eastern Equatorial Pacific Ocean by combining analyses of geochemical proxies and interpretations of the microfaunal assemblages.

Myself, the main author of this dissertation, and the co-authors of the following chapters want this study to provide useful chemical and carbonate dissolution proxy data that can help other scientists to constrain the variables involved into carbon cycle modeling.

1.2. Organization of this dissertation

This work is organized in three main chapters that correspond to research papers that have been published and/or submitted to peer-reviewed journals. Each chapter contains its own introduction, methods, results, discussion, and conclusions. At the end, there is section for closing remarks and an appendix with initial results of an ongoing research that involves similar objectives to those delineated above but expanded into the rest of the Eocene sedimentary record. Below I summarize the content and questions addressed in subsequent chapters.

Chapter 2 concentrates on the complex history of carbonate accumulation of the ODP Site 1215 by using several chemical and dissolution proxies: stable carbon and

oxygen isotopes, carbonate content, planktic/benthic foraminiferal ratio, planktic foraminiferal fragmentation and abundance. The proxy records reveal four horizons with similar isotopic and lithological expressions represented by negative excursions of $\delta^{13}\text{C}_{\text{bulk}}$ and $\delta^{18}\text{O}_{\text{bulk}}$, strong dissolution of calcium carbonate, and nearly complete dissolution of planktic foraminifers. These same perturbations have been described in other marine sites, which confirm the global nature of these events. The character of the ^{13}C isotopic excursions of these events indicate that they were caused by massive and rapid releases of ^{13}C depleted carbon into ocean/atmosphere system that ultimately produced increase in global temperatures (hyperthermals) and reduced pelagic carbonate sedimentation (temporary rise of the lysocline and the CCD). The first and most important of these events correspond to the PETM (55.5 Ma) followed by H1 (53.7 Ma), I1 (53.2 Ma), and K (52.5 Ma). Interestingly, and as predicted by carbon cycle modelers, after each one of the events, the sedimentary record shows enhanced carbonate content and general improvement in the foraminiferal assemblages, which correspond to rapid falls of lysocline and CCD or periods of recovery that followed each “hyperthermal”.

In *Chapter 3*, various component accumulation rates are calculated from the record of ODP Site 1215 (carbonate MAR, planktic foraminifera accumulation rates (PFAR), benthic foraminifera (BFAR), and fish debris (FDAR) to quantitatively assess how much carbonate accumulated on the seafloor and/or how dissolution particularly affected the carbonate-made microfossils during the several fluctuations of the lysocline and the CCD throughout the Early Paleogene in this region. Additionally, microfossils from this site are used to make inferences on the paleoclimate in the Equatorial Pacific during this time. This analysis shows that hyperthermals are characterized by very low accumulation rates of

carbonate, as well as low planktic and benthic foraminiferal accumulation rates. During these intervals of high dissolution the most commonly preserved genera are *Acarinina* and *Praetenuitella*. Within 200 kyr after each event, there is an overall improvement in carbonate accumulation, foraminiferal preservation, and diversity. In general, detailed analyses of the planktic assemblages indicate that foraminifers follow a pattern of selective dissolution. The genus *Acarinina* is preferentially preserved over *Morozovella*, which are preferentially preserved over *Subbotina*, *Igorina* and *Globanomalina*. The genus *Praetenuitella* seems resistant to dissolution; interestingly, it was not previously reported in early Paleogene sediments of any other site before. Despite the imprint of dissolution, changes in the oxygen isotope record and foraminiferal assemblages suggest that, at Site 1215, the hyperthermal events were superimposed on a slight long-term cooling between 55.3 and 52.6 Ma. Thus, warm-water, mixed layer dwellers (*Acarinina* and *Morozovella*) appear right after the hyperthermals, but those probably more tolerant to colder temperatures (*Praetenuitella*) prevail over the long-term. This long-term cooling may reflect northward tectonic migration of the site into a zone of upwelling and greater productivity.

Chapter 4 is a careful study of planktic foraminifers attributed to the genus *Praetenuitella* and are formally placed into a new species *Praetenuitella antica* n.sp. The finding of individuals belonging to this taxon deserved a more extensive inspection for two reasons: (1) the presence of this genus in Site 1215 seemed odd because in previous taxonomic works, the oldest tenuitellids (*Praetenuitella* and *Tenuitella*) were identified in upper Eocene sediments (Huber et al., 2006), and (2) this genus was an important component of several samples from ODP Site 1215. Thus, it became necessary to confirm

its taxonomic identification and to further study the implications of its presence in the record. This study documents the presence of *P. antica* n.sp. in two deep-sea drilling sites of the Equatorial Pacific (ODP Site 1215 and IODP Site U1333). *Praetenuitella antica* n.sp. shares several characteristics with other tenuitellids: (1) monolamellar wall that in the earliest chambers is macroperforate and moderately pustulose, and in the latest chambers becomes microperforate and sparsely pustulose; (2) small size ~100 μm of diameter with 4 to 5 chambers in the last whorl that slowly increase in size. Therefore, this new species may indeed represent the earliest form of the tenuitellid plexus that is therefore placed about 20 myr older than previously documented. Stable isotopic data indicate that *Praetenuitella antica* incorporated a proportion of isotopically ^{13}C -depleted metabolic carbon was incorporated into the calcite shell. Comparison of 3D crossplots of relative abundance vs. carbonate content vs. $\delta^{18}\text{O}_{\text{bulk}}$ between *Praetenuitella* and *Acarinina* (the genus with the highest resistance to dissolution) indicate that *Acarinina* is definitely the most abundant genus when carbonate content is less than 50%. Nonetheless, the presence of the small size *Praetenuitella* is also notable when carbonate content is low, which confirms its importance as probably the second most resilient planktic genus to carbonate dissolution. Stable oxygen isotopic analyses on *Praetenuitella antica* indicates that this species probably lived in a wide range of temperatures between 18.3 and 23.6 $^{\circ}\text{C}$; while *Acarinina*, is restricted to warmer sea-surface temperatures.

The last part of the dissertation, Chapter 5, collects the principal findings and interpretations made from the analyses of lower Paleogene sediments of the ODP Site 1215, which serves as a framework for future work. This would involve similar objectives and analyses at other ODP/IODP Sites in the Equatorial Pacific Ocean covering the middle to

late Eocene. We are currently exploring some of these lines of investigation at the IODP Site U1332 and U1333. **Appendix A** contains a data report for core analyses conducted at IODP Site U1332 Hole A and B, and Site U1333 Hole A This section presents some preliminary results of stable isotope and carbonate content analyses conducted in these sites. These initial results and their preliminary interpretation are set as the outline for future research following this dissertation. **Appendix B** is a repository containing all the data used in this study.

Chapter 2

Constraints on Ocean Acidification Associated with Rapid and Massive Carbon Injections: the Early Paleogene Record at Ocean Drilling Program Site 1215, Equatorial Pacific Ocean

Lizette Leon-Rodriguez^{a,*} and Gerald R. Dickens^{a,b}

^aDepartment of Earth Sciences, Rice University, MS-126 P.O. Box 1892, Houston
TX, 77281-1892, USA

^bInstitutionen för Geologiska Vetenskaper, Stockholms Universitet, 106 91
Stockholm, Sweden

Published November 2010:

Palaeogeography, Palaeoclimatology, Palaeoecology 298 (2010) 409-420

ABSTRACT

Massive amounts of ^{13}C -depleted carbon rapidly entered the ocean more than once during the early Paleogene, providing a geological framework for understanding future perturbations in carbon cycling, including ocean acidification. To assess the number of events and their impact on deep-sea carbonate accumulation, we investigated a 42 m thick unit of upper Paleocene-lower Eocene carbonate ooze, which was deposited on a subsiding flank of the East Pacific Rise. Age control was established using calcareous nannofossils and planktonic foraminifera, as well as stable carbon isotopes of bulk carbonate. Carbonate content, foraminiferal test fragmentation, and planktonic/benthic foraminiferal ratio were measured to ascertain changes in carbonate dissolution. Based on these analyses, carbonate preservation generally increased from the late Paleocene (56 Ma) through the early Eocene (51.4 Ma), after which it became poor to negligible. This trend was punctuated by three (and probably four) short-term intervals characterized by carbonate dissolution and negative $\delta^{13}\text{C}$ excursions. These horizons almost assuredly correspond to the PETM (~55.5 Ma), H1/ETM-2 (~53.7 Ma), I1 (~53.2 Ma), and K/X (~52.5 Ma) events. Carbonate preservation also increased within 200 kyr after two and perhaps all four intervals. We suggest the lysocline and calcite compensation depth (CCD) generally deepened between 56 to 51.4 Ma but shoaled and subsequently overcompensated during and after three and likely four intervals of rapid and massive carbon injection. Oxygen isotope data further suggests these intervals were times of anomalous warmth.

Keywords: Eocene, Ocean Acidification, Carbon, CCD, Lysocline, Pacific Ocean, Hyperthermal

2.1. Introduction

It is “virtually certain” that current and future release of CO₂ by anthropogenic activities will decrease pH and calcium carbonate solubility in the ocean (Denman et al., 2007). This expected “ocean acidification” will reduce CO₂ uptake from the atmosphere to the ocean, may impact marine organisms that calcify, and should modify certain physical properties of seawater, such as sound and light propagation (Brewer and Hester, 2009; Doney et al., 2009; Feely et al., 2009). Basic responses of the ocean carbon cycle to future CO₂ inputs have been predicted (e.g., Walker and Kasting, 1992; Caldeira and Wickett, 2005; Orr et al., 2005, 2009; Tans et al., 2009). However, the magnitudes remain unconstrained because they depend on a multitude of factors (e.g., Zachos et al., 2008; Kump et al., 2009; Tans et al., 2009).

The late Paleocene through early Eocene, nominally 58 to 50 million years ago (Ma), is perhaps the best past time interval in which to understand ocean acidification (Zachos et al., 2008; Kump et al., 2009; Zeebe et al., 2009; Ridgwell and Schmidt, 2010). Carbon isotope and seafloor carbonate records spanning this time strongly suggest long-term ($>10^5$ yr) and short-term ($<10^5$ yr) perturbations to ocean carbon chemistry (e.g., Dickens et al., 1997; Hilting et al., 2008; Zachos et al., 2008). Among these are profound changes across the Paleocene-Eocene Thermal Maximum (PETM) ca. 55 Ma, a geologically brief event characterized by a 5 to 9 °C rise in Earth surface temperatures and numerous biotic turnovers (e.g. Sluijs et al., 2007a), including those of calcifying marine organisms (Bralower, 2002; Kelly, 2002; Raffi et al., 2005, Thomas 2007; Kump et al.,

2009). The onset of the PETM is marked by a prominent negative carbon isotope excursion (CIE) in globally distributed marine and terrestrial sediment sequences, and by carbonate dissolution in widely separated deep-sea sediment sections (e.g., Kennett and Stott, 1991; Lu and Keller, 1993; Zachos et al., 2005, 2007; Sluijs et al., 2007a; Zachos and Zeebe, 2007). A tremendous and rapid ($<10^5$ yr) addition of ^{13}C -depleted CO_2 into the ocean/atmosphere system produced these signals, although the source and mass of the input remain uncertain (e.g., Dickens et al., 1997; Kump et al., 2009; Zachos et al., 2005, 2007, 2008; Zeebe et al., 2009; Ridgwell and Schmidt, 2010).

Carbonate dissolution in deep-sea sediment across the PETM almost certainly reflects ocean acidification, more specifically rises in the lysocline and calcite compensation depth (CCD) (Dickens et al., 1997; Dickens, 2000; Kump et al., 2009; Ridgwell and Schmidt, 2010; Zachos et al., 2005, 2008; Zeebe and Zachos, 2007; Zeebe et al., 2009). These are "depth horizons" in the ocean related to calcite accumulation (Bramlette, 1961; Peterson, 1966; Broecker and Broecker, 1974, Takahashi and Broecker, 1977): the former is where calcite dissolution begins to increase significantly, such that accumulation decreases markedly; the latter is where calcite dissolution balances calcite rain, such that accumulation effectively drops to zero (Boudreau et al., 2010). Basically, when massive amounts of CO_2 entered the ocean during the PETM, the pH and CO_3^{2-} concentration dropped, and depths of diminished carbonate accumulation shoaled.

Three open issues have emerged in recent discussions of the PETM and its associated ocean acidification. First, how does deep-sea carbonate dissolution across the PETM vary from one section to another? Cores recovered from several areas, such as in the central Atlantic (ODP Sites 999 and 1001 in the Caribbean Sea; ODP Sites 1262-1267 on

Walvis Ridge) and the southern Indian (ODP Site 738) show pronounced dissolution across the event (e.g., Lu and Keller, 1993; Bralower et al., 1997; Zachos et al., 2005). This has been argued to represent major (> 1 km) global rises in the lysocline and CCD (Zachos et al., 2005; Sluijs et al., 2007a). However, cores from other locations, such as in the Southern Atlantic (ODP Site 690 on Maud Rise), eastern Indian (DSDP Site 259 in Perth Basin) or Pacific (ODP Site 1209 on Shatsky Rise), exhibit limited dissolution (e.g., Hancock et al., 2007; Zeebe and Zachos, 2007; Zeebe et al., 2009). Second, was the PETM one of several similar events during the early Paleogene? Some explanations for the carbon injection, for example impact of a carbonaceous comet (Kent et al., 2003) or rapid generation and release of thermogenic methane by intrusive sills (Svensen et al., 2004), have implicitly considered it a unique event. By contrast, recent papers (e.g., Lourens et al., 2005; Nicolo et al., 2007; Agnini et al., 2009; Sluijs et al., 2009; Stap et al., 2009, 2010; Galeotti et al., 2010) have suggested that the PETM was the most pronounced of a series of early Paleogene “hyperthermals”, each characterized by massive injection of ^{13}C depleted carbon. Other postulated events include short intervals centered at ~53.7 Ma (called H1 or ETM-2), at ~53.2 Ma (I1), and at ~52.5 Ma (K or X) (Appendix 1). Third, what was the average depth of the CCD and lysocline before and after the PETM? Some reconstructions of the CCD through the late Paleocene and early Eocene (van Andel, 1975; Shipboard Scientific Party, 2002a; Rea and Lyle, 2005) have it relatively shallow (~3,200 m) and constant. However, others suggest it deepened through this interval (Hancock et al., 2007). The answers to these questions are uncertain but essential for understanding and modeling the impacts of massive carbon addition upon ocean carbon chemistry (Panchuck et al., 2008; Kump et al., 2009; Zeebe et al., 2009; Ridgwell and Schmidt, 2010).

To better understand late Paleocene-early Eocene carbon cycle variations, especially during the postulated carbon injection events, stable isotope and carbonate dissolution records across this time interval are needed from multiple sites of different ocean basins. Here we generate records at ODP Site 1215 in the Eastern Pacific Ocean (**Figure 2.1**). This site was chosen because it should have been located near or below the lysocline between 58 and 50 Ma. We show that it has an important but complex history of carbonate accumulation. From the late Paleocene through the early Eocene, the site likely subsided as the lysocline and CCD deepened; superimposed on this long-term trend are major rises and falls in the lysocline and CCD during and after at least three (and possibly four) suspected hyperthermal events.

2.2. Site and Samples

Site 1215 (**Figure 2.1**) is located northeast of Hawaii in the central Pacific (26°01.77'N, 147°55.99'W) at 5396 meters below sea level (Shipboard Scientific Party, 2002a). It lies on oceanic crust of the Pacific Plate formed during the youngest part of magnetic polarity C26r (Shipboard Scientific Party, 2002a), which corresponds to 58 Ma (Cande and Kent, 1995).

Two holes (A and B) were drilled and cored at Site 1215. The recovered section (**Figure 2.2**) comprises ~70 m of sediment, divided into three units, as well as underlying basalt pebbles (Shipboard Scientific Party, 2002a). For the sediment, Unit I is red clay from the seafloor to 26 m below seafloor (mbsf), Unit II is clayey calcareous ooze to 68 mbsf, and Unit III is metalliferous oxide ooze to basalt at 70 mbsf. Biogenic silica is not a major

component, although chert nodules and horizons are scattered throughout Unit II (Shipboard Scientific Party, 2002a).

Shipboard stratigraphy indicates late Paleocene to Holocene deposition for the sediment section. However, only depths within Units II and III could be assigned a reasonable (~1 Myr) chronology. This interval (26-70 mbsf) is upper Paleocene to lower Eocene (**Figure 2.2**). The magnetostratigraphy for this unit includes several data gaps, and is not interpreted easily without additional constraints. Biostratigraphic zones were not defined very well in initial studies because of low sample resolution.

Magnetic susceptibility (MS) of sediment at Site 1215 varies significantly (**Figure 2.2**). Unit I and Unit II are characterized generally by high and low MS, respectively. However, several short intervals of high MS lie between 26 and 60 mbsf. The MS of deep-marine sediment often correlates inversely to carbonate content (e.g., Ellwood et al., 2000, Lourens et al., 2005). Consequently, these MS “highs” in Unit II may represent carbonate dissolution horizons. A prominent MS high occurs at ~54.7 mbsf, which corresponds to the PETM according to shipboard biostratigraphy (Shipboard Scientific Party, 2002a). Overlying MS peaks in Unit II might, therefore, correlate to suspected hyperthermals of the early Eocene.

We collected 117 10-cc “tubes” of sediment between 20 and 60 mbsf from Hole 1215A. These were taken every 30 to 50 cm with increased resolution of every 5 to 10 cm across dark horizons with high MS. Samples were selected to avoid disturbed intervals caused by drilling and coring.

2.3. Methods

2.3.1. Sample Processing

All samples were cleaned with 18 M Ω deionized water to eliminate salts that precipitated from interstitial water. After freeze-drying, three aliquots were taken from each sample: ~0.1 g for stable isotope analyses; ~0.4 g for CaCO₃ content analyses; 2 - 5 g for biostratigraphy. For 100 samples of the latter set, smear slides were prepared for calcareous nannoplankton biostratigraphy at the ExxonMobil Micropaleontological Laboratory (EMML). These and 7 additional “biostratigraphy” samples were washed gently on a 63 μ m sieve to collect foraminiferal tests and other fragments.

2.3.2. Nannofossil Biostratigraphy

Identification of nannofossils was made using a Zeiss AxioImager petrographic microscope at EMML. For obtaining ages, we used the biostratigraphic zonation scheme proposed by Martini (1971) as amended by Raffi et al. (2005).

2.3.3. Planktonic Foraminifer Biostratigraphy

Identification of planktonic foraminifers was carried out using a Leica MZ6 binocular microscope. Classification of species was based on the taxonomic reference for the Eocene (Pearson et al., 2006), with supplementary sources (Berggren, 1977; Olsson et al., 1999; Blow, 1979). To constrain ages, we used the tropical to subtropical planktonic foraminiferal zonation of Berggren and Pearson (2005).

2.3.4. Geochemistry

Stable isotope compositions of bulk sediment were measured using a VG / Micromass (now GV Instruments) PRISM Series II isotope ratio mass spectrometer housed at the University of Florida Stable Isotope Mass Spectrometry Laboratory. Samples were loaded into stainless steel boats and placed into a 44-position Isocarb preparation system. All isotope results are reported in standard delta notation relative to Vienna Pee Dee Belemnite (VPDB). Accuracy and precision were calibrated by multiple measurements (n=38) of NBS-19 carbonate standard ($\delta^{13}\text{C} = 1.95\text{‰}$, $\delta^{18}\text{O} = -2.20\text{‰}$), and multiple measurements (n=18) of sample replicates. Analytical accuracy and precision are better than $\pm 0.07 \text{‰}$ for carbon and oxygen isotopes.

Carbonate contents of bulk sediment samples were measured in the Geochemistry Laboratory at Rice University using a “Karbonat-bombe”. This technique (Müller and Gastner, 1971; Birch, 1981) measures the volumetric change of CO_2 produced by the reaction of a dried and powdered sample of unknown carbonate content with 10 ml 10% HCl. The analytical error of these analyses is $\pm 2.0\%$, calculated from numerous measurements (n=25) of a CaCO_3 standard.

2.3.5. Fragmentation and Planktonic/Benthic Foraminiferal Ratio

Foraminifera tests tend to break into fragments as they dissolve. Benthic foraminifera also resist dissolution more than planktonic foraminifera (e.g., Berger, 1973). Indeed, dissolution can modify planktonic foraminiferal assemblages (e.g. Bé et al., 1975; Berger, 1968; Thunell and Honjo, 1981). Although there are caveats, the degree of foraminifera fragmentation and the ratio of planktonic and benthic foraminifera can be used

to assess carbonate dissolution (e.g., Berger, 1970; Bé et al., 1975), including in Paleogene sediment (Hancock and Dickens, 2005; Colosimo et al., 2005).

Planktonic foraminiferal fragmentation was quantified as follows. First, we counted the total number of tests preserved in the >63 μm size fraction, as well as the number with indications of fragmentation. Specifically, we looked for missing, broken, or partially dissolved chambers, as well as tests of muricate taxa where only the marginal keel of pustules was preserved. We also considered those tests with signs of significant peeling on the wall structure (**Figure 2.3**). Second, the degree of fragmentation (FRAG) was calculated as follows:

$$\text{FRAG (\%)} = [(\#f / 8) / ((\#f / 8) + \text{whole tests})] * 100$$

where #f is the number of fragments in a sample, which is divided by 8 to account for average number of fragments upon breakage of a whole test (Le and Shackleton, 1992). In samples where no fragments and no whole tests exist, a value of infinity (∞) is assigned (**Figure 2.4**).

From our counts, we also determined the numbers of planktonic (P) and benthic (B) foraminifers that were moderately to well preserved (i.e., no obvious signs of dissolution). The relationship of planktonic to benthic foraminifers was calculated as $P/(P+B)$, and we refer to this as the "P/B ratio".

2.4. Results

2.4.1. Age Model

Our analyses enhance the previous calcareous nannofossil biostratigraphy at Site 1215 (Shipboard Scientific Party, 2002; Raffi et al., 2005), and confirm that Unit II sediment was deposited from the late Paleocene to the early Eocene (**Figure 2.2**). A common presence of *Fassiculithus* spp. (*F. richardii*, and *F. shaubii*) is found at 55.38 mbsf; this corresponds to the topmost part of NP9 (Raffi et al., 2005). The lowest occurrence (LO) of *Tribrachiatus bramlettei*, which marks the base of NP 10, is found at 54.32 mbsf. The LO and HO of *T. contortus* are found at 44.76 mbsf and at 36.32 mbsf, respectively; the latter correlates to the top of the NP10. The lowest common occurrence (LCO) of *Discoaster lodoensis* is found at 28.95 mbsf; this equates to the NP11/NP12 boundary. Calcareous nannofossils useful for biostratigraphy are absent in sediment above 25.73 mbsf (**Figure 2.2**).

Planktonic foraminifers are present throughout Unit II but absent from Unit I. For Unit II, tests generally have poor to moderate preservation, with clear signs of recrystallization (**Figure 2.3**). Globanomalinids and acarininids are present from 59.09 to 54.58 mbsf. Above 53.72 mbsf, acarininids become the most common taxon while globanomalinids nearly disappear. Morozovellids are scarce throughout Unit II. Moreover, their preservation is especially poor, making taxonomic identification difficult. Despite these complications, bioevents of stratigraphic value can be found. The LO of *Acarinina pseudotopilensis* is at 53.73 mbsf; this suggests the base of E1, although the biozone marker *A. sibayaiensis* (Berggren and Pearson, 2005, 2006a) is not present. The LO of *Morozovella*

subbotinae also occurs at 53.73 mbsf, although this usually occurs at the base of P5 elsewhere (Berggren and Pearson, 2006). The HO of *Morozovella acuta*, at 46.47 mbsf, may mark the end of E2. The HO of *Morozovella marginodentata*, or at least relicts of tests ascribable to this species, occurs at 30.79 mbsf (**Figure 2.3**) and suggests zone E3 (Berggren and Pearson, 2005, 2006). Although the E1/E2, E3/E4 and E4/E5 boundaries cannot be resolved, because key bioevents are missing, the planktonic foraminifera stratigraphy agrees with that of the nannofossils.

Given the calcareous nannofossil assemblages, two age models are offered for the Unit II sediment sequence (**Figure 2.2**). The first conforms to the widely used Geomagnetic Polarity Time Scale (GPTS) (Berggren et al., 1995; Cande and Kent, 1995). However, recent work suggests that absolute ages on this scale are imprecise for the late Paleocene and early Eocene (Westerhold and Röhl, 2009). The second age model is based on studies of lower Paleogene sediment at ODP Site 1262, which allow revised ages for calcareous nannoplankton bioevents (Agnini et al., 2007) based on orbital tuning of cycles (Westerhold et al., 2007, 2008). The first and second age models indicate that the studied interval of the Unit II (i.e., 59.09 to 25.28 mbsf) was deposited between 52 and 55.2 Ma or 51.4 and 56.0 Ma, respectively.

Shipboard work identified intervals of normal and reversed magnetism within and above Unit II (**Figure 2.2**). These were assigned to polarity chrons (Shipboard Scientific Party, 2002a), but probably incorrectly. For example, the normal magnetism between ~25.0 and 29 mbsf was correlated to C23n; however, the NP11/NP12 boundary is found within this chron, so it must be C24n or more specifically C24n.1n (Agnini et al., 2007). Considering multiple magnetic anomalies between 51 and 53 Ma (Cande and Kent, 1995),

and incomplete magnetostratigraphy at Site 1215, calcareous nannoplankton biozones provide the best age constraints for Unit II.

2.4.2. Stable Isotopes

Bulk carbonate $\delta^{13}\text{C}$ varies from 3.43 to 1.02 ‰ across the studied interval (**Figure 2.2**). Three salient features appear in this record. The highest $\delta^{13}\text{C}$ values, between 3.43 and 3.02‰, are found between 59.09 and 55.37 mbsf. By contrast, values generally decrease from 2.41 to 1.02‰ between 54.31 and 25.28 mbsf. Superimposed on these "background values" are three or four short intervals marked by negative CIEs (**Figures 2.2, 2.4**).

The lowest and most pronounced CIE spans the Paleocene/Eocene Boundary as identified by biostratigraphy, and separates the two carbon isotope trends noted above. The $\delta^{13}\text{C}$ values drop from 3.10‰ to 1.08‰ between 55.40 and 54.31 mbsf, increase to 2.00‰ by 53.72 mbsf, and then to 2.23‰ by 50.99 mbsf. The recovery in $\delta^{13}\text{C}$ is complex, and values do not reach those before the excursion. A second obvious CIE begins at 34.37 mbsf, where $\delta^{13}\text{C}$ drops from 1.81 to 1.42‰; above, the $\delta^{13}\text{C}$ record partly recovers to 1.67‰ by 33 mbsf, and then gradually to prior values by 32.23 mbsf. A third, subtle CIE is found at 29.90 mbsf. The $\delta^{13}\text{C}$ values decrease from 1.81 to 1.67‰, and then recover to preexisting values by 29.24 mbsf. A fourth pronounced and short CIE lies just below the top of Unit II. The $\delta^{13}\text{C}$ drops from 1.98 to 1.02‰ at 28.60 mbsf, and recovers to 1.92‰ by 28.05 mbsf.

Somewhat similarly, the bulk carbonate $\delta^{18}\text{O}$ record has overall trends and short negative excursions (**Figure 2.4**). A lower interval, between 59.09 and 56.29 mbsf, contains the highest $\delta^{18}\text{O}$ values, from -0.62 to -1.69‰. A decrease from -0.62 to -2.26‰ occurs

between 56.3 to 54.3 mbsf, which coincides with the lowermost CIE. Values then increase between 54.13 and 52.27 mbsf, reaching -2.17‰. A generally positive trend, where $\delta^{18}\text{O}$ values fluctuate between -1.99 to -1.39 ‰, continues to the top of Unit II. Three negative $\delta^{18}\text{O}$ excursions punctuate this trend, and these correspond to the CIEs (**Figure 2.4**). The $\delta^{18}\text{O}$ drops from -1.57 to -1.70‰ across the second CIE, from -1.46 to -1.73‰ across the third CIE, and from -1.40 to -2.23‰ across the uppermost CIE.

2.4.3. Carbonate Content

Bulk carbonate in Unit II mostly consists of calcareous nannoplankton but contains minor amounts of foraminifers and rare ostracods. Like the stable isotope records, the record of carbonate content shows both trends and anomalies through Unit II (**Figure 2.4**). Most samples have values between 50 and 100%, and suggest a general increase up through the section. Mean carbonate contents are 68.6% between 59.09 and 54.97 mbsf, 76.7% between 53.72 and 34.48 mbsf, and 82.0% between 34.00 and 30.37 mbsf. Carbonate content remains relatively high between 29.75 and 28.64 mbsf and between 28.42 and 25.28 mbsf, averaging 68.7% and 53.8%, respectively, but drops below detection above 24.86 mbsf.

Four short horizons of low carbonate content punctuate the general upcore increase (**Figure 2.4**). These coincide with the aforementioned CIEs and the negative excursions of $\delta^{18}\text{O}$. Carbonate content decreases to 7.3% between 54.58 and 54.51 mbsf, to 34.1% at 34.37 mbsf, to 38.3% at 30.0 mbsf, and 1.4 % at 28.6 mbsf.

2.4.4. Fragmentation of Foraminiferal Tests

The record of fragmentation at Site 1215 is complicated (**Figure 2.4**). Overall, FRAG fluctuates between 0 and 100%. Within the lowest few meters of the section, FRAG remains below 20%. However, it rises to ∞ at 54.51 mbsf, which corresponds to the lowermost CIE and interval of low carbonate content. FRAG recovers to about 11% at 54.13 mbsf but then varies significantly over the next 20 m, generally within 0 and 36%, but 100% at 41.31 mbsf. Across the second CIE (34.31 mbsf), FRAG drops to 0%. Above this depth values increase to nearly 10% (30.61 mbsf) and then to 100% (30.0 mbsf). FRAG drops to 15% at ~29.90 mbsf, where the third CIE is found. Values remain below 20% for the next 94 cm, and then rise to ∞ at the fourth and highest CIE. FRAG varies from 0 to 100% between 28.37 and 24.05 mbsf; above this, FRAG increases to ∞ because neither fragments nor whole tests are preserved.

Following previous work (e.g., Le and Shackleton, 1992; Hancock and Dickens, 2005), our initial expectation was that FRAG would increase across intervals of low carbonate content, assuming they resulted from dissolution. However, portions of the CIEs are characterized by low FRAG (**Figure 2.4**). Intense dissolution may dissolve fragments as well as whole tests; it may also affect planktonic foraminifera differently. It is therefore worth considering the absolute number of foraminifera fragments as well as planktonic foraminifera assemblages.

The FRAG record is complicated in certain intervals because the number of fragments is low. Notably, samples across the first, second, and fourth CIEs contain from 0 to 2 fragments. Samples above 23.62 mbsf also lack foraminifera fragments.

Furthermore, planktonic foraminiferal assemblages display interesting changes in composition. In particular, within some horizons, there are no fragments of muricate taxa (i.e. *Acarinina* and *Morozovella*) but low numbers of a small planktonic microperforate taxon, herein called '*Tenuitella*' (Figure 2.3), remain without signs of dissolution. Consequently, some samples have very few or no foraminiferal fragments but a significant number of whole tests, which renders low FRAG values despite strong dissolution. We discuss the importance of these observations more fully in a forthcoming article.

2.4.5. Planktonic/Benthic Foraminiferal Ratio

The P/B ratio fluctuates from 0.00 to 0.79 but generally increases up the section (Figure 2.4). Values are from 0.12 to 0.27 between 59 and 57.5 mbsf. Above and until 54.13 mbsf, the P/B ratio is from 0.0 to 0.18. It increases to 0.74 mbsf across the lowermost CIE. Values fluctuate from 0.00 to 0.87 in the overlying 19 m, but are mostly above 0.15. The P/B ratio does not significantly decrease across the second CIE but does increase above this horizon. The P/B ratio drops to 0.00 across the third CIE. Within 1 m above this horizon, the P/B ratios increase, although they do not exceed 0.50. Values drop to another low across the fourth CIE. However, they do not recover in overlying sediment, instead remaining below 0.15 until 26 mbsf.

Again, it is useful to consider total numbers, in this case planktonic foraminifera tests in processed samples. Fairly low numbers (< 87) exist between 59.09 to 54.97 mbsf. This drops to 2 or less between 54.97 to 54.13 mbsf, which roughly coincides with the lowermost CIE. Above, the number of planktonic specimens per sample increases to 138 at 53.06 mbsf, and to 307 at 46.46 mbsf but then fluctuates from 0 to 50 between 46.11 and

34.48 mbsf. The interval that corresponds to the second CIE has 6 specimens per sample. Above the second CIE, sediment again has high numbers of planktonic specimens, almost 300 per sample. Between 30.37 and 30.0 mbsf, and where the third CIE occurs, there is a decline from 214 to 0. The recovery that follows is not as pronounced as with the preceding CIEs, as the number of planktonic tests does not exceed 32 per sample. There is a drop to 0 across the fourth CIE, and no significant recovery after this horizon.

2.5. Discussion

2.5.1. The Overall Carbonate Unit at Site 1215

The basic lithology and stratigraphy of Site 1215 cores (**Figure 2.2**) conform to a predictable history, considering past plate motion and subsidence of oceanic crust. Basalt was emplaced at the crest of the East Pacific Rise (EPR) toward the end of Chron 26r (~58 Ma) at about 11°N latitude (Shipboard Scientific Party, 2002a). The overlying metalliferous ooze (Unit III), a mixture of hydrothermal particulates and pelagic calcareous organisms, reflects ridge axis proximity. Moreover, Unit III contains nannofossils of NP 8 (Shipboard Scientific Party, 2002a), which occurred between ~58 and 57.2 Ma (Agnini et al., 2007).

Deposition of Unit II probably initiated near the ridge crest. According to the biostratigraphy (**Figure 2.5**), it accumulated during the latest Paleocene and the early Eocene (57 to 51.4 Ma). This age is consistent with the bulk $\delta^{13}\text{C}$ record at Site 1215, which can be described loosely as two segments separated by the first and most pronounced CIE. Values are relatively high in the bottom segment, averaging 3.11‰; values are relatively low in the top segment, averaging 1.87‰. A similar trend, including a prominent

CIE, is found in other bulk carbonate (e.g., Cramer et al., 2003; Hollis et al. 2005) and foraminifera (e.g., Zachos et al., 2001) $\delta^{13}\text{C}$ records that span this time interval (**Figure 2.6**).

Sediment in Unit II averages 66% carbonate. For open ocean locations far away from terrigenous sources, such values typify sites below the lysocline (Gardner, 1975; Archer, 1996; Lisitzin, 1996). Microfossil assemblages support this inference. Nannofossils dominate the carbonate, and further show "fragmentation and loss of morphological features such as central areas in placolith and zygodisc assemblages" (Shipboard Scientific Party, 2002a). Planktonic foraminifers also display obvious signs of dissolution (e.g., fragmentation and "peeling" on the wall structure of muricate taxa). Moreover, the P/B ratio is generally low. Thus, Unit II very likely represents a section of sediment that propagated north and west away from the ridge axis, as the seafloor subsided below the lysocline for nominally 6 million years (**Figure 2.5**). At ~ 51.4 Ma and at about 14°N , the seafloor passed below the CCD (Lyle and Wilson, 2006).

The present-day lysocline and CCD between 10 and 20°N latitude in the central Pacific are found at about 3000 and 4000 m water depth, respectively (Archer, 1996). An intriguing issue is whether these depths were significantly different during deposition of Unit II in the early Paleogene. Two factors confound a simple answer: unknown water depths in the past and temporal variations in the carbonate accumulation horizons.

Subsidence curves, which relate ridge flank basalt age to water depth, allow a means to reconstruct past water depths (Van Andel, 1975; Parsons and Sclater, 1977). Regarding Site 1215, however, there are several problems. First, gridded interpolations of

water depths for 0-2 Myr crust on the modern EPR range from 2700 to 3400 m (Calcagno and Cazenave, 1994). This heterogeneity in "zero age" depth likely relates to underlying mantle properties and likely occurred in the past (Calcagno and Cazenave, 1994). Second, subsidence rates along portions of the EPR vary from 200 to 400 m/Myr^{1/2} (Calcagno and Cazenave, 1994). Third, the section of the EPR that generated basalt at Site 1215 has subducted. Collectively, this makes any subsidence curve for this location somewhat speculative. In discussing carbonate deposition at Site 1215, Rea and Lyle (2005) used a generic EPR subsidence curve: $z \text{ (mbsl)} = 2750 \text{ m} + 357 \text{ m/Myr}^{1/2}$. This implies that Unit II accumulated when the seafloor subsided from about 3100 to 3700 mbsl (including minor sediment loading). Subsidence curves appropriate for the last 60-70 Myr also have been derived for ridge perpendicular "corridors" containing and surrounding Site 1215; these can be approximated as (Calcagno and Cazenave, 1994): $z \text{ (mbsl)} = 2350 \text{ m} + 375 \text{ m/Myr}^{1/2}$. This implies that Unit II accumulated when the seafloor subsided from about 2700 to 3400 mbsl.

Carbonate records on Shatsky Rise, about 5,000 km northwest of Site 1215, provide an upper constraint on early Paleogene lysocline depths in the north Pacific. Like Site 1215, Sites 1209 and 1211 were located on the Pacific Plate and in an open ocean environment with low elevated surface water productivity during the Paleocene and early Eocene. However, the water depths of these sites were about 2000 m and 2500 m, respectively (Bralower et al., 2002). For sediment deposited between 57 and 51.4 Ma at Sites 1209 and 1211, carbonate content mostly exceeds 80%, FRAG generally ranges between 30 and 50%, and the P/B ratio is typically low (Hancock and Dickens, 2005). These observations suggest the sites were near or above the lysocline between 57 and 51.4 Ma.

In a general sense, Unit II at Site 1215 represents pelagic deposition on the flank of the EPR as it subsided below a lysocline shallower than present-day and passed through a CCD also shallower than present-day at 51.4 Ma (**Figure 2.5**). However, subsidence does not explain the trends and anomalies in the carbonate records; rather, these likely signify global variations in lysocline and CCD depths during the early Paleogene.

The overall upward increases in carbonate content and planktonic foraminiferal abundance through Unit II (**Figure 2.4**) suggest enhanced carbonate accumulation in younger sediment. This is opposite to expectations for seafloor subsiding by 600-700 m below a stationary lysocline. However, these records are consistent with a view that lysocline and CCD depths generally increased between about 57 and 51 Ma (Hancock et al., 2007). This postulated deepening of carbonate dissolution horizons coincides with the long-term drop in $\delta^{13}\text{C}$ at Site 1215 (**Figures 2.2, 2.4**) and elsewhere (e.g., DSDP Site 259), and may reflect slow input of ^{13}C -depleted carbon to the ocean (Hancock et al., 2007; Hilting et al., 2008). On time-scales $>10^5$ yr, carbon addition to the atmosphere should enhance chemical weathering and delivery of HCO_3^- and Ca^{2+} to the ocean (e.g., Walker et al., 1981; Kump et al., 2009). Within this context, the top of the carbonate unit marks a rise in the CCD and the culmination of carbon input. One might speculate that this coincides with beginning of long-term Cenozoic cooling (Zachos et al., 2008).

2.5.2. Early Eocene Carbon Isotope Excursions and Multiple Carbon Injection

Events

Although long-term ($>10^5$ yr) massive carbon addition to the ocean (or atmosphere) should deepen the lysocline and CCD, short-term ($<10^5$ yr) injections should cause a

different response (e.g., Walker and Kasting, 1992; Dickens, 2000; Caldeira and Wickett, 2003; Ridgwell and Zeebe, 2005, Kump et al., 2009). Initially, seawater pH and carbonate saturation should decrease (i.e., ocean acidification), which would shoal the lysocline and CCD. After the carbon input, however, accelerated chemical weathering should remove CO_2 from the atmosphere, raise seawater pH, and increase the supply HCO_3^- and Ca^{2+} to the ocean. This should deepen the lysocline and CCD, but by more than before the carbon input (i.e., an “overshoot” of carbonate saturation horizons) because relevant inputs now exceed the steady-state outputs. The magnitude and timing of these responses at a given location should depend on various boundary conditions (e.g., ocean and atmosphere chemistry, direction of thermohaline circulation, etc.) as well as the nature and location of carbon addition (Dickens, 2000; Zeebe and Zachos, 2007).

Superimposed on long-term trends in carbonate content and preservation at Site 1215, short-term variations characterize the four negative CIEs (**Figure 2.4**). All four CIEs are marked by lows in carbonate content. Indeed, between 55 and 25 mbsf, these short depth intervals are the times of lowest carbonate content (**Figure 2.4**). As observed for the PETM and H1/ETM-2 in Atlantic cores (Kelly et al., 2005, 2010; Stap et al., 2009), enhanced carbonate preservation follows the lower two CIEs. Within ~200 kyr after the excursions, carbonate content increases significantly and planktonic foraminifers dominate assemblages. Partial evidence for carbonate overshoots also follows the upper two CIEs. The four intervals very likely reflect a series of rapid and massive additions of ^{13}C -depleted carbon between 56 and 51 Ma. This is because of the telltale carbonate dissolution and recovery, and because the CIEs most probably correlate to similar CIEs at other locations (**Figure 2.2**).

The lowest and most pronounced CIE occurred during C24r, at the NP9/NP10 boundary, and near the P5/E1 boundary. This corresponds to the PETM (e.g., Agnini et al., 2007). Indeed, this horizon already was suspected to mark the PETM, given shipboard biostratigraphy and identification of a Benthic Foraminiferal Extinction Event (BFEE) (Shipboard Scientific Party, 2002a).

The second CIE happened within the lower part of NP11. This is the stratigraphic position of the H1/ETM-2 event at several locations (Lourens, et al. 2005; Stap et al., 2008; Nicolo et al., 2007; Galeotti, et al., 2010) (**Figure 2.6**), although we note two caveats with this correlation. First, the magnitude of this CIE (0.38‰) is about 20% of that across the PETM (**Figures 2.4 and 2.6**). This is proportionally less than observed elsewhere (e.g., Lourens et al., 2005; Nicolo et al., 2007; Galeotti et al., 2010). For example, on Walvis Ridge, the magnitude of the H1/ETM-2 CIE is roughly half that of the PETM (Stap et al., 2009). Second, according to shipboard magnetostratigraphy (Shipboard Scientific Party, 2002a), the position of this event occurred within a normal polarity chron (which we would assign to C24n.3n). However, recent early Eocene calibrations place the H1/ETM-2 event near the top of chron C24r (Agnini et al., 2007; Westerhold and Röhl, 2009, Galeotti et al., 2010). These discrepancies may relate to the aforementioned magnetostratigraphy problems at Site 1215, concatenation of the record at Site 1215 (discussed below), or both.

The third CIE occurred near the top of NP11 but in sediment without a clear magnetic signal (**Figure 2.2**). The biostratigraphic position approximates that of the I1 event (**Figure 2.6**) identified in multiple sections (Cramer et al., 2003; Nicolo et al., 2007). According to current stratigraphic alignments (Agnini et al., 2007; Westerhold and Röhl, 2009), the event corresponds to a set of short normal and reversed sub-chrons near the top

of C24. This may explain the uncertain magnetic signal. We also note the magnitude of the CIE (0.14‰) is less than that for the H1/ETM-2 event. This agrees with previous findings (Cramer et al., 2003; Nicolo et al., 2007; Galeotti et al., 2010).

The uppermost CIE happened at the transition between NP11 and NP12 and during a normal polarity chron (**Figures 2.2, 2.4**). Assuming the polarity chron is C24n.1n, this is the stratigraphic position of the K/X event documented at other locations (Agnini et al., 2007, 2009; Galeotti et al., 2010). At Site 1215, absolute $\delta^{13}\text{C}$ values drop to the same as those during the PETM, although the magnitude of the CIE is about 50%. This is similar to the findings at the Contessa section in Italy (Galeotti, et al., 2010).

2.5.3. Complications and Highlights of Lower Eocene Records at Site 1215

Stable carbon isotope records at several locations (e.g., DSDP Sites 550 and 577, ODP Site 1051, Cramer et al., 2003; ODP Sites 1262-1267, Stap et al., 2009, 2010; Mead and Dee Streams, Nicolo et al., 2007) show "minor" negative CIEs that do not appear in our $\delta^{13}\text{C}$ record. In particular, the H2 and I2 CIEs follow the H1 and I1 CIEs (respectively) by about 100 kyr. Small CIEs also may have occurred before and after the K/X event (Cramer et al., 2003). The absence of these CIEs may highlight a basic problem facing interpretations of carbonate and carbon isotope records at Site 1215.

The average compacted sedimentation rate for Unit II is ~ 0.8 cm/kyr (Figure 17 in Shipboard Scientific Party, 2002a). This is lower than that of most other lower Paleogene sections with $\delta^{13}\text{C}$ records, as expected for an open-ocean location below the lysocline. Moreover, these rates are even less across CIEs because of carbonate dissolution. Given the low sedimentation rates and evidence for bioturbation at Site 1215, it is entirely possible

that signatures of carbon injection events have been modified. For instance, changes in various records across the H1/ETM-2 event at Site 1215 may in fact represent integrated changes of conditions spanning H1/ETM-2, H2, and intervening time. Such concatenation of the sedimentary record would impact interpretations because the magnitude of the CIEs and carbonate dissolution may be "smeared" in the time domain (e.g., Zachos et al., 2007; Stap et al., 2009). Nonetheless, records from Site 1215 provide important information in which to address the link between rapid, massive carbon addition and seafloor carbonate accumulation.

The PETM is the most pronounced and best-studied early Paleogene carbon injection event, and our Site 1215 records display two features of special significance in this regard. First, carbonate preservation diminishes before the PETM (**Figure 2.4**). About 2 m below the CIE, the numbers of fragments and planktonic foraminifera progressively decrease. This signal might be ascribed to carbonate dissolution of previously deposited sediment (e.g., Dickens, 2000). However, for sites on Shatsky Rise, such "burn-down" before the PETM was <20 cm (Colosimo et al. (2005), an amount similar to that inferred in various modeling exercises (e.g., Dickens, 2000; Zeebe and Zachos, 2007). It is possible that significant carbonate dissolution (i.e., a rise in the lysocline) began before the CIE, at least in the Pacific Ocean. We offer no mechanism for such a change but note that environmental perturbations preceded the CIE of the PETM elsewhere (e.g., Sluijs et al., 2007b).

Second, carbonate content does not drop below 7% at the PETM. This is true even for a very small sample taken from the darkest interval within the CIE (i.e., presumably a horizon with the lowest carbonate content). This finding is consistent with data from other

sites in the Pacific Ocean (ODP Site 1209, Colosimo et al, 2005), as well sites within the southern Indian and southern Atlantic oceans (e.g., DSDP Site 259, Hancock et al., 2007; ODP Site 690, Kelly et al., 2005). However, it contrasts with observations at some sites in the central and North Atlantic Ocean, where carbonate content drops to 0% at the PETM (e.g., Zachos et al., 2005; Zeebe and Zachos, 2007). Some authors have suggested, based on Atlantic records, that the lysocline and CCD rose by over 2 km during the PETM (e.g., Zachos et al., 2005). No site in the Pacific Ocean, including Site 1215, supports this inference. Indeed, a straightforward interpretation of the Site 1215 record is that this location was nominally halfway between the lysocline and CCD before the PETM, at or near the CCD during the PETM, and near the lysocline after the PETM (**Figure 2.5**).

There is strong interest in comparing perturbations across the different CIEs, as this may constrain the range of impacts resulting from massive carbon injection (e.g., Zachos et al., 2008). The similarities and differences in carbonate responses spanning the PETM and the H1/ETM-2 events hint at the power and problem with this goal. The magnitude of the CIE is greater across the PETM than the H1/ETM-2 event at Site 1215 and elsewhere (e.g., Cramer et al., 2003; Nicolo et al., 2007; Stap et al., 2010), suggesting a larger input of ^{13}C -depleted carbon during the first interval (Dickens, 2003). All proxies for carbonate dissolution also are greater during the PETM (**Figure 2.4**), which supports this idea. However, the recovery of carbonate preservation, as signified by records of bulk carbonate content, the percentage and number of foraminiferal fragments, and the P/B ratio, was greater following the H1/ETM-2 event (**Figure 2.4**). In fact, the number of planktonic foraminiferal tests within 200 kyr after the H1/ETM-2 event is at least twice that following the PETM. In other words, seafloor carbonate dissolution was greater during the PETM, but

subsequent carbonate preservation was greater after H1/ETM-2 (**Figure 2.5**). This is not predicted by modeling (e.g., Dickens, 1997, 2000; Zachos et al., 2008), unless boundary conditions were different. One explanation incorporates the aforementioned notion that the lysocline and CCD generally deepened from the late Paleocene through the early Eocene. Specifically, the PETM occurred when the long-term lysocline and CCD were shallower than when H1/ETM-2 occurred. Model comparisons of Paleogene carbon injection events need to consider this possibility.

Carbonate signals across the I1 event are problematic at Site 1215 (**Figure 2.6**) and elsewhere. A significant and apparently correlative CIE has been documented at widely separated sites in different depositional environments (Cramer et al., 2003; Nicolo et al., 2007; Galeotti et al., 2010). However, an obvious CIE or lithological expression has not been found at all sites (e.g., the Possagno section, Agnini et al., 2009); indeed, this suspected hyperthermal has been omitted in the ad hoc ETM nomenclature (Appendix 1). This may imply that the carbon input was relatively small compared to that during the PETM and H1/ETM-2. At Site 1215, the suspected I1 has a small CIE and higher carbonate preservation than the earlier two events. The subsequent recovery is also complex. The carbonate content following the event is similar to that after H1/ETM-2, but the number of fragments and the P/B ratio do not show major recoveries (**Figure 2.4**).

The relatively large magnitude of the CIE across the K/X event here and elsewhere (Rohl et al., 2006; Agnini et al., 2009; Galeotti et al., 2010) suggest a carbon injection with a mass between those of the PETM and H1/ETM-2. However, it is uncertain whether proxies for carbonate dissolution (**Figure 2.6**) support this notion. The carbonate content decreased to 1.4% during the K/X event, and with such dissolution neither foraminifers nor

their fragments were preserved. About 200 kyr later, the carbonate content approached 100%, which was subsequently followed by a gradual decrease such that values reached 0% about 1 Myr after the event. Within the "carbonate overshoot", P/B values are high, although the number of planktonic foraminifers does not exceed 10 specimens per sample (**Figure 2.4**). These unusual signals may reflect a combination of bathymetric position and the termination of the postulated "long-term" carbon input. Given plate motion and subsidence, the site likely sat at about 14°N latitude and between 3400 and 3700 mbsl during the K/X event. This is several hundreds of km north and several hundreds of m deeper than when the PETM occurred (**Figure 2.5**). In the first regard, it is possible that the site was on the northern fringe of the Paleogene equatorial Pacific productivity belt during this time (Moore, 2004). If ideas of reduced pelagic productivity during hyperthermals are correct (Bralower, 2002; Tremolada and Bralower, 2004), the lysocline and CCD might show atypically strong dissolution and subsequent preservation at Site 1215. In any case, once the long-term carbon input ceased, carbonate accumulation horizons shoaled relatively fast.

2.5.4. Evidence for Multiple Hyperthermals

The PETM has been studied extensively because it may serve as a past analog in which to address future climate change. Over the last 15 years, it has become abundantly clear that this geologically brief time interval was somehow linked to massive input of ¹³C-depleted carbon, extreme global warming, and profound environmental change (e.g., Sluijs et al., 2007a). An open issue is whether other, lesser CIEs in the lower Paleogene sediment are correlated and linked to global warming. Recent papers have provided affirmative

evidence for H1/ETM-2 (Lourens et al., 2005, Stap et al., 2009; Sluijs et al., 2009) and possibly I1 (Nicolo et al., 2007).

The four CIEs found at Site 1215 were accompanied by negative $\delta^{18}\text{O}$ excursions in bulk carbonate (**Figure 2.4**). The most pronounced $\delta^{18}\text{O}$ excursion occurred during the PETM. The K/X event also has a prominent $\delta^{18}\text{O}$ excursion, while H1/ETM-2 and I1 events have relatively small excursions. Although these depletions in $\delta^{18}\text{O}$ are measured in bulk carbonate and may represent complex signatures, they most probably relate to temporary rises in sea surface temperature. The $\delta^{18}\text{O}$ record at Site 1215 may indicate that all four CIEs were related to a rise in global temperature and that there was a first order correspondence between the mass of carbon injected into the atmosphere-ocean system and Earth surface warming. This supports the notion that major CIEs of the early Paleogene were indeed “hyperthermals” linked to greenhouse gas emissions.

2.6. Conclusions

The sedimentary record at Site 1215 contains a 42 m thick interval of carbonate ooze. This lithologic unit (Unit II) was deposited between 57 and 51.4 Ma, during which the seafloor subsided and moved northwest away from the crest of the EPR. The section accumulated below the lysocline, and the termination of Unit II represents passage through the CCD. However, during this time, the depth of the lysocline varied significantly.

Overall, the carbonate content increased and the preservation of planktic and benthic foraminifera improved upcore through Unit II. This suggests that the lysocline (and CCD) generally deepened at this location from the late Paleocene through the early Eocene.

Such an interpretation has been made at other locations, and may signify an increase in the flux of carbon to the ocean. This is important to models of early Paleogene carbon cycling and climate because it implies that one or more boundary conditions are changing during this time.

Unit II also has four relatively short intervals of carbonate dissolution characterized by low carbonate content and poor carbonate preservation. These are interpreted as geologically brief rises in the lysocline; they also correspond with three and possibly four negative CIEs that have been documented at other locations. The combined dissolution and carbon isotope records at Site 1215 strongly suggest that there were at least four intervals of fairly rapid and massive injection of ^{13}C -depleted carbon that led to ocean acidification. These events are the PETM (55.5 Ma), H1/ETM-2 (53.7 Ma), I1 (53.2 Ma) and K/X (52.5 Ma). This concept is further supported at Site 1215 by carbonate "overshoots". Within 200 kyr after each CIE, the carbonate content, the abundance and preservation of planktonic foraminifers, or both increase, sometimes considerably. These are probably short-term drops in the lysocline, which should occur after the initial carbonate dissolution as weathering removed CO_2 from the atmosphere and supplied excess Ca^{2+} and HCO_3^- to the ocean (e.g., Dickens et al., 1997). Carbonate overshoots have also been found in sediment records from the Atlantic Ocean following the PETM and ETM-2/H-1 (Kelly et al., 2005, 2010; Stap et al., 2009).

2.7. Acknowledgements

We thank scientists and staff of the Gulf Coast Repository at College Station for sample collection, and T.C. Huang of ExxonMobil Exploration Company for identifying

the nannofossils. The senior author was guided by Chengjie Liu (ExxonMobil Exploration Company) on taxonomic identification of planktonic foraminifera. William Berggren and Richard Olsson lent several planktonic foraminiferal slides from type localities and DSDP sites. Glen Snyder aided with SEM images, which were taken in conjunction with the Rice Shared Equipment Authority. Jason Curtis performed the stable isotope analyses at the Stable Isotope Mass Spectrometry Laboratory, University of Florida. This study was partially supported by a Geological Society of America Student Grant. We thank two referees for valuable comments that improved this paper.

2.8. Appendix 1

The K event has been called X event and ETM-3 (Eocene Thermal Maximum-3, Röhl et al., 2006; Sluijs et al., 2007a; Agnini et al., 2009; Galeotti et al., 2010). We refrain from usage of the latter because there is likely at least one significant hyperthermal between H1 and K (Nicolo et al., 2007; Galeotti et al., 2010). This event, “missing” in the tentative “ETM nomenclature” and already the source of some confusion, is referred to as I1 (Cramer et al., 2003; Nicolo et al., 2007).

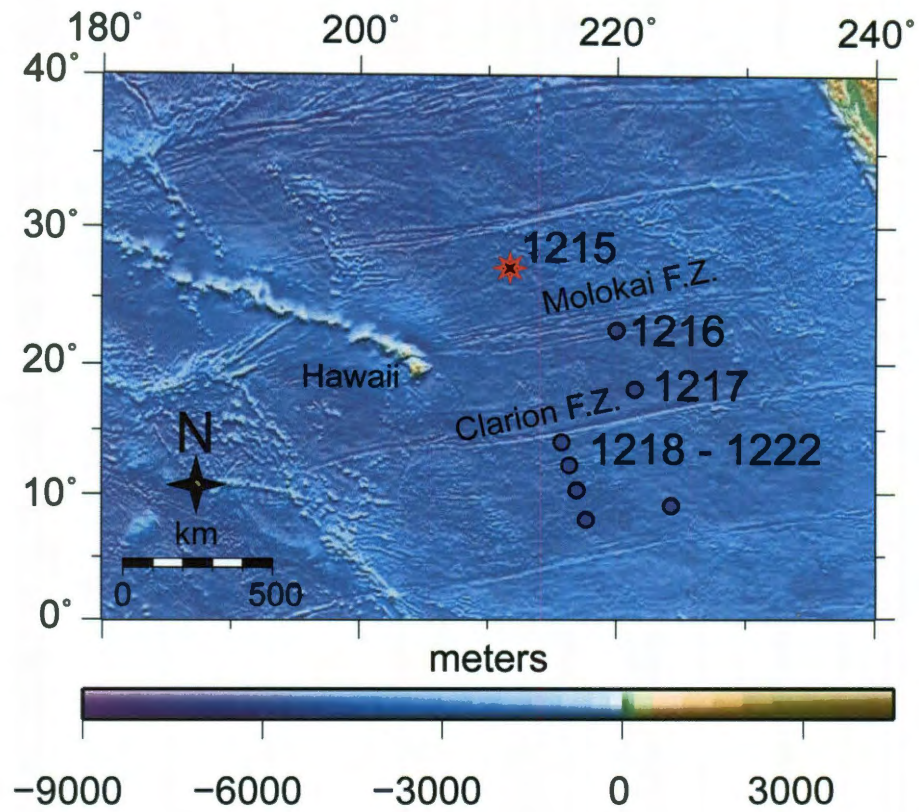


Figure 2.1 – Location of Site 1215 and other sites drilled by ODP Leg 199 (Shipboard Scientific Party Leg 199, 2002). Topography and bathymetry from Smith and Sandwell (1997).

Figure 2.2

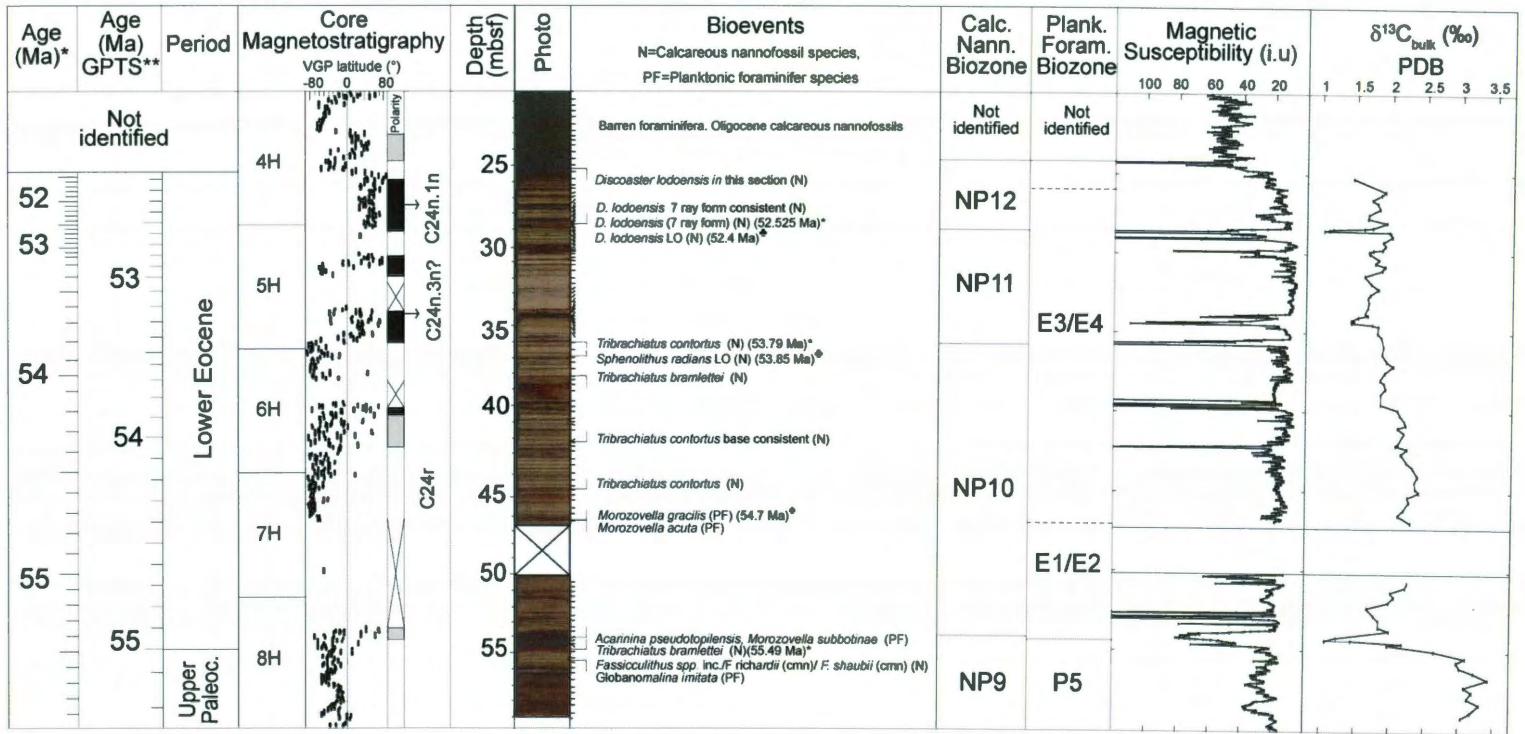


Figure 2.2 – Lithology and stratigraphy at ODP Site 1215. Lithologic units, paleomagnetic information and magnetic susceptibility data from Shipboard Scientific Party Leg 199 (2002); other records mostly from this study. Absolute ages are for both * = the revised datums by Agnini et al. (2007) and ** = the widely used datums by Cande and Kent (1995). Small lines on the right side of the core photo show the position of samples used for this study. ♣= Datum reported by Raffi et al., 2005. ♠= Datum reported by Shipboard Scientific Party (2002). cmn= common occurrence. We chose MS = 150×10^{-6} SI as the background in which enhanced accumulation of magnetic minerals could be detected.

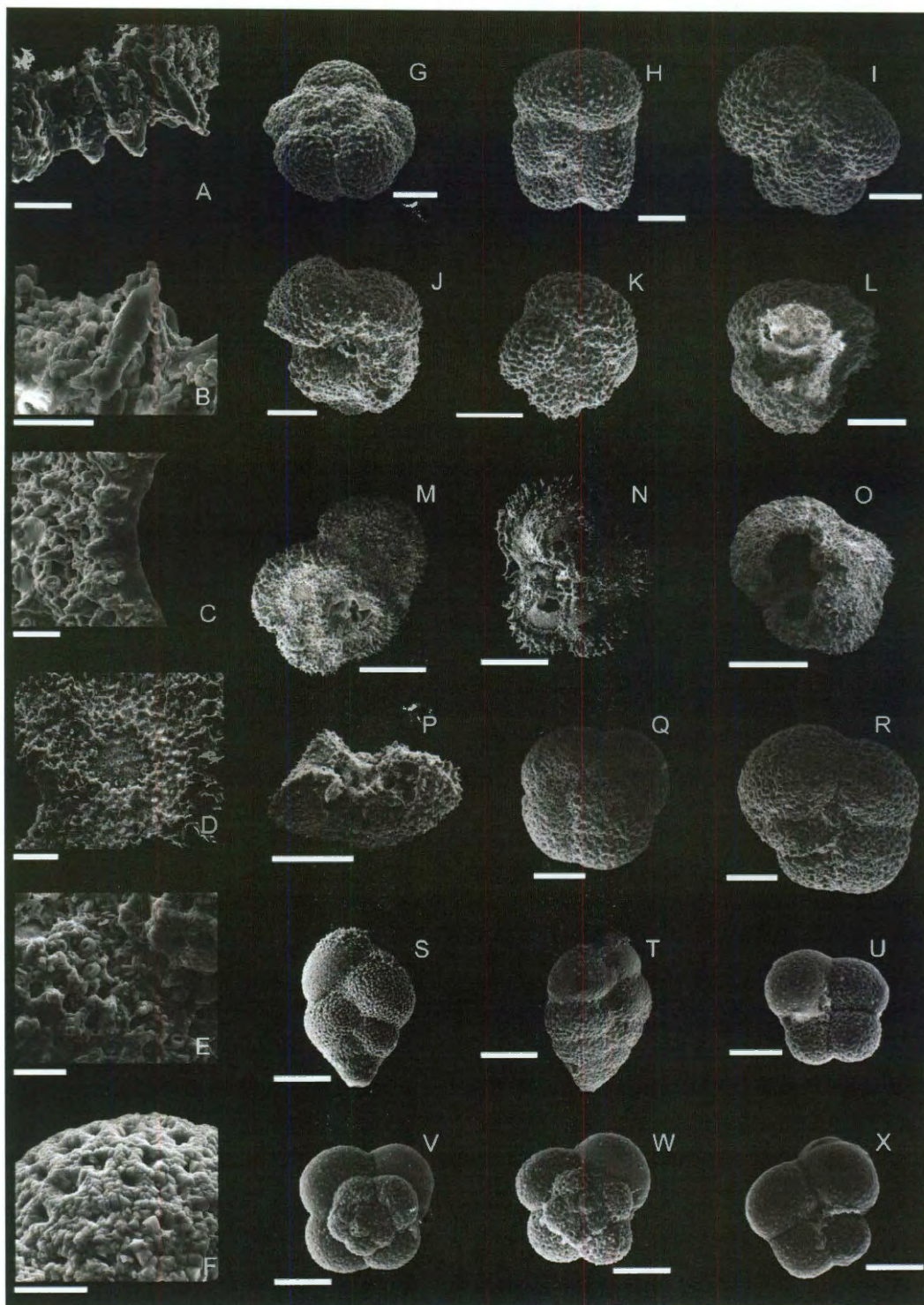


Figure 2.3

Figure 2.3 – Late Paleocene and early Eocene planktonic foraminifers at IODP Hole 1215A. A - B. *Acarinina* spp. Chamber fragments with partially dissolved pustules, C. *Acarinina* sp. Detail of broken chamber and partially dissolved wall. D. *Morozovella subbotinae* Dissolution of test. Penultimate chamber “peeled off”, E. *Acarinina* sp. Recrystallized wall and coccoliths filling pores, F. *Paragloborotalia?* sp. Recrystallized and partially dissolved test. Overgrown euhedral calcite crystals on wall, G. *Acarinina esnehensis?* 53.725 mbsf H. *A. pseudotopilensis* 53.725 mbsf, I. *A. angulosa*, J. *A. soldadoensis?* 53.725 mbsf K. *Acarinina* sp. small test L. *Acarinina* sp. Broken test, M – N. *M. subbotinae* Partially dissolved tests 45.61 mbsf, O. *Acarinina* sp. Test with missing chambers and signs of corrosion, P. *M. subbotinae* Fragmented test (side view) with partially corroded chambers, Q – R. *Paragloborotalia?* spp. Overgrown calcite crystals on the test walls, S – T. *Chiloguembelina crinita* 31.89 mbsf, U – X. “*Tenuitella*” spp. at 30.37 mbsf, 35.885 mbsf, 52.275 mbsf, and 59.095 mbsf. White bar in A - D, and F= 20µm; in E, Q, and R= 50µm; in G – L, S - T= 100µm, in M – O= 200µm; in U – X= 40µm.

Figure 2.4 – Stable isotope records of bulk carbonate and various carbonate records at ODP Site 1215. FRAG, and P/B ratio as defined in the Methods. ∞ = samples where FRAG is infinity because there are no whole tests of planktonic foraminifera. Dashed red lines correspond to the depths of pronounced CIEs in the record.

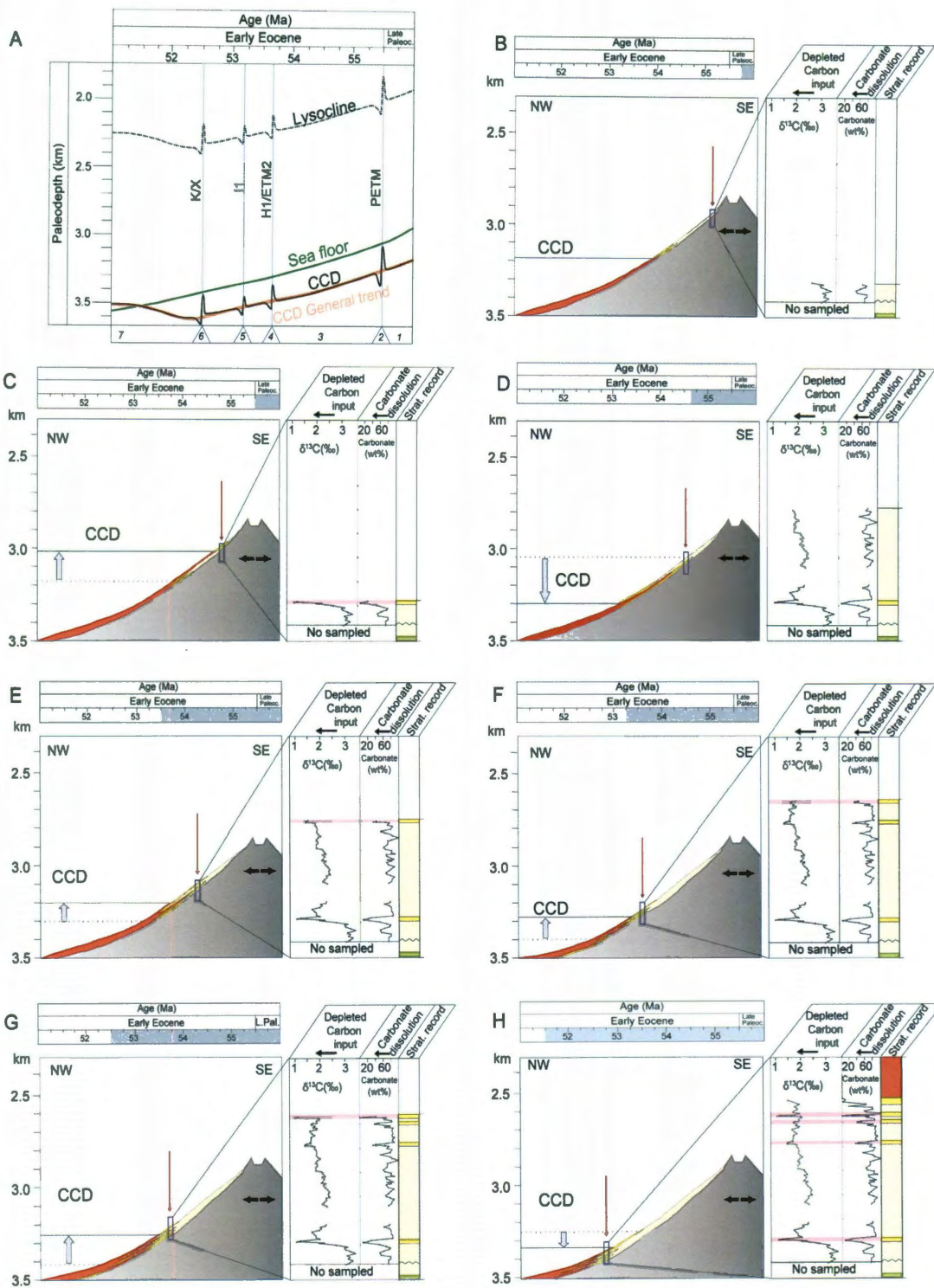


Figure 2.5

Figure 2.5 – Hypothetical evolution of the CCD (solid black line) and the lysocline (dashed line) in the Equatorial Pacific during the early Eocene. Thermal subsidence predicted for Site 1215 (Rea and Lyle, 2005; green line). B-H. Cross-section and “snapshots” of the evolution of the ODP site 1215. Red arrows indicate latitudinal position of the ODP Site 1215 at different times. Dashed line corresponds to previous position of the CCD. Continuous line indicates CCD position at that specific time. Color scheme: Green is basalt of the oceanic crust of the Pacific Plate; right yellow is red clay with low carbonate content; orange is red clays; pale yellow are nanofossil oozes and carbonate-rich sediments. Double direction arrows indicate center of the spreading center and relatively plate tectonic movement.

Figure 2.6

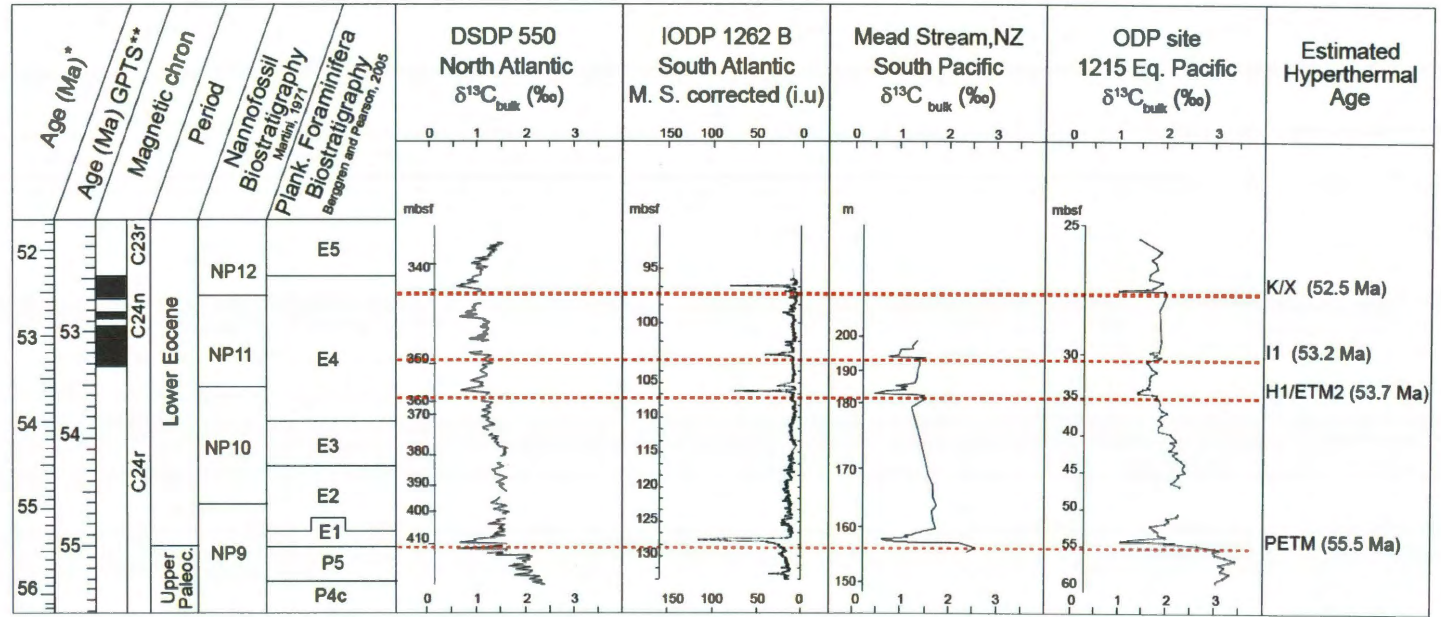


Figure 2.6 – Age correlation of 4 early Eocene Hyperthermals at different location. ODP Site 550 (Cramer et al., 2003), Magnetic Susceptibility (Shipboard Scientific Party, 2004), Mead Stream, New Zealand (Nicolo et al., 2007), ODP Site 1215 (this study). * Biochronology and Age data by Agnini et al. (2007). **Time scale by Cande and Kent, 1995. Dashed red lines correspond to the position of pronounced early Paleogene hyperthermals.

Chapter 3

Lower Paleogene Carbonate and Planktic Foraminiferal Accumulation at ODP Site 1215, Eastern Equatorial Pacific Ocean

Lizette Leon-Rodriguez^{a,*}, Gerald R. Dickens^{a,b}, and R. Mark Leckie^c

^aDepartment of Earth Sciences, Rice University, MS-126 P.O. Box 1892, Houston TX,
77281-1892, USA

^bInstitutionen för Geologiska Vetenskaper, Stockholms Universitet, 106 91 Stockholm,
Sweden

^cDepartment of Geosciences, University of Massachusetts, 611 North Pleasant Street, 233
Morrill Science Center, Amherst, MA 01003-9297, USA

A manuscript to be submitted to:

Marine Micropaleontology

November 13, 2011

ABSTRACT

Carbonate accumulation and planktic foraminiferal preservation are examined in sediment deposited at ODP Site 1215 before, during, and after four hyperthermal events of the early Paleogene (PETM, ~55.5 Ma; H1/ETM2, ~53.7 Ma; I1, ~53.2 Ma, and K/X, ~52.5 Ma). The hyperthermals are characterized by very low accumulation of carbonate and planktic and benthic foraminifers. Within 200 kyr after each event, there is an overall improvement in carbonate accumulation and foraminiferal preservation. In general, the planktic foraminiferal assemblages follow a predicted pattern for selective dissolution. Species of *Acarinina* are preferentially preserved over *Morozovella*, which are preferentially preserved over *Subbotina*, *Igorina* and *Globanomalina*. A previously overlooked genus that made small tests, *Praetenuitella*, also appears resistant to dissolution. Despite the imprint of dissolution, changes in the oxygen isotope record and foraminiferal assemblages suggest that the hyperthermal events at Site 1215 were superimposed on a slight long-term cooling between 55.3 and 52.6 Ma. Thus, warm-water dwellers (*Acarinina* and *Morozovella*) appear soon after the hyperthermals, but cooler-water dwellers (*Praetenuitella*) prevail over the long-term. This long-term cooling differs from most locations, and may reflect northward tectonic migration of the site towards cooler regions during this time.

Keywords: Planktic foraminifera, Early Eocene, Hyperthermal, Ocean acidification, Equatorial Pacific, Paleocene-Eocene Thermal Maximum

3.1. Introduction

Earth experienced a series of short-term (<200 kyr) global warming episodes in the early Paleogene between ca. 58 and 50 million years ago (Ma) (Lourens et al., 2005; Zachos et al., 2005; Nicolo et al., 2007; Sluijs et al., 2007b; Zachos et al., 2008; Leon-Rodriguez and Dickens, 2010). These “hyperthermals” were characterized by widespread environmental perturbations, including prominent drops in the $^{13}\text{C}/^{12}\text{C}$ ratio of the exogenic carbon cycle, which reflect massive addition of ^{13}C -depleted CO_2 to the ocean and atmosphere (Dickens et al., 1997; Dickens, 2000; Zachos et al., 2005; Stap et al., 2009; Leon-Rodriguez and Dickens, 2010). The most pronounced and best studied of these events was the PETM (Paleocene-Eocene Thermal Maximum; ~55.5 Ma) (Sluijs et al., 2007a; McInerney and Wing, 2010). However, at least three subsequent intervals of warming and carbon injection occurred; these are called tentatively ETM-2 or H1 (~53.7 Ma), I1 (~53.2 Ma), and K or X (~52.5 Ma) (Cramer et al., 2003; Lourens et al., 2005; Nicolo et al., 2007; Agnini et al., 2009; Sluijs et al., 2009; Stap et al., 2009; Galeotti et al., 2010; Leon-Rodriguez and Dickens, 2010; Stap et al., 2010; Zachos et al., 2010). The early Paleogene hyperthermals, including the PETM, have become a magnet for investigations concerning rapid global change of the past and carbon cycling (e.g., Sluijs et al., 2007a; Zachos et al., 2008; McInerney and Wing, 2010).

Basic ocean chemistry models consistently show that rapid and massive CO₂ injections cause strong carbonate dissolution followed by enhanced carbonate preservation (“overshoots”) on the seafloor (Dickens et al., 1997; Kump et al., 2009; Zachos et al., 2010; Cui et al., 2011). However, the magnitude, timing and spatial distribution of these responses relate to the source(s) and location(s) of carbon input, as well as carbon outputs through chemical weathering and organic carbon sequestration (Kelly et al., 2005; Zachos et al., 2005; Kelly et al., 2010). Changes in deep-sea sediment carbonate dissolution and preservation during the early Paleogene remain poorly constrained because of limited records and different responses between available locations; certainly, carbonate accumulation was not uniform across ocean basins surrounding the PETM (Zeebe and Zachos, 2007).

Given scientific boreholes drilled to date, the sedimentary record recovered at Ocean Drilling Program (ODP) Site 1215 in the eastern equatorial Pacific Ocean (**Figure 3.1**) offers a rare window for examining deep-sea carbonate accumulation and calcareous microfossil preservation across the early Paleogene hyperthermals. The sequence was deposited on ocean crust formed at a mid-ocean ridge several million years before the PETM, and it was recovered using advanced hydraulic piston coring (HPC) techniques. This means that deposition occurred within the lysocline across the time interval of interest, and that sediment recovery was reasonably good. We previously have presented the stratigraphy and various

records regarding carbonate dissolution and preservation at this site (Leon-Rodriguez and Dickens, 2010). This work strongly suggests that the four main hyperthermal events between 58 and 50 Ma were characterized by carbonate dissolution followed by enhanced preservation (Leon-Rodriguez and Dickens, 2010), as predicted from geochemical modeling pertaining to massive inputs of depleted ^{13}C carbon (Dickens et al., 1997; Dickens, 2000; Kelly et al., 2005; Zachos et al., 2005; Kelly et al., 2010).

Changes in carbonate accumulation rates and foraminiferal assemblages during and between the hyperthermal events were not addressed in our previous work at Site 1215. Orbitally-tuned carbon isotope and geochemical (XRF) records are now available for the early Paleogene interval at Site 1262 in the Atlantic Ocean (Westerhold et al., 2007; Westerhold et al., 2008; Westerhold and Röhl, 2009; Zachos et al., 2010). Moreover, experimental data are now available regarding how carbonate dissolution affects early Paleogene foraminiferal assemblages (Nguyen et al., 2009). These recent studies “open the door” for further assessment as to how massive past injections of CO_2 impact carbonate deposition and microfossil preservation. In this paper, we return to the sedimentary record at Site 1215 and present accumulation rates of carbonate (and various other components) as well as assemblage data of planktic foraminifera before, during and after each of the four main hyperthermals. The hyperthermal events almost assuredly represent a series of massive ^{13}C -depleted carbon releases to the ocean-atmosphere system, but

intriguing complications remain when trying to understand and quantify past deep-sea carbonate dissolution in the early Paleogene.

3.2. Background

3.2.1. Site and Samples

Ocean Drilling Program (ODP) Site 1215 (**Figure 3.1**) comprises two holes located ~1,000 km northeast of Hawaii ($26^{\circ}01.77'N$, $147^{\circ}55.99'W$) at 5,396 meters below sea level (Shipboard Scientific Party, 2002c). Hydraulic piston coring in the holes (A and B) recovered a sedimentary sequence that ranges from the Holocene to the upper Paleocene. It has been divided into three lithological units: Unit I is red clay from the seafloor to 26 m below seafloor (mbsf), Unit II is clayey calcareous ooze from 26 to 68 mbsf, and Unit III is metalliferous oxide ooze to basalt from 68 to 70 mbsf (Shipboard Scientific Party, 2002c).

Deep-sea drilling typically recovers incomplete sediment sequences with gaps between successive cores (Shipboard Scientific Party, 2002a). Thus, records from adjacent drill holes are often “spliced” together to make a composite sequence (Shipboard Scientific Party, 2002a). We have done this for Site 1215, using the magnetic susceptibility (MS) records (Shipboard Scientific Party, 2002c), after removing severely disturbed intervals and horizons with nodules (**Figure 3.2**). Such splicing often results in a composite sequence longer than that drilled, which then should be compressed (Shipboard Scientific Party, 2002a). Our composite depth scale for Site 1215, reported as

core composite depth below seafloor (mccsf), following recent methodology and terminology (Expedition 320/321 Scientists, 2010) was compressed by 8%, so that it has the correct total depth (Shipboard Scientific Party, 2002a).

We focused on the upper Paleocene-lower Eocene interval between 20.7 and 57.8 mccsf (**Figure 3.2**), because this spans the early Paleogene hyperthermals (Leon-Rodriguez and Dickens, 2010). As part of a previous effort (Leon-Rodriguez and Dickens, 2010), we collected and examined 117 samples of 10 cc of sediment from Hole 1215A at every 30 to 50 cm with a higher resolution of every 5 to 10 cm across dark horizons. Most samples were selected to avoid disturbed intervals caused by drilling and coring.

3.2.2. Age Model and Isotope Stratigraphy

A tentative age model for Site 1215 was based on revised depths and dates of calcareous nannofossil, planktic foraminiferal, and magnetostratigraphic datums (Leon-Rodriguez and Dickens, 2010). However, this age model can be improved through carbon isotope stratigraphy. As is true for many early Paleogene marine sections, there is a fairly good correlation between carbon isotope records at Site 1215 (Leon-Rodriguez and Dickens, 2010) and other locations, such as Site 1262 on Walvis Ridge in the southeast Atlantic (Zachos et al., 2010). Notably, the $\delta^{13}\text{C}$ record at Site 1262 contains four pronounced CIEs, which can be used as additional age constraints (**Figure 3.3; Table 3.1**).

3.3. Methods

3.3.1. Sample Processing

All samples were cleaned with 18 M Ω deionized water to eliminate salts that precipitated from interstitial fluids. After freeze-drying, between 2 and 5 g of each sample were carefully weighed. These aliquots were subsequently washed with deionized water on a 63 μ m sieve to collect foraminifers and other biogenic material. Stable isotope compositions of bulk sediment were measured using a VG/Micromass PRISM Series II isotope ratio mass spectrometer housed at the University of Florida. The analytical accuracy and precision were better than $\pm 0.07\text{‰}$ for both carbon and oxygen isotopes, and the data have been reported previously by Leon-Rodriguez and Dickens (2010).

3.3.2. Abundance of Foraminifers

Planktic foraminifers and benthic foraminifers were collected in cardboard micropaleontological slides and counted (Appendix A). Planktic foraminifers were determined to the species level when preservation permitted. Identification followed the an updated taxonomic guide for the Eocene (Pearson et al., 2006), with supplementary sources (Berggren, 1977; Blow, 1979; Olsson et al., 1999). It should be noted, though, that a newly described species of foraminifera, *Praetenuitella antica* n. sp., occurs within this sediment section (Leon-Rodriguez et al., Submitted). Relative abundances of planktic foraminifers were calculated using all the genera within assemblages excluding those that did not represent more 1%, as their relative abundance is not statistically significant.

3.3.3. Mass and Component Accumulation Rates

Carbonate mass accumulation rates and component accumulation rates were calculated as follows:

$$AR_x = X * SR * DBD , \quad (\text{Eq. 1})$$

where X is either the weight percent of carbonate or the number of individuals of component X per dry sample weight, SR is the (compacted) sedimentation rate (cm/kyr), and DBD is the dry bulk density (g/cm³). Carbonate contents of bulk dry sediment samples have been published previously (Leon-Rodriguez and Dickens, 2010). For other components, such as benthic and planktic foraminifers, or fish debris, X was calculated from counts of biogenic residues collected from the 63µm fraction of weighed samples.

Sedimentation rates were derived from stratigraphic datums, including prominent changes in carbon isotopes (**Figure 3.3**). However, they were estimated through two different approaches. First, conventional linear sedimentation rates (LSRs) were determined by fitting straight lines through age datums. This gives a series of sedimentation steps. Second, smoothed sedimentation rates (SSRs) were determined from the first derivative of the fourth order polynomial that best fit the overall age model. The result is a sedimentation curve expressed by: $SSR = -1.1494273928z^3 + 184.8112527899z^2 - 9899.2023533302z + 176649.87912498$, where z is depth expressed in mccsf. Ideally, both approaches should give similar first-order results.

The dry bulk density (DBD) was measured for several sediment horizons at Hole 1215A (Shipboard Scientific Party, 2002c). We took the available measurements within our interval of interest and determined the average DBD for carbonate-rich (0.62 g/cm^3) and clay-rich horizons (0.31 g/cm^3), as well as for the entire thickness (0.57 g/cm^3). Mass accumulation rate curves are affected minimally by the choice of DBD, so results presented hereafter consider different densities for clay and carbonate-rich horizons.

3.4. Results

3.4.1. Relative Abundance of Planktic Foraminifera

Four intervals in Unit II can be distinguished on the basis of planktic foraminiferal assemblages (**Figure 3.4**). These intervals are separated by horizons where counts of planktic foraminifers are extremely low, and only a few individuals of praetenuitellids and small acarininids are preserved.

The first interval lies between 57.81 and 54.48 mccsf, and was deposited during the latest Paleocene (**Figure 3.4**). Assemblages consist of *Globanomalina* (30-80%), *Praetenuitella* (15-70%), *Paragloborotalids* and *Subbotinids* (33-63% collectively), and *Acarinina* (0-33%). Throughout of this interval, foraminifers are uncommon (< 100 individuals per sample) and have moderate to poor preservation. Some identifiable species in this part of the section include: *Globanomalina imitata/ovalis*, *Acarinina soldadoensis*, *Praetenuitella* sp., and *Paragloborotalia griffinoides*?

The second interval lies between 52.95 and 35.51 mcsf, and was deposited in the earliest Eocene (**Figure 3.4**). Samples throughout have a very different assemblage than those of the underlying interval. *Acarinina* is the most abundant genus (30-100%); the next most abundant are *Praetenuitella* (0-75%) and *Morozovella* (0-25%). In the lower part of this interval, between 52.95 and 45.87 mcsf, and just above the PETM (**Figure 3.4**), the number of individuals (~50-300 specimens per sample), preservation and diversity of planktic species is relatively high. Species identified include: *A. soldadoensis*, *A. pseudotopilensis*, *A. soldadoensis*, *A. wilcoxensis*, *A. coalingensis*. *M. subbotinae*, *M. acuta*, *M. cf. acuta*, and *Praetenuitella* sp. (**Plates 3.1-3.3**). The relative and absolute abundances of other genera (i.e., *Globanomalina*, *Igorina*, *Subbotina*, *Paragloborotalia*, and *Parasubbotina*) are generally low (<20%) within this interval (**Figure 3.4**), and throughout the lower Eocene sedimentary record. In the upper part of the second interval, between 45.87 and 35.60 mcsf, absolute counts of all planktic genera diminish (<100 specimens per sample).

The third interval lies between 35.40 and 31.39 mcsf, and was deposited between the H1 and I1 events. Planktic foraminifers are abundant. In the lower part, between 35.40 and 33.54 mcsf, assemblages are dominated by *Acarinina* (50-85%) and *Morozovella* (2-20%), which are represented by species such as *A. esnaensis*, *A. alticonica*, *M. lensiformis*, and *M. marginodentata* (**Plate 3.1-3.2**). Both acarininids and morozovellids display relatively good preservation, although morozovellids are often broken or “peeled”. In the upper part of the third interval, between 32.46 and 31.39 mcsf, *Praetenuitella* becomes more abundant (8-75%) than muricates (**Figure 3.4**).

Other species present throughout the third interval include: *Igorina lodoensis?* (0-2%), *Chiloguembelina crinita* (2-11%), and *Subbotina* spp. (0-3%).

Scarce planktic foraminifers are found in the fourth interval between 30.96 and 28.29 mccsf. Here, samples usually contain a few individuals of *A. soldadoensis*, *Praetenuitella* sp., small unidentifiable acarininids, and fragments of morozovellids (**Figure 3.4, Appendix B**). Planktic foraminifers disappear from the record above 28.29 mccsf.

The horizons separating the above intervals correspond to the PETM (54.48 – 52.95 mccsf), H1 event (35.51 – 35.40 mccsf), and I1 event (31.48 – 30.96 mccsf). Carbonate dissolution is much more pronounced within these horizons (Leon-Rodriguez and Dickens, 2010; Appendix B).

3.4.2. Mass and Component Accumulation Rates

3.4.2.1. Carbonate MAR

Carbonate MAR records have been generated using both sedimentation rate approaches (**Figure 3.5**). Distinctive changes mark both records.

The LSR approach indicates a series of broad steps separated by extreme lows across the hyperthermals. Carbonate MARs before the PETM average 0.35 g/cm²/kyr, but drop to ~ 0.03 g/cm²/kyr at the PETM. A maximum occurs within the first 2 m above the PETM (up to 0.56 g/cm²/kyr). From this peak to H1, average rates are ~0.49 g/cm²/kyr. During H1, carbonate MAR declines to ~ 0.11 g/cm²/kyr. Rates increase again with several meters above this interval, to ~0.56

g/cm²/kyr. Another major drop in the carbonate MAR (to 0.02 g/cm²/kyr) happens at I1, which is followed by a slight recovery (~0.07 g/cm²/kyr). The K/X event is characterized by no carbonate accumulation (~0.00 g/cm²/kyr), which is followed by a subtle increase (~0.11 g/cm²/kyr) before the end of Unit II.

The SSR approach gives a smoother curve. An obvious difference is the relatively lower carbonate MARs between H-1 and I1 using the SSR. Overall, however, the two approaches yield similar curves, suggesting that primary features in accumulation records are independent of the specific method for estimating sedimentation rate.

3.4.2.2. Fish Debris Accumulation Rate (FDAR)

Fish debris counted in this study includes fish teeth, otoliths and phosphatic bone debris. As for carbonate MARs, both LSR and SSR approaches give similar FDAR records (**Figure 3.5**). We suggest two general depth intervals with distinct characteristics, and these are separated by the PETM. In the lower one (between 57.81 and 54.48 mccsf), FDARs vary from ~0.11 to 1.3 indiv/cm²/kyr. In the upper one (between 52.95 and 27.60 ccsf), FDAR values are generally <1 indiv/cm²/kyr. However, within this second interval, FDARs reach a maximum just before I1. FDARs are very low (~0.00 indiv/cm²/kyr) between 27.60 and 20.73 mccsf.

3.4.2.3. Benthic Foraminiferal Accumulation Rate (BFAR)

Benthic foraminifers are usually present in Unit II samples, and preservation ranges from very good to poor. The BFAR records can be subdivided into two main

intervals, separated by the PETM horizon, where benthic foraminifers become scarce ($< 0.5 \text{ indiv/cm}^2/\text{kyr}$) (**Figure 3.5**).

Within the lower interval, BFARs average around $31 \text{ indiv/cm}^2/\text{kyr}$ (LSR) and $20 \text{ indiv/cm}^2/\text{kyr}$ (SSR). By contrast, the upper interval has lower rates, around $8 \text{ indiv/cm}^2/\text{kyr}$ (LSR) or $9 \text{ indiv/cm}^2/\text{kyr}$ (SSR). These average BFARs above the PETM have high variance amongst samples ($0 \text{ to } 40 \text{ indiv/cm}^2/\text{kyr}$). A rapid increase occurs just above the PETM (up to $20 \text{ indiv/cm}^2/\text{kyr}$). We also observe three horizons characterized by extremely low BFARs ($0 \text{ to } 2 \text{ indiv/cm}^2/\text{kyr}$) within the upper interval. These horizons coincide with the negative CIEs of the H1, I1, and K/X events. Furthermore, the upper interval has a horizon right below the I1 event (31.83 mccsf) that has exceptionally high BFARs ($114 \text{ indiv/cm}^2/\text{kyr}$, LSR; $51 \text{ indiv/cm}^2/\text{kyr}$, SSR).

3.4.2.4. Planktic Foraminiferal Accumulation Rate (PFAR)

Four broad depth intervals with distinct PFARs are identified in Unit II (**Figure 3.5**). Interval 1 ($57.81\text{-}54.48 \text{ mccsf}$) is characterized by relatively low PFARs ($\sim 10 \text{ indiv/cm}^2/\text{kyr}$). Interval 2a ($52.95\text{-}47.20 \text{ mccsf}$) displays generally higher, but widely varying accumulation rates ($\sim 0 \text{ to nearly } 64 \text{ indiv/cm}^2/\text{kyr}$). Interval 2b ($47.20\text{-}35.51 \text{ mccsf}$) is defined by generally low values ($< 11 \text{ indiv/cm}^2/\text{kyr}$). Interval 3 ($35.40\text{-}31.39 \text{ mccsf}$) shows relatively high and widely varying accumulation rates. Here, the range depends significantly on the sedimentation rate method used: $4 \text{ to } 76 \text{ indiv/cm}^2/\text{kyr}$ (LSR) and $2 \text{ to } 46 \text{ indiv/cm}^2/\text{kyr}$ (SSR). Interval 4 ($30.96\text{-}28.29 \text{ mccsf}$) is distinguished by very low PFARs ($\sim 0 \text{ to } 2 \text{ indiv/cm}^2/\text{kyr}$). The intervals are similar though not exactly the same as those defined by assemblages.

The horizons that correspond to the hyperthermals have very low to no planktic foraminifers. PFARs in these intervals are between ~ 0 and ~ 4 indiv/cm²/kyr (**Figure 3.5**).

In addition to determining bulk PFARs, we calculated rates for specific genera. The same four intervals described above appear in these records (**Figure 3.5**). Interval 1 is characterized by *Globanomalina* accumulation rates of <10 indiv/cm²/kyr and *Praetenuitella* rates of 1 to 3 indiv/cm²/kyr. Interval 2a shows rates as follows: *Acarinina* (0 to 45 indiv/cm²/kyr), *Morozovella* (~ 0 to 8 indiv/cm²/kyr), and *Praetenuitella*, *Chiloguembelina*, and *Subbotina* gr. (<1 indiv/cm²/kyr). Interval 2b is mostly characterized by low accumulation of acarininids and praetenuitellids (<7 indiv/cm²/kyr each). Interval 3 is interesting because of widely varying rates. *Acarinina* accumulation rates are initially high (15 to 45 indiv/cm²/kyr, LSR; 11 to 30 indiv/cm²/kyr, SSR) but drop at 32.77 mccsf (<12 indiv/cm²/kyr, LSR; <7 indiv/cm²/kyr, SSR); *Morozovella* and *Chiloguembelina* accumulation rates show similar trends, but remain below 5 indiv/cm²/kyr. By contrast, *Praetenuitella* displays an opposite trend. At 35.42 mccsf, accumulation rates of this genus are relatively low (<8 indiv/cm²/kyr, LSR; <5 indiv/cm²/kyr, SSR) but these rates increase at 33.23 mccsf (>19 indiv/cm²/kyr, LSR; >11 indiv/cm²/kyr, SSR). Interval 4 is characterized by very low rates of *Acarinina* and *Praetenuitella* (<0.5 indiv/cm²/kyr).

3.5. Discussion

3.5.1. Carbonate Accumulation at ODP Site 1215

Carbonate accumulation at Site 1215 likely expresses a complex depositional history that involves changes in location, water depth and ocean chemistry. During the late Paleocene, the site was located close to the crest of the East Pacific Rise, and beneath the northern fringe of the paleoequatorial zone (Lyle and Wilson, 2006; Leon-Rodriguez and Dickens, 2010). The site then subsided and propagated northwest away from the ridge axis through the Cenozoic. Superimposed on this “tectonic migration”, a series of lysocline and CCD fluctuations occurred during the early Paleogene (Leon-Rodriguez and Dickens, 2010). Previous work tried to reconstruct this history at Site 1215, but without an assessment of carbonate accumulation (Leon-Rodriguez and Dickens, 2010). We expand upon and support the earlier effort, proposing the following explanation for changes in carbonate accumulation.

Carbonate MARs were generally lower in the latest Paleocene (0.25 to 0.35 g/cm²/kyr) compared to the first ~1.8 Myr of the early Eocene (0.45 to 0.55 g/cm²/kyr from the end of the PETM to the H1 event). This is intriguing because, with constant oceanographic conditions, one would predict the opposite, given thermal subsidence of oceanic crust on the flank of a mid-ocean ridge. The simplest and most plausible explanation is that the lysocline and the CCD generally deepened from the latest Paleocene through the earliest Eocene (Leon-Rodriguez and Dickens, 2010). This is consistent with information at other sites in the Indian and Pacific Oceans (Hancock et al., 2007). Carbonate MARs generally declined from the H1 event (using SSR approach)

until ~51.5 Ma (**Figure 3.5**), when carbonate stopped accumulating at the paleo-location of Site 1215. This interval is more complicated to interpret because the lysocline and CCD still may have deepened (Hancock et al., 2007), but not as fast as the site subsided. Records from multiple sites suggest that global CCD horizons began to rise rapidly sometime around 50-51.5 Ma (Rea and Lyle, 2005; Hancock et al., 2007), although this cannot be deciphered from Site 1215 records alone.

Carbonate accumulation rates surrounding the PETM exhibit important changes. The boundary itself is marked by strong carbonate dissolution, where carbonate MARs drop from ~0.35 to 0.06 g/cm²/kyr. However, values rise to 0.56 g/cm²/kyr afterward, or 40% greater than before the event. Major carbonate dissolution overlain by enhanced carbonate preservation (a “carbonate overshoot”) have been documented across the same general time interval in cores from the Atlantic Ocean, namely at ODP Sites 690 and 1262 (Kelly et al., 2010). Geochemical models predict this sedimentary response during and after massive CO₂ addition to the ocean and atmosphere (Dickens, 2000; Kump et al., 2009).

The H1 and I1 events are characterized by carbonate MAR declines to ~0.11 g/cm²/kyr and 0.06 g/cm²/kyr, respectively. Another carbonate “overshoot” appears above H1, as carbonate MARs are 0.39 (LSR) to 0.49 (SSR) g/cm²/kyr before the event, and 0.35 to 0.56 g/cm²/kyr after the event. However, such an “overshoot” is not obvious at Site 1215 following the I1 or K/X events. In the first case, carbonate MARs decrease from 0.25 (SSR) to 0.53 (LSR) g/cm²/kyr before the event to 0.08 (LSR) to 0.13 g/cm²/kyr (SSR) after the event. The overall low carbonate MARs during and after the I1 and K/X events may reflect a combination of factors. First, the seafloor at Site 1215 was

probably very near the CCD by this time, given long-term subsidence and variations in the CCD. Second, both events may have been associated with smaller carbon inputs than at the start of PETM and H1.

3.5.2. Planktic Foraminiferal Preservation

The quality of preservation and abundance of planktic foraminifers at Site 1215 is significantly lower (Appendix A) than that at time correlative sites in the North Pacific, such as at Allison Guyot or Shatsky Rise (Bralower et al., 1995; Petrizzo, 2007; Petrizzo et al., 2008). For example, at ODP sites 1209 and 1210 to the northwest on Shatsky Rise, the number of planktic foraminifers can exceed 10,000 specimens/g of sediment within and after the PETM; by contrast, at Site 1215, the number never exceeds 300 specimens on such a mass-normalized basis (Appendix A). There has been a latitudinal difference between the sites since emplacement of basement; nonetheless, the primary reason for the two or three orders of magnitude discrepancy in foraminiferal test abundance was likely water depth. During most of the late Paleocene and early Eocene, cored sites on Shatsky Rise were at a paleodepth of between 2,000 m and 2,500 m (Shipboard Scientific Party, 2002b) and probably above or in the uppermost part of the lysocline (Hancock and Dickens, 2005), while Site 1215 subsided from >2,700 m, or from below the lysocline to below the CCD (Leon-Rodriguez and Dickens, 2010).

Any analysis of foraminiferal records within Unit II at Site 1215 becomes complex because the assemblages, both planktic and benthic, are almost assuredly modified by dissolution such that they represent a skewed view of original abundance and diversity. Leon-Rodriguez and Dickens (2010) partially addressed this problem in

their previous work, and concluded that carbonate dissolution was particularly pronounced during the PETM, H1, I1, and K events, which display low numbers of planktic foraminiferal tests, low P/B ratios, and low percentages of foraminiferal fragments.

Experimental studies demonstrate that planktic and benthic foraminifer assemblages can be affected strongly by selective dissolution (Bé et al., 1975; Hecht et al., 1975; Thunell and Honjo, 1981; Nguyen et al., 2009). Waters corrosive to carbonate dissolve foraminifer tests, so they become weaker and prone to fragmentation. Additionally, it is known that benthic foraminifers are more resistant to dissolution than planktic foraminifers, and that planktic foraminifers exhibit differential corrosion (Bé et al., 1975; Hecht et al., 1975; Thunell and Honjo, 1981). Recently, dissolution experiments have been conducted on foraminiferal assemblages from upper Paleocene and lower Eocene sedimentary rocks from Egypt (Nguyen et al., 2009). This study concluded that, among planktic foraminifers, the genera *Acarinina* and *Morozovella* are more resistant to dissolution than *Subbotina*. Similar inferences were made from analyses of planktic foraminifer counts from late Paleocene and early Eocene sediment at ODP Sites 1209 and 1210 (Petrizzo, 2007; Petrizzo et al., 2008). These works invite an interesting question: do planktic foraminiferal assemblages and accumulation rates across Unit II at Site 1215 suggest changes in carbonate dissolution and preservation?

Samples from horizons with low carbonate MARs (i.e., the PETM, H1, and I1) have a few specimens of *Acarinina* and *Praetenuitella* (**Figure 3.5; Appendix B**). By contrast, samples from intervals with higher carbonate MARs, particularly the

carbonate “overshoots” after these events, show high abundances of *Acarinina*, *Praetenuitella*, and *Morozovella*. Higher diversity, better preservation, bigger size tests, higher relative abundances, and a greater number of planktic foraminifers are also observed in these intervals of relatively high carbonate accumulation.

Globanomalina, *Chiloguembelina*, *Igorina*, and *Subbotina* abundances are always poor throughout Unit II; they only increase subtly after the PETM, but not after other CIEs at Site 1215 (**Figures 3.4 and 3.5**). A straightforward explanation is that carbonate dissolution preferentially affects all planktic foraminifera, particularly these genera. This is consistent with experimental results of Nguyen et al. (2009). In other words, sediment deposition at Site 1215 began beneath the lysocline (Leon-Rodriguez and Dickens, 2010), so that dissolution susceptible genera (e.g., *Subbotina* and *Globanomalina*) have a very low abundance in Unit II.

Cross-plots showing absolute and relative abundance of planktic foraminifers against carbonate content also support this interpretation (**Figures 3.6a and 3.6b**). Samples with >50% carbonate content display greater numbers of genera and specimens, with *Acarinina* and *Praetenuitella* generally more abundant than *Morozovella*, *Globanomalina*, *Igorina*, *Chiloguembelina*, and *Subbotina*. Samples with <50% carbonate content have lower numbers of genera and specimens, with *Acarinina* and *Praetenuitella* as the predominant genera.

The small-size (~100 μm) specimens of the proposed planktic foraminifer genus *Praetenuitella* (**Plate 3.3**) have not been described formally in previous work (Leon-Rodriguez et al., Submitted). Specimens are found along with *Acarinina* in

samples spanning the PETM, H1, and I1 events; they also are found in samples with low carbonate content toward the top of Unit II, where acarininids become scarce. Despite their small size, *Praetenuitella* may be especially resistant to carbonate dissolution. They may have become an important component of assemblages at Site 1215 for this very reason.

3.5.3. Evidence for Paleoenvironmental Changes?

Selective dissolution has very likely biased early Paleogene foraminiferal assemblages at Site 1215. A few paleoecological interpretations can be offered given the array of chemical and micropaleontological records, but these must be qualified; indeed, they highlight potential “pitfalls” when interpreting early Paleogene foraminiferal records.

Planktic foraminiferal assemblages deposited in the latest Paleocene at Site 1215 contrast markedly from those of the earliest Eocene (**Figures 3.4 and 3.5**). The former contain relatively more *Globanomalina* (smooth-walled taxon), *Praetenuitella* (macro to microperforate taxon), and *Subbotina* (spinose taxon) than contemporaneous *Acarinina* and *Morozovella* (muricate symbiont-bearing taxa). *Globanomalina* probably lived in deep habitats and cooler waters along with *Parasubbotina* and *Subbotina* (Boersma and Premoli-Silva, 1983; Olsson et al., 1999; Luciani et al., 2007). By contrast, *Acarinina* and *Morozovella* likely were specialized surface water dwellers with a preference for warm water (e.g., (Boersma and Premoli-Silva, 1983; Olsson et al., 1999; Pearson et al., 2001; Sexton, 2005; Luciani et al., 2007)). It is possible that waters overlying Site 1215 were slightly cooler than surrounding equatorial regions during the latest Paleocene, which

would have precluded high abundances of warm water dwellers. The $\delta^{18}\text{O}_{\text{bulk}}$ record at Site 1215 (**Figures 3.4 and 3.5**) shows maximum values between 55.6 and 56.0 Ma, and this may support relatively cool sea-surface temperatures.

In the late Paleocene, BFARs were relatively high. However, just prior to the PETM, they progressively drop. Assuming the BFAR record serves as a proxy for paleoproductivity (Herguera and Berger, 1991; Herguera, 1992), this could indicate a drop in primary production before the PETM. However, it could also suggest that significant carbonate dissolution began before the PETM (Leon-Rodriguez and Dickens, 2010). In either case, the interpretations would support the overall notion that paleoenvironmental changes began before the PETM, as argued from records at other locations (Luciani et al., 2007; Sluijs et al., 2007b).

The onset of the PETM at Site 1215 is characterized by a significant drop in the $\delta^{18}\text{O}$ of bulk carbonate (**Figure 3.5**), presumably because of major rise in sea-surface temperature, as documented in many locations (Kennett and Stott, 1991; Zachos et al., 2003; Sluijs et al., 2007a). The lack of planktic foraminifers across the PETM, because of carbonate dissolution, prevents us from assessing any potential response of planktic foraminifers during the environmental perturbation. However, substantial changes within the upper water column most probably occurred. The inference comes from the planktic foraminifera assemblages preserved immediately above the PETM, which are characterized by abundant warm-water genera (e.g., *Acarinina*, *Morozovella*) known for harboring algal symbionts in oligotrophic environments (Kelly et al., 1996; Norris, 1996; Kelly et al., 1998; Kelly, 2002; Luciani et al., 2007). The assemblage change probably supersedes effects of dissolution because *Globanomalina*, a dweller of cooler water found

in uppermost Paleocene assemblages, becomes scarce above the PETM. If the change was caused solely by dissolution, one would predict abundant *Acarinina* and *Morozovella* tests in samples below the PETM, which is not the case.

Benthic foraminifers experienced a major extinction during the PETM (Kennett and Stott, 1991; Thomas and Shackleton, 1996; Thomas, 1998). Although BFARs rose within 200 kyr after the PETM (~15 indiv/cm²/kyr; **Figure 3.5**), they did not reach levels before this event (20 - 30 indiv/cm²/kyr). Other analyses of benthic foraminiferal assemblages at Site 1215 (Shipboard Scientific Party, 2002c; Nomura and Takata, 2005) further indicate that diversity decreased after the PETM. Interestingly, certain species (e.g., *Nuttallides truempyi*, *Abyssamina inflata*, and *Abyssamina poagi*) became more abundant. The high abundance of *N. truempyi* has been interpreted as an indicator of oligotrophy (Thomas, 1998; 2007), and this may imply that, at the location of Site 1215, the earliest Eocene was a time of low food availability at the seafloor.

Following the PETM and the ensuing recovery (54.7 – 53.8 Ma), planktic foraminifers fail to show high accumulation rates, despite relatively high carbonate accumulation rates (**Figure 3.5**). Correlative records at Shatsky Rise (Biozones E3-E4) with fairly broader sampling resolution also show relatively lower abundances of *Acarinina*, *Morozovella*, and *Subbotina*, low species diversity, and fairly high planktic foraminiferal fragmentation (Hancock and Dickens, 2005; Petrizzo, 2007; Petrizzo et al., 2008). Thus carbonate dissolution likely controlled the preservation of the planktic assemblages in all of these pelagic locations at least after the post-PETM carbonate “overshoot” until the H1 event. Nonetheless, low PFARs, BFARs, FDARs, and low diversity benthic foraminiferal assemblages (Nomura and Takata, 2005) at Site 1215 also

provide supporting evidence that ecological conditions likely remained oligotrophic throughout this time.

The abundances of *Acarinina*, *Morozovella*, *Praetenuitella*, and *Chiloguembelina* increase following H1. While this may indicate enhanced preservation (Leon-Rodriguez and Dickens, 2010), paleoenvironmental conditions also may have favored taxa adapted to warm and oligotrophic surface waters (*Acarinina* and *Morozovella*) and to accompanying intermediate waters (*Chiloguembelina*, *Praetenuitella*). Certainly, some authors have suggested that ocean warming facilitated the supremacy of *Acarinina* and *Morozovella* during the PETM (Luciani et al., 2007; Petrizzo, 2007; Petrizzo et al., 2008).

Muricates, mostly acarininids, are dominant during the carbonate “overshoot” following H1; however, they diminish before the I1 event. This is opposite to the trend of *Praetenuitella* (Figures 3.4 and 3.5). Despite enhanced dissolution, changes in surface water temperature, nutrient levels, or both may have caused this transition from typical warm-and-oligotrophic-water dwellers (acarininids and morozovellids) to presumably cooler-water taxa (praetenuitellids). This may be supported by maxima in BFARs and FDARs.

3.5.4. A Cooling Trend with Global Warming Episodes?

The bulk sediment oxygen isotope record at Site 1215 suggests rapid increases of sea-surface temperature at the PETM (~55.5 Ma), H1 (~53.7 Ma), I1 (~53.2 Ma) and K (~52.5 Ma) events (Figure 3.4). These “hyperthermals” (Nicolo et al., 2007; Sluijs et al., 2007a; Sluijs et al., 2009; Stap et al., 2009; Leon-Rodriguez and Dickens, 2010; Stap et

al., 2010) are generally thought to have occurred during a time interval characterized by long-term warming (Zachos et al., 2008).

A comparison of early Eocene bulk carbonate $\delta^{18}\text{O}$ records at Site 1262 on Walvis Ridge in the south-central Atlantic (Zachos et al., 2010) and at Site 1215 (**Figure 3.7**) shows two notable differences. First, there is a $>0.6\text{‰}$ offset in $\delta^{18}\text{O}$ between the locations. Second, the records at Walvis Ridge remain low after the PETM, while that at Site 1215 generally increases by 0.6‰ (**Figure 3.7**). This may reflect the past locations of the sites. Paleo-reconstructions indicate that Site 1262 moved northwest and towards warmer surface waters between 56 and 52 Ma (O'Connor and Duncan, 1990; Bowles, 2006). By contrast, Site 1215 migrated northwest from about 11°N and at the northern fringe of equatorial upwelling to about 14°N during this time (Huber, 2002; Leon-Rodriguez and Dickens, 2010).

3.6. Summary and Conclusions

The sedimentary record at Site 1215 contains a 40 m thick carbonate-rich unit that was deposited on the flank of a spreading ridge during the early Paleogene. Within this unit are found four short intervals characterized by low carbonate content, prominent carbon isotope excursions (CIEs), and negative $\delta^{18}\text{O}$ excursions. These intervals correspond to the PETM (55.5 Ma), H1 (53.7 Ma), I1 (53.2 Ma), and K (52.5 Ma) hyperthermal events.

Carbonate MARs were low, but fairly similar for much of the unit. Because deposition occurred as the site was subsiding, this suggests a long-term drop in the

lysocline during the early Paleogene. Very low carbonate MARs, BFARs, and PFARs occur across the hyperthermals, which is consistent with results from carbon cycle modeling when massive amounts of carbon are rapidly added to the ocean and carbonate dissolves on the seafloor (Dickens, 2000; Kump et al., 2009). Increases in carbonate MARs, PFARs and BFARs mark the ~200 kyr of sediment deposited after the PETM, H1, and I1 events. These “carbonate overshoots” are also predicted by models, which render lysocline “over-compensations” after rapid carbon injections, ultimately because of greater weathering on continents.

Detailed analysis of planktic foraminiferal assemblages suggests that suspected lysocline changes strongly influence accumulation of carbonate microfossils. More specifically, some genera appear more resistant to carbonate dissolution than other genera. Accumulation rates and abundances *Acarinina* are relatively high throughout most of the unit; *Praetenuitella* also appears in many samples. By contrast, *Morozovella*, *Chiloguembelina*, *Globanomalina*, *Igorina*, and *Subbotina* are only found in samples with high carbonate content (> 50%). These observations confirm and expand upon recent ideas regarding the impact of dissolution on early Paleogene planktic foraminiferal assemblages (Nguyen et al., 2009). Thick walled and relatively robust *Acarinina* tests seem to be particularly resistant to carbonate dissolution. Despite their small size, tests of the genus *Praetenuitella* appear fairly resilient to dissolution.

Paleoenvironmental interpretations from the carbonate-rich unit at Site 1215 are difficult to make on the basis of foraminifera alone. Sea-surface temperatures seem to have been cooler in the late Paleocene compared to the early Eocene. This is based on the relatively high abundances of cold and intermediate-water dwellers (*Globanomalina* and

Praetenuitella), but also on more positive $\delta^{18}\text{O}$ values in bulk carbonate. However, the very latest Paleocene (~150 kyr prior the onset of the PETM) is characterized a decrease of the PFARs, BFARs, and FDARs and by a negative excursion in $\delta^{18}\text{O}$. This may indicate an initial rise in sea surface temperature slightly before the onset of the PETM, as suggested by other workers (e.g., Luciani et al., 2007; Sluijs et al., 2007c). Furthermore, the earliest Eocene is distinguished by relatively high abundances of *Acarinina* and *Morozovella*, which are known for being highly specialized taxa (symbiont-bearing) that thrived under warm and oligotrophic conditions. These low-productivity conditions may explain the relatively low BFARs, the low diversity of benthic foraminifers, and the higher abundances of *Nuttallides truempyi*.

A progressive influence of *Praetenuitella* and *Chiloguembelina* as well as a general, drop in $\delta^{18}\text{O}$ characterize sediment between the PETM and the X events. Although the earliest Eocene was significantly warmer than the late Paleocene, sea surface temperatures above Site 1215 may have declined across the early Eocene. This may reflect northward migration of the site. However, short temperature rises appear to mark the CIE PETM, H1, I1, and K hyperthermals. This is evidenced by the presence of warm water species like *Acarinina* and *Morozovella* immediately after the PETM and H1.

3.7. Acknowledgments

We thank the scientists and staff of the Integrated Ocean Drilling Program's (IODP) Gulf Coast Repository (GCR) at College Station for sample collection. Glen

Snyder aided with SEM images, which were taken in conjunction with the Rice Shared Equipment Authority. This study was partially supported by the Geological Society of America Student Grant. Kind regards to Francois Paquay, Benjamin Slotnick, and Fermin Fernandez-Ibanez for their valuable comments and corrections to the initial drafts of this document.

3.8. Appendix 1: Taxonomic List

Acarinina alticonica? (El Naggar) = *Globorotalia africana* El Naggar, 1996

Acarinina angulosa (Bolli) = *Globigerina soldadoensis angulosa* Bolli, 1957

Acarinina coalingensis (Cushman and Hanna) = *Globigerina coalingensis* Cushman and Hanna, 1927

Acarinina decepta? (Martin) = *Globorotalia (Acarinina) decepta* (Martin) as in Blow, 1979

Acarinina esnaensis (Le Roy) = *Globigerina esnaensis* Le Roy, 1953

Acarinina interposita Subbotina, 1953

Acarinina mckannai (White) = *Globigerina mckannai* White, 1928

Acarinina nitida (Martin) = *Globigerina nitida* Martin, 1943

Acarinina pseudotopilensis Subbotina, 1953

Acarinina soldadoensis (Bronnimann) = *Globigerina soldadoensis* Bronnimann, 1952

Chiloguembelina crinita (Glaessner) = *Guembelina crinita* Glaessner, 1937

Chiloguembelina trinitatensis (Cushman and Renz) = *Guembelina trinitatensis* Cushman and Renz, 1942

Globanomalina imitata (Subbotina) = *Globorotalia imitata* Subbotina, 1953

Globanomalina planoconica (Subbotina) = *Globorotalia planoconica* Subbotina, 1953

Globanomalina compressa (Plummer) = *Globigerina compressa* Plummer, 1926

Globanomalina pseudomenardii (Bolli) = *Globorotalia pseudomenardii* Bolli, 1957

Globorotaloides quadrocameratus = *Globorotaloides quadrocameratus* Olsson, Pearson, and Huber, 2006

Igorina lodoensis (Mallory) = *Globorotalia broedermanni* Cushman and Bermúdez var. *lodoensis* Mallory, 1959

Igorina tadjikistanensis (Bykova) = *Acarinina tadjikistanensis* Bykova, 1953

Morozovella acuta (Toulmin) = *Globorotalia wilcoxensis* Cushman and Ponton var. *acuta* Toulmin, 1941

Morozovella aequa (Cushman and Renz) = *Globorotalia crassata* (Cushman) var. *aequa* Cushman and Renz 1942

Morozovella formosa (Bolli) = *Globorotalia formosa formosa* Bolli 1957

Morozovella gracilis (Bolli) = *Globorotalia formosa gracilis* Bolli, 1957

Morozovella lensiformis (Subbotina) = *Globorotalia lensiformis* Subbotina, 1953

Morozovella marginodentata (Subbotina) = *Globorotalia marginodentata* Subbotina, 1953

Morozovella passionensis (Bermúdez) = *Pseudogloborotalia passionensis* Bermúdez, 1961

Morozovella subbotinae (Morozova) = *Globorotalia subbotinae* Morozova, 1939

Morozovella velascoensis (Cushman) = *Pulvinulina velascoensis* Cushman, 1925

Paragloborotalia griffinoides Olsson and Pearson, 2006

Parasubbotina varianta (Subbotina) = *Globigerina varianta* Subbotina, 1953

Subbotina eocaena (Guembel) = *Globigerina eocaena* Guembel, 1868

Subbotina patagonica (Todd and Kniker) = *Globigerina patagonica* Todd and Kniker,
1952

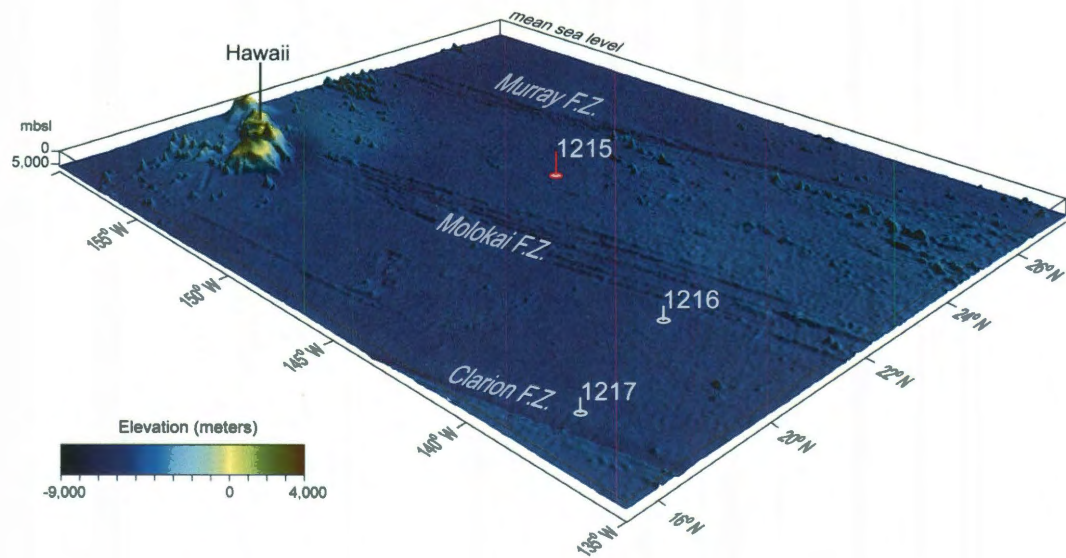


Figure 3.1 – Location of Site 1215 and other sites drilled by ODP Leg 199 (Shipboard Scientific Party, 2002a). Topography and bathymetry from Smith and Sandwell (1997).

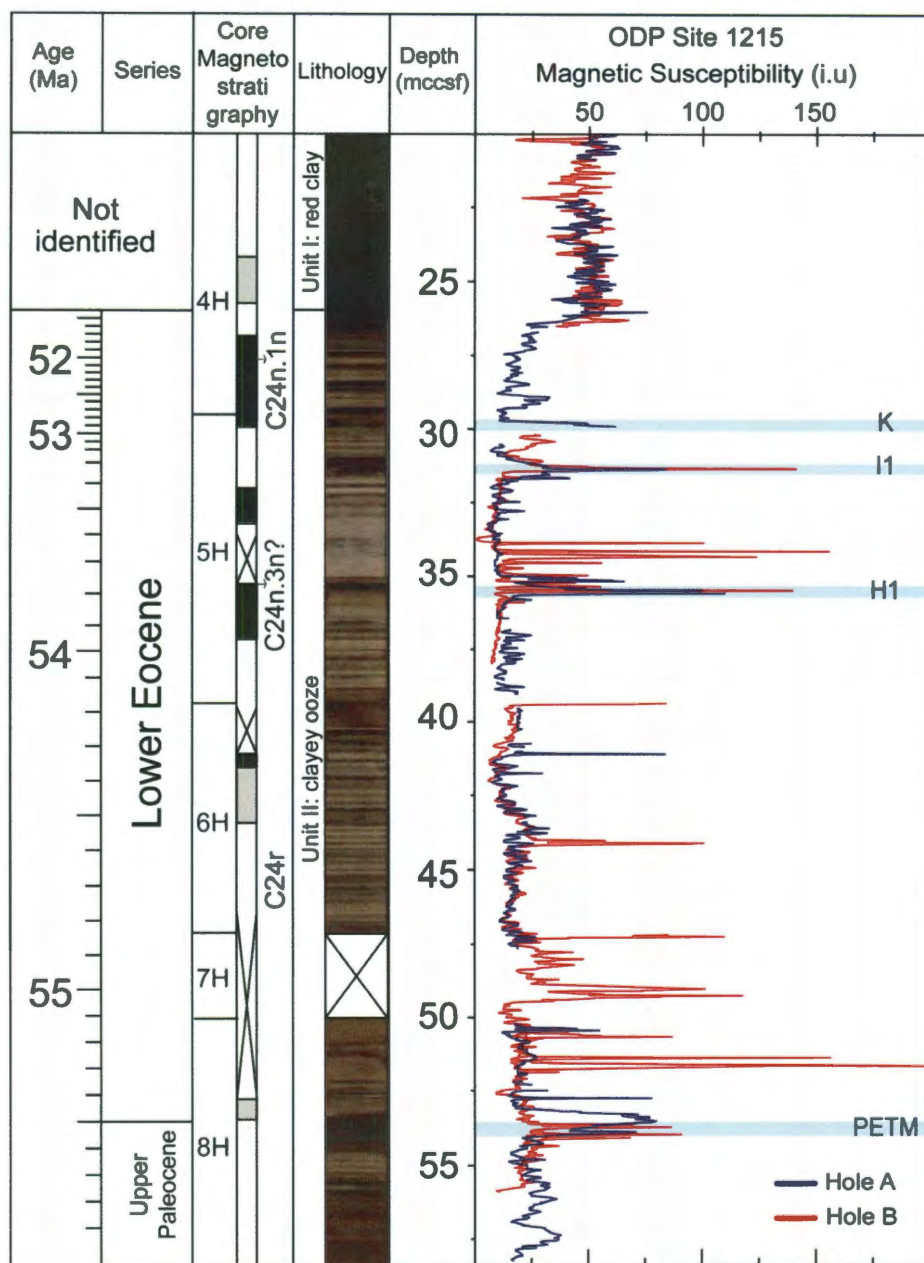


Figure 3.2 – ODP Site 1215 lithological record and splice using magnetic susceptibility from Holes A and B (Shipboard Scientific Party, 2002b). Gray shadow boxes: undefined magnetostratigraphic chron. Green rectangles: Position of the CIE events.

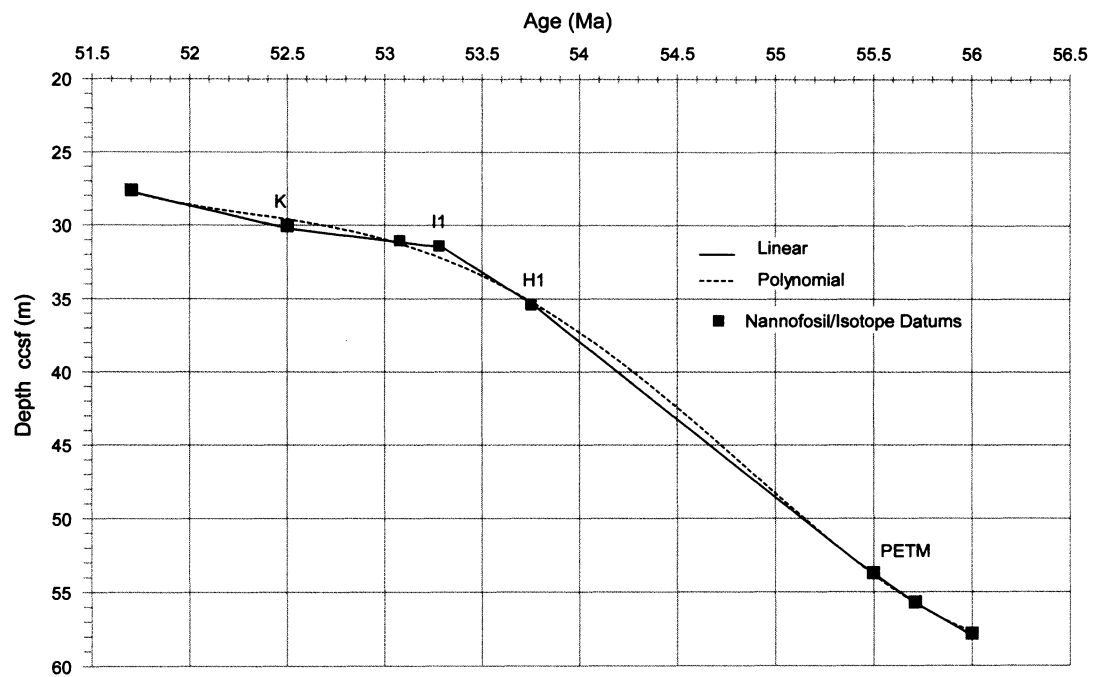


Figure 3.3 - Age model for ODP Site 1215. Linear and polynomial curves based on nannofossil and isotope datums as published by Leon-Rodriguez and Dickens (2010) and Zachos et al. (2010). Polynomial curve is defined by the equation: $y = -0.2873568482x^4 + 61.6037509296x^3 - 4949.6011766348x^2 + 176649.8791239090x - 2362980.8151503400$. Solid line corresponds to linear fit and dashed line corresponds to polynomial fit.

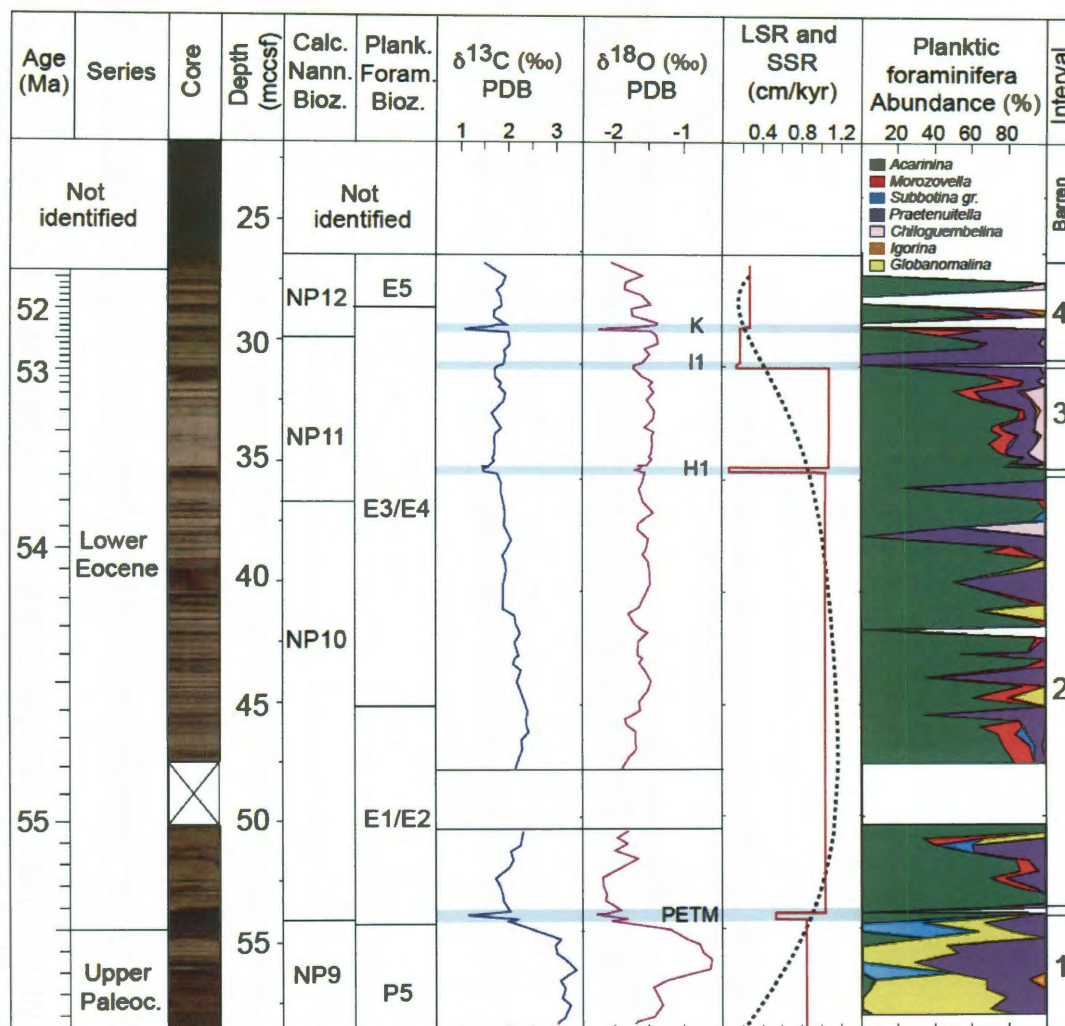


Figure 3.4 – Isotope stratigraphy, Linear Sedimentation Rate (LSR), Smooth Sedimentation Rate (SSR), and Relative abundances of planktic foraminifera at ODP Site 1215. Solid red line corresponds to LSR and dashed black line corresponds to SSR. Planktic foraminiferal zonation of Berggren and Pearson (2005); Calcareous nannofossil zonation scheme proposed by Martini (1971) as amended by Raffi et al. (2005). Biostratigraphic datums are available in Leon-Rodriguez and Dickens (2010).

Figure 3.5

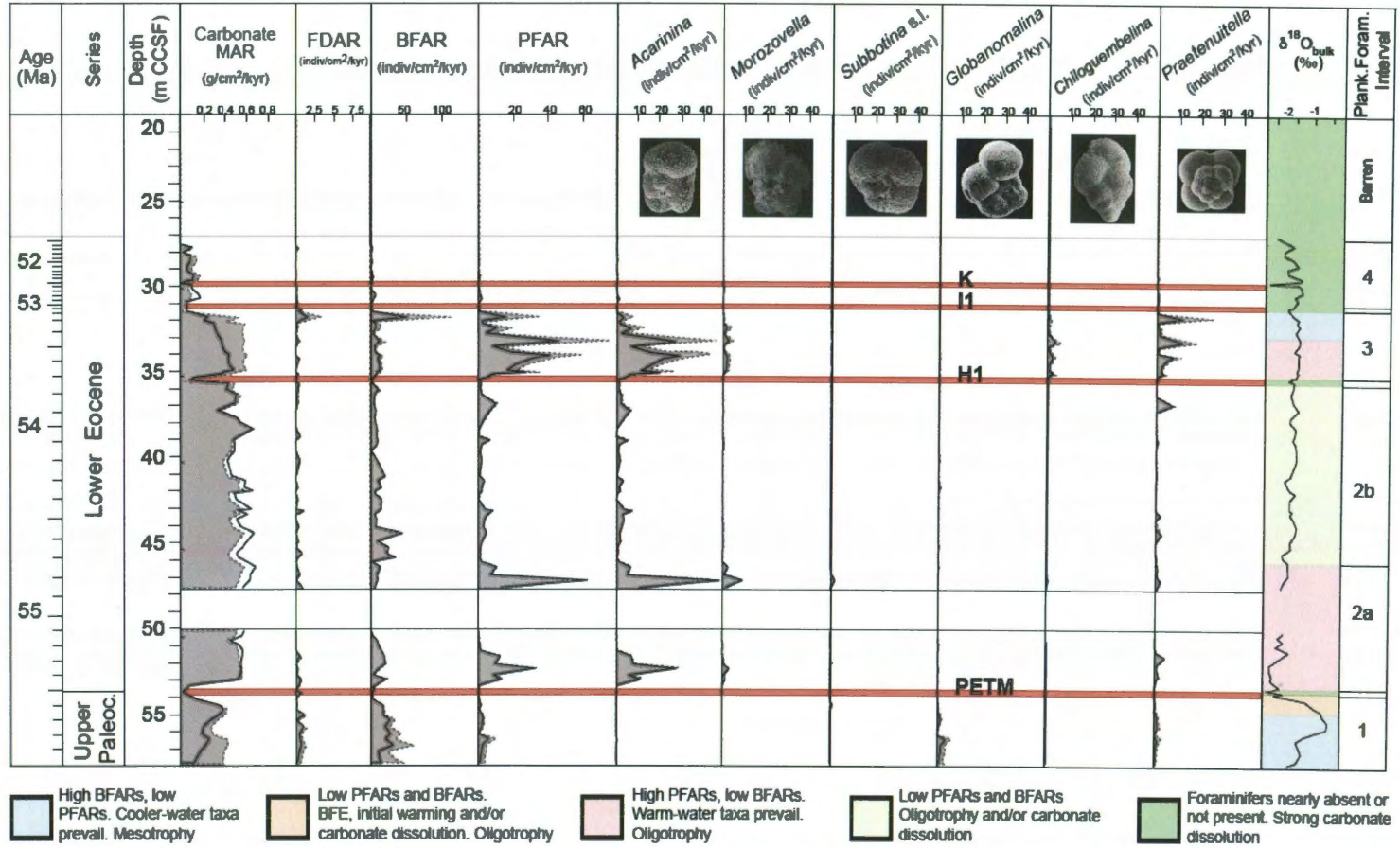


Figure 3.5 - Carbonate Mass Accumulation Rate (carbonate MAR), Fish Debris Accumulation Rate (FDAR), Benthic Foraminiferal Accumulation Rate (BFAR), Planktic Foraminiferal Accumulation Rate (PFAR), and accumulation rates for selected planktic foraminiferal genera at the ODP Site 1215. Color shaded areas correspond to outstanding features as interpreted from carbonate and/or genera records. Solid line with grey shaded area corresponds to accumulation rates calculated with LSR. Dashed line corresponds to accumulation rates calculated with SSR.

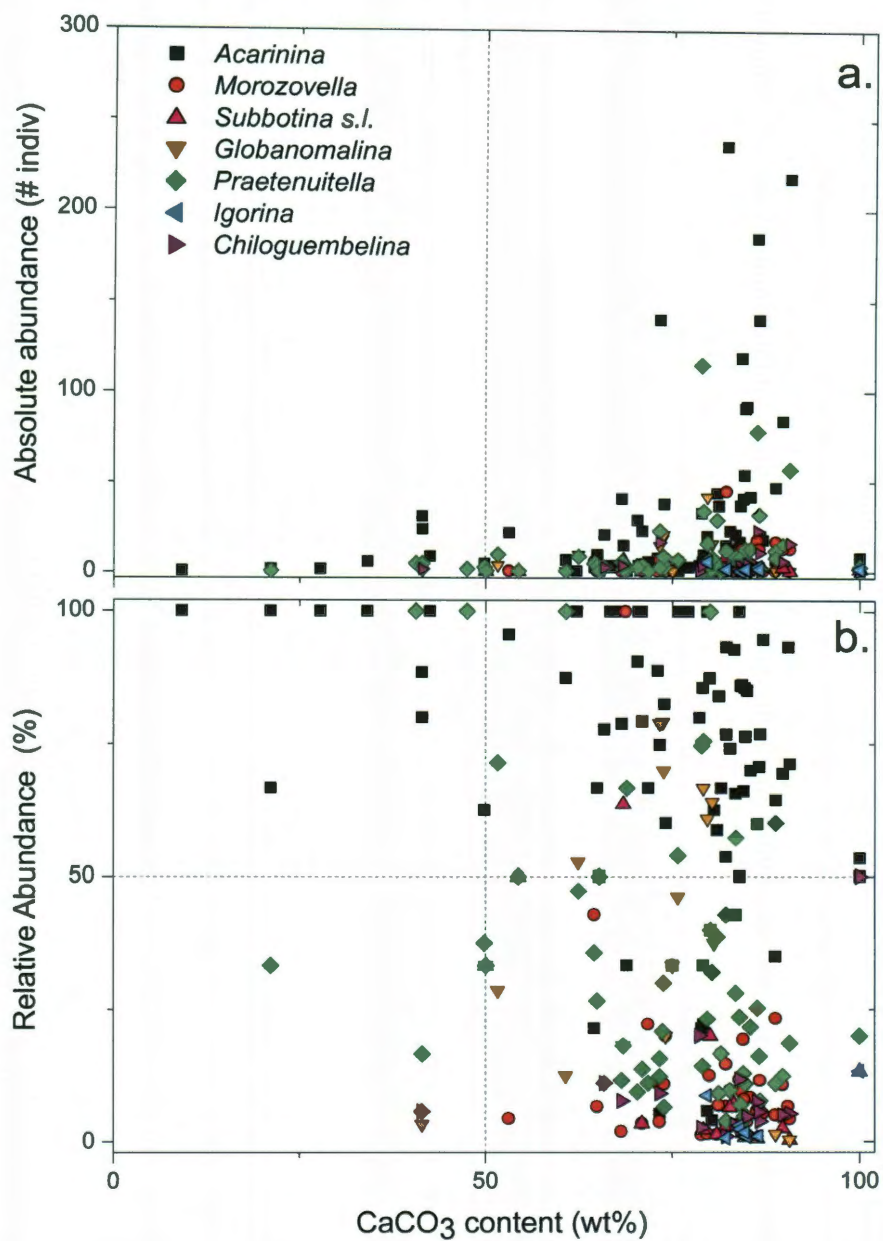


Figure 3.6 - Crossplots of (a) Carbonate content vs. absolute abundance of planktic foraminifera, and (b) Carbonate content vs. relative abundance of planktic foraminifera.

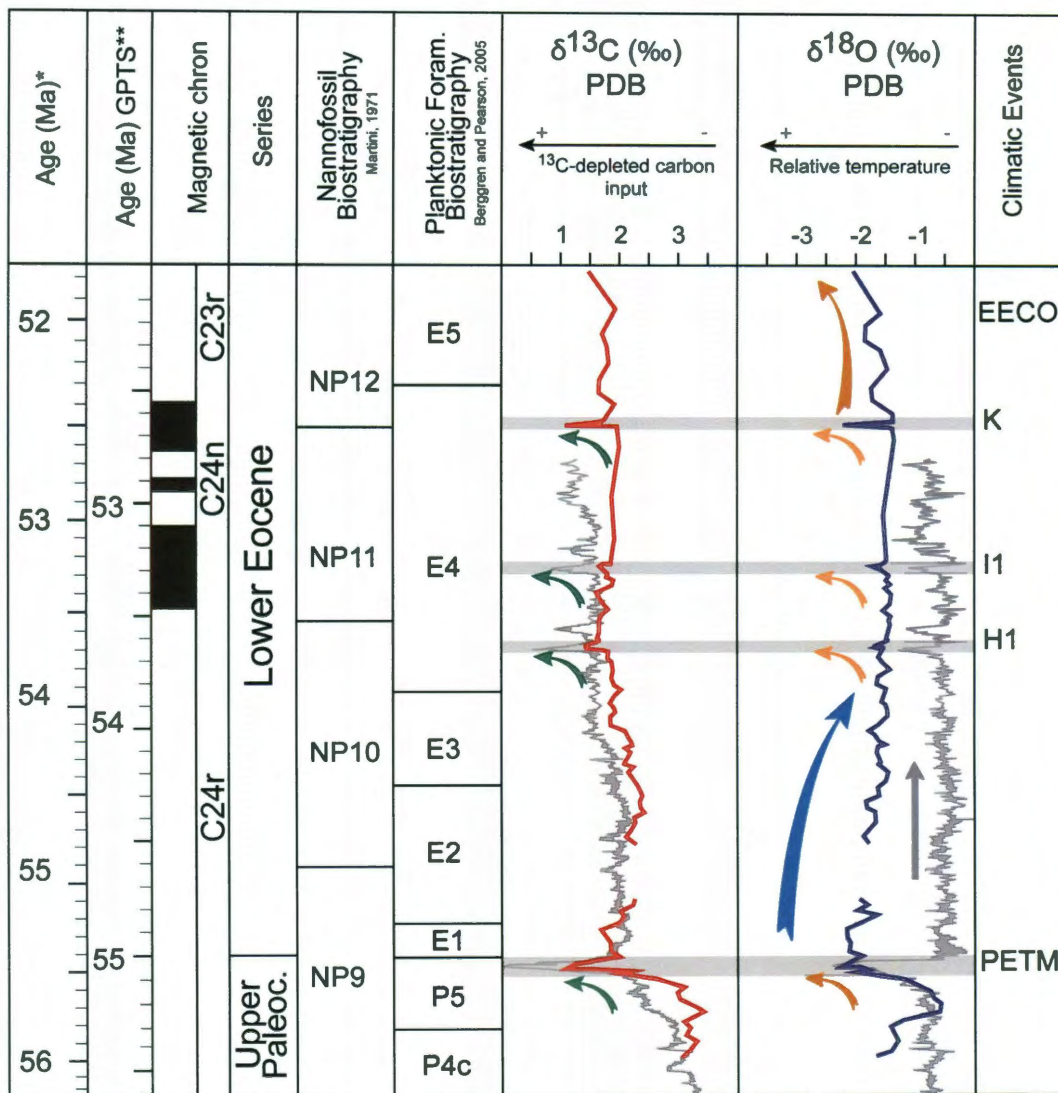


Figure 3.7 - Comparison of $\delta^{13}\text{C}_{\text{bulk}}$ and $\delta^{18}\text{O}_{\text{bulk}}$ records from the eastern equatorial Pacific Ocean, ODP Site 1215 (blue and red color) and the South Atlantic Ocean, ODP Site 1262 Walvis Ridge (in grey; taken from Zachos et al., 2010).

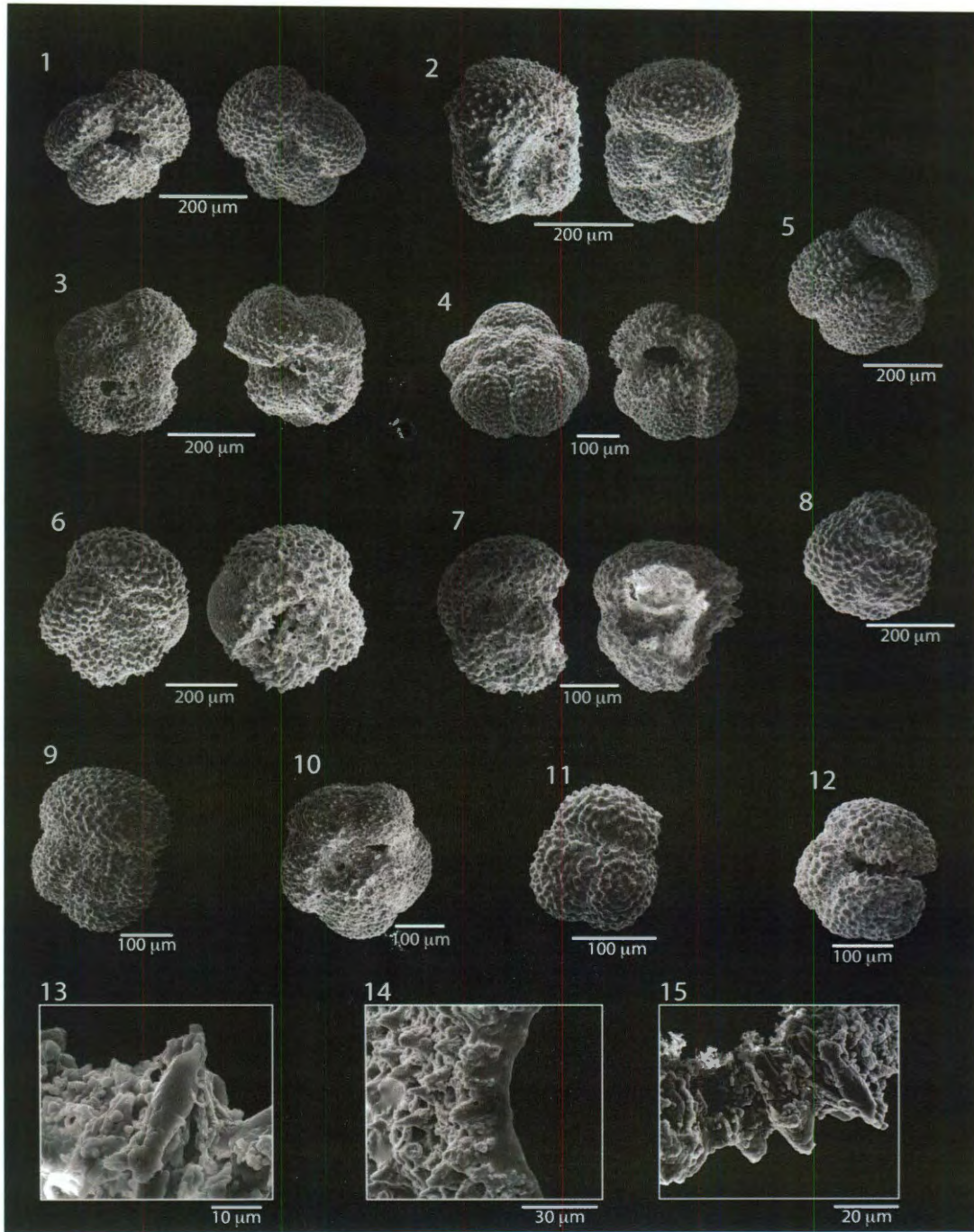


Plate 3.1

Plate 3.1 - Selected early Eocene acarininids from ODP Site 1215. 1. *Acarinina angulosa*, 2. *A. pseudotopilensis*, 3. *A. cf. esnehensis*, 4. *Acarinina* sp., 5. *A. soldadoensis*, 6. *Acarinina* sp. with bulla 7. *Acarinina* sp. partially fragmented, 8. *Acarinina* sp. small specimen, 9. *Acarinina coalingensis*, 10. *Acarinina cf. pentacamerata*, 11. *Acarinina coalingensis*, 11. *Acarinina cf. coalingensis* small specimen, 13-15. *Acarinina* spp. with partially dissolved chambers and pustules.

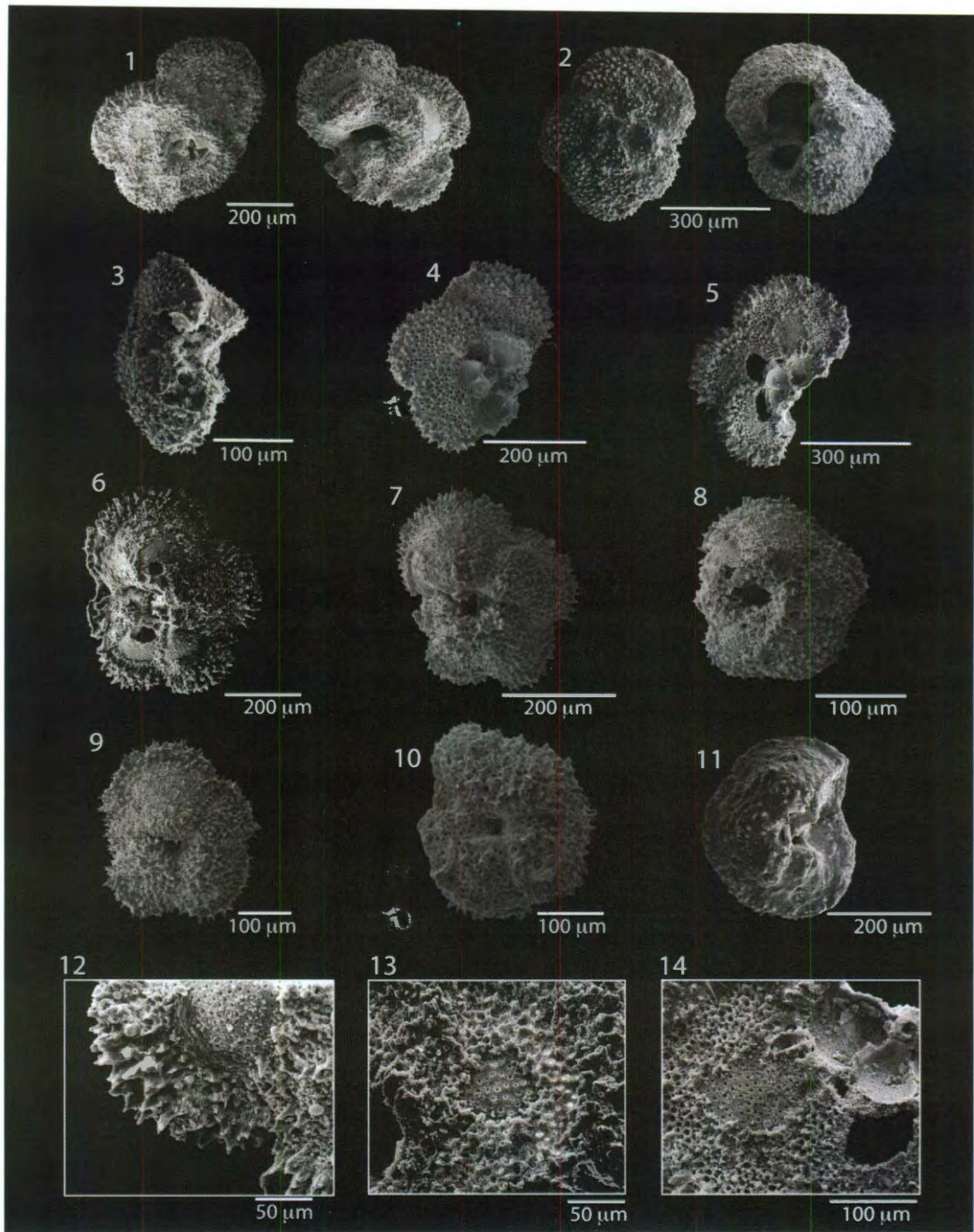


Plate 3.2

Plate 3.2 - Selected early Eocene morozovellids from ODP Site 1215. 1. *Morozovella subbotinae*, 2-5. *Morozovella* sp. with features of dissolution, 6-7. *Morozovella subbotinae/marginodentata* 8-10. *Morozovella* sp pustules and chambers partially dissolved, 11. *Morozovella acuta*, 12-14. Detail of “peeled-off” walls in *Morozovella* spp.

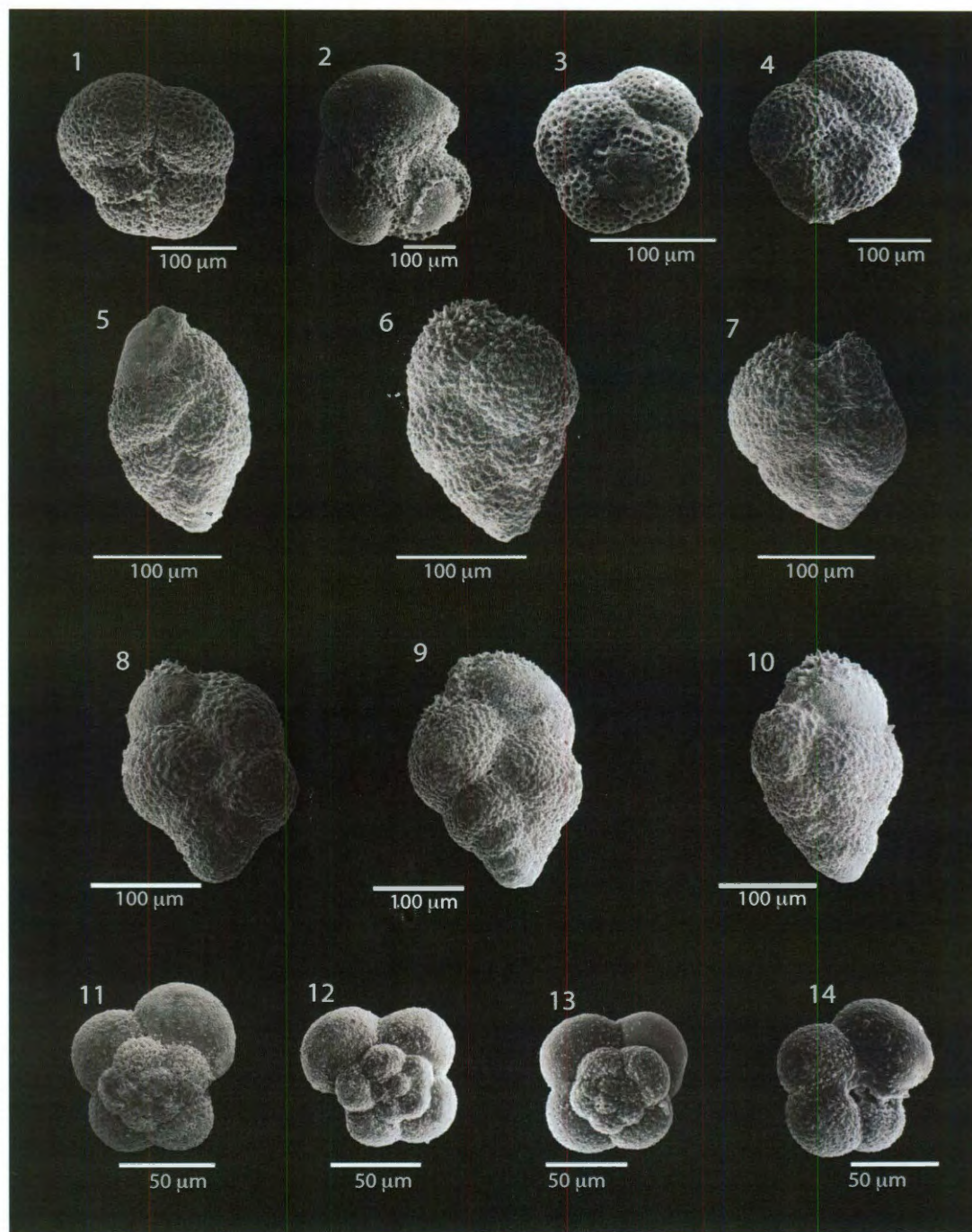


Plate 3.3

Plate 3.3 - Selected late Paleocene and early Eocene subbotinids, igorinids, chiloguembelinids, and tenuitellids from ODP Site 1215. 1. *Parasubbotina* sp., 2. *Subbotina* sp. test partially dissolved, 3-4., *Igorina tadjikistanensis*, 5. *Chiloguembelina* sp., 6-10. *Chiloguembelina crinita*, 11-14. *Praetenuitella* sp..

CIE Events	Age (Ma)	Depth (m ccsf)	$\delta^{13}\text{C}$ Excursion (‰)	$\delta^{18}\text{O}$ Excursion (‰)
K or X or ETM3	52.5	29. 90-29.78	From 1.98 to 1.02	From -1.40 to -2.23
I1	53.7	31.39-30.96	From 1.81 to 1.67	From -1.46 to -1.73
H1 or ETM2	53.2	35.51-35.40	From 1.81 to 1.42	From -1.57 to -1.70
PETM	55.5	54.48-52.95	From 3.10 to 1.08	From -0.62 to -2.26

Table 3.1 – CIE events at the ODP Site 1215. Data from Leon-Rodriguez and Dickens (2010).

***Praetenuitella antica* n. sp.:**
A Macro to microperforate Planktic
Foraminifer from the Lower to Middle
Eocene of the Equatorial Pacific Ocean

Lizette Leon-Rodriguez^{1,*}, R. Mark Leckie², and Gerald R. Dickens^{1,3}

¹Department of Earth Sciences, Rice University, MS-126 P.O. Box 1892, Houston TX,
77281-1892, USA

²Department of Geosciences, University of Massachusetts, 611 N. Pleasant St., 01003,
Amherst, MA, USA

³Institutionen för Geologiska Vetenskaper, Stockholms Universitet, 106 91 Stockholm,
Sweden

A manuscript to be submitted to:

Journal of Foraminiferal Research

November 15, 2011

ABSTRACT

We describe *Praetenuitella antica*, a newly identified species of planktic foraminifer that lived during the latest Paleocene to middle Eocene. It is reported after examining sediment at two deep-sea drilling sites in the eastern Pacific Ocean (ODP Site 1215 and IODP Site U1333). Specimens show characteristics of the genus *Praetenuitella* Li, which is resurrected and emended in this study. The new species has a monolamellar wall that is macroperforate and moderately pustulose in the earliest chambers, and is microperforate and sparsely pustulose in the latest chambers. Morphometric analysis shows that this species is very small (~100 μm maximum diameter), with 4 to 5 chambers in the last whorl that slowly increase in size. Intraspecific variability is low, although specimens occasionally have a kummerform last chamber. Considering possible phylogenetic relationships, the genus *Praetenuitella* is likely related to *Tenuitella* suggesting that this plexus is 20 Myr older than previously recorded. Stable carbon isotope data on *Praetenuitella antica* n.sp. range from -0.63 to -0.47 ‰, values that are significantly lower than co-existing acarininids and morozovellids. These data may indicate that this species had rapid growth rates with a proportion of isotopically ^{13}C -depleted metabolic carbon incorporated into the calcite test. Stable oxygen isotope data on this species range from -2.64 to -1.5‰, which implies that the species lived in a wide range of temperatures between 18.3 and 23.6°C. Despite their small size, tests of the species are fairly resistant to dissolution, and specimens are preserved in horizons with low carbonate content.

4.1. Introduction

The discovery of *Praetenuitella antica* n.sp. arose during a detailed study of foraminiferal assemblages in lower Paleogene sediment at Ocean Drilling Program (ODP) Site 1215. This site presently lies at 5396 m water depth, and about 1000 km northeast of Hawaii (**Figure 4.1**). Surface sediment at this location is “red clay”. However, Site 1215 lies above mid-ocean ridge basalt emplaced during polarity Chron C26r at 58 Ma (Shipboard Scientific Party, 2002). As such, the location was shallower (2700-3400 m) and about 3700 km to the southeast between 51.5 and 56 Ma (Leon-Rodriguez and Dickens, 2010). During this time, a 45-m thick section of calcareous ooze accumulated between the lysocline and calcite compensation depth (CCD) on the subsiding flank of the East Pacific Rise (Shipboard Scientific Party, 2002).

Our initial aim was to constrain the evolution of early Paleogene carbonate saturation horizons in the tropical Pacific (Leon-Rodriguez and Dickens, 2010; Leon-Rodriguez et al., submitted), because this is crucial to understanding carbon cycling over this time interval (Zeebe and Zachos, 2007; Zeebe et al., 2009; Dickens, 2011; Zeebe, 2011). As part of these studies, we detailed the planktic foraminiferal assemblages, in order to assess preferential dissolution among genera. We concluded that *Acarinina* and an unknown species were more resistant to carbonate dissolution than *Morozovella*, *Globanomalina*, and *Igorina* (Leon-Rodriguez et al., Submitted). A similar pattern, excepting the new species of interest, has been observed in dissolution experiments

conducted on sediment deposited during the near the Paleocene-Eocene Thermal Maximum (PETM) (Nguyen et al., 2009).

The unknown planktic foraminiferal specimens were initially described as “*Tenuitella*” sp. (Leon-Rodriguez and Dickens, 2010) because they had strong morphological similarities to the late Eocene genus *Tenuitella* (Li, 1987; Huber et al., 2006), and because they likely correspond to rare species referenced as cf. *Tenuitella* sp. in initial examinations of sediment at Site 1215 (Shipboard Scientific Party, 2002). These characteristics included a small size, four to five globular chambers in the last whorl, and a pustulose wall texture. In this study, we formally describe and present stable isotope analyses of the unknown planktic foraminifers. We name them *Praetenuitella antica* n. sp., which we believe is the sole species of the genus found at Site 1215.

The genus *Praetenuitella* was initially proposed by Li (1987) to describe three new late Eocene species that were small and had a peculiar wall texture. This genus was related but ancestral to the late Eocene-late Miocene genus, *Tenuitella*. In the original description, *Praetenuitella* had a finely macroperforate wall in the initial chambers but became microperforate in the later chambers, while *Tenuitella* was entirely microperforate. Huber et al. (2006), in the Atlas of Eocene of Planktonic Foraminifera, reviewed the validity of both genera and dismissed *Praetenuitella* based on SEM images of one the earliest tenuitellids, *T. insolita* (formerly assigned to the genus *Praetenuitella*). The images revealed that the entire wall structure of *T. insolita* was microperforate. However, we present SEM imaging and morphometric studies of new specimens that allow the resuscitation of this genus; they fit within the original description of

Praetenuitella, which among other features is characterized by macroperforations in the earlier chambers and microperforations in the later chambers.

Our interpretations extend the tenuitellid plexus into the late Paleocene, which is roughly 20 Myr older than previously recorded (Li, 1987; Huber et al., 2006). Therefore, the phylogenetic relationships of the tenuitellids are still not understood, as there is a gap of at least 12 Myr years between the latest praetenuitellids of this study and the earliest tenuitellids found in other marine sites. Nonetheless, it is likely that *Praetenuitella* is phylogenetically related and may be “ancestral” to the late Eocene-late Miocene genus *Tenuitella*, based on the morphological comparison of the two genera but also on the carbon isotope data suggesting that this new taxon had high metabolic rates and rapid growth as it appears was the case for *Tenuitella* as well (Huber et al., 2006).

Besides the phylogenetic value of *P. antica* n.sp., our documentation is important because this species comprises a significant part of planktic foraminiferal assemblages in several horizons at Site 1215 (Leon-Rodriguez et al., Submitted). We attribute this finding to a combination of two factors: tests of the species are fairly resistant to carbonate dissolution and the species could tolerate a wide range of shallow water temperatures, as shown by cross-plots of the abundance of this species versus carbonate content and $\delta^{18}\text{O}_{\text{bulk}}$ isotopes.

4.2. Materials and Methods

One hundred and seventeen sediment samples of $\sim 10 \text{ cm}^3$ were taken from cores through the lower Paleogene interval in Hole 1215A. From these samples, 3-5 g aliquots were examined for micropaleontological analyses. Samples were placed in 63 μm sieve, gently washed with 18 M Ω deionized water, and subsequently dried at room temperature. Taxonomic identification and total numbers of planktic foraminifers were done employing a Leica MZ6 binocular microscope. The most recent taxonomic concepts were used (Pearson et al., 2006), but several other references were consulted for comparative and discussion purposes e.g., (Li, 1987; Huber, 1991; Chaisson and Leckie, 1993; Leckie et al., 1993; Li et al., 1995; Poag and Commeau, 1995; Liu et al., 1998; Olsson et al., 1999; Li et al., 2003; Li et al., 2004)

A single sediment sample of $\sim 10 \text{ cm}^3$ was taken from IODP Hole U1333A. This site is about $\sim 2000 \text{ km}$ southeast of Hawaii (**Figure 4.1**) and currently lies at 4865 m water depth (Expedition_320/321_Scientists, 2010). This sample (U1333A/20X/2W/63-65cm) was collected at $\sim 200 \text{ mccsf-a}$ (meters core composite depth below seafloor) and from the lowest section of the middle Eocene nannofossil ooze collected at this site. It was processed following the same procedures used for samples taken from ODP Site 1215. Absolute counts were not carried out on this sample, as our purpose was to confirm the presence of the new species at another site of the Equatorial Pacific Ocean.

4.2.1. SEM Imaging and Morphometrics

We mounted 30 specimens for SEM imaging with their dorsal/spiral side facing upward in such way that coiling axis was almost perpendicular to the mounting button. Another 33 specimens were mounted to display their ventral/umbilical side and their periphery; at least 10 of them were purposely broken apart. SEM images were taken using a FEI Quanta 400 ESEM FEG at the Rice Shared Equipment facility at Rice University under HV, 25-30K. We used images to examine type of wall, pore size, sutures, umbilicus, apertural arch, apertural lip, coiling direction, total number of chambers in the last whorl. Broken specimens were used to inspect in a greater detail wall structure and size of pores at the interior of the chambers. We measured height, intersutural length of the chambers, and maximum test diameter (**Figure 4.2**) following the methodology of Pearson et al. (2001).

The Chamber Expansion Index (CEI) and the Dorsal Chamber View Index (DCVI) were calculated as follows (Pearson et al., 2001):

$$CEI = [(ISL_{T-1} * H_{T-1}) / (ISL_{T-3} * H_{T-3})]^{1/3}$$

(1)

$$DCVI = ISL_{T-1} / H_{T-1}$$

(2)

The first index calculates the average areal increase in the size of the chambers in the last whorl. The second index measures the degree of elongation of the penultimate

chamber as seen from the spiral side (Pearson et al., 2001). These calculations complement morphological descriptions and can be used for future morphometric comparisons with other tenuitellids.

4.2.2. Stable Isotopes

Samples were analyzed on ThermoElectron Delta Advantage mass spectrometer in a Kiel III automated carbonate preparation device at the Stable Isotope Laboratory at the University of Massachusetts, Amherst. Samples were reacted with phosphoric acid at 70°C to liberate CO₂ gas. Values are reported relative to the Vienna Peedee Belemnite standard (VPDB) standard via regular calibration to an internal laboratory standard. Precision is better than 0.06‰ for δ¹⁸O and 0.02‰ for δ¹³C. These samples comprised batches of between 50 and 120 specimens of *P. antica* n.sp, between 3 and 16 specimens of *Acarinina* spp., *Morozovella* spp., *Subbotina* spp., and *Nuttallides truempyi*; and 70 specimens of *Chiloguembelina* spp. Several rounds of gentle washing were carried out to assure good cleansing of the specimens.

4.2.3. Cross-plots

A series of measurements have been made on lower Paleogene sediment from Site 1215, including carbonate content (wt%), and the stable oxygen isotope composition of bulk carbonate (δ¹⁸O_{bulk}; Leon-Rodriguez and Dickens, 2010). To evaluate how carbonate dissolution and paleotemperature might impact the abundance of *P. antica* n.sp., we compared carbonate content and δ¹⁸O_{bulk} to the relative abundance of *P. antica* n.sp. in the same samples. We did the same with *Acarinina* spp. because this is a well-known

genus with three generally accepted characteristics: it was a photosymbiont-bearing, mixed layer dweller; it had a preference toward warm and oligotrophic environments; and it made tests particularly resistant to dissolution (Petrizzo, 2007; Petrizzo et al., 2008; Nguyen et al., 2009).

4.3. Results

4.3.1. Sytematic Taxonomy

Family GUEMBELITRIIDAE Montanaro and Galitelli, 1957

Genus *Praetenuitella* Li, 1987 Emendation

Description

Type of wall: Monolamellar, radial calcite wall. Test is finely macroperforate on the earliest chambers (1.2 – 2.0 μm pores) but progresses into microperforate (<1 μm pores) on the latest chambers. Moderately pustulose wall on the earliest chambers but later sparsely pustulose.

Test morphology: Test small (<150 μm), low to moderate trochospiral, periphery subrounded, chambers globular to ovate, 4-6 chambers in the final whorl; sutures radial on both sides. Small, closed umbilicus. Aperture extraumbilical low arch with thin to slightly wider flap-like lip.

Taxonomic Discussion

This genus was originally described by Li (1987) in order to distinguish late Eocene planktic foraminifers that display the following characteristics “1. very low trochospiral test; 2. Finely-macroperforate walls in the earlier test, developing into a microperforate wall in the adult chambers; and 3. a wide and open umbilicus”. The original species recognized under this genus included: *P. impariapertura* (now *T. insolita*), *P. patefacta* (now *T. patefacta*), and *P. praegemma* (now *T. praegemma*). Later, Huber et al. (2006) disregarded the validity of the genus and synonymized *Praetenuitella* Li (1987) within *Tenuitella* Fleischer (1974) based on SEM images of *Tenuitella insolita*, which showed that the early chambers of this species were not finely macroperforate but instead microperforate as observed in other species of *Tenuitella*. However, SEM images taken from late Paleocene to early Eocene foraminifers (Plates 1-3) led us to resuscitate the genus *Praetenuitella*, because specimens show characteristics similar to those described by Li (1987). These specimens have moderately to weakly pustulose and possess a macroperforate wall in the earliest chambers that later progresses into finely and sparsely pustulose and microperforate wall, particularly on the last two chambers of the last whorl. Moreover, our praetenuitellid specimens from sediment at the ODP Site 1215 are moderately trochospiral and have a closed umbilicus rather than a wide and open umbilicus as initially described by Li (1987). These morphological features are not particularly different from other late Eocene-late Miocene tenuitellids e.g., (Li, 1987; Leckie et al., 1993). We therefore emend the *Praetenuitella* taxonomic description to accommodate the distinctive wall texture of the late Paleocene-early Eocene specimens from the equatorial Pacific.

Phylogenetic Relationships

The origin of the tenuitellids remains uncertain. Huber et al. (2006) disregard *Pseudohastigerina micra* (Cole) as an ancestor of the earliest tenuitellids as proposed by Li (1987). This is because several morphological changes should have happened in order to for nearly planispiral and smooth-walled representatives of *Pseudohastigerina* to become a genus with low to moderate trochospiral and macro to microperforate wall. Instead, Huber et al. (2006) suggest a different ancestor: *Cassigerinella eoacaenica* Cordey, which share some features with *Tenuitella* such as microperforate wall, small size test, and high, narrowly arched aperture but has a distinctive triserial trochospiral arrangement that *Tenuitella* does not have. We suggest *P. antica* n.sp. is likely phylogenetically closer to *Tenuitella*, because both genera share features like their monolamellar and finely pustulose wall, small size (100 - 150 μm), have similar trochospiral chamber arrangement, and have very similar carbon isotopic characteristics. Although, the wall in *Praetenuitella* is macroperforate in its first chambers, later it becomes microperforate just as in *Tenuitella*. Furthermore, carbon stable isotope data indicate that praetenuitellids probably had similar paleobiology as *Tenuitella*, which is discussed below.

Nearly 20 Myr separates our early Eocene praetenuitellids at Site 1215 from *Tenuitella insolita* (Jenkins). We were able to find *Praetenuitella* in a sample (~200 mcsf-a) of middle Eocene sediment at IODP Site U1333 (~47 Ma). Carbonate dissolution in samples above did not allow tracking this genus further up in the section. However, this still means praetenuitellids and *Tenuitella insolita* (Jenkins) are separated by nearly 12 Myr. Given this time difference, early Eocene praetenuitellids were probably not direct ancestors of the late Eocene *Tenuitella* spp. Instead, the genus could

be a primitive ancestor with a micro/macroporifera wall, higher trochospirality, and an extraumbilical aperture, which later evolved into a genus with a fully microperforate wall, a lower trochospiral coiling, and an aperture from extraumbilical to intra-extraumbilical and interiomarginal. *Cassigerinella eocaenica* Cordey might be closely related to *Tenuitella* and *Praetenuitella*, but certainly does not appear to be the direct ancestor of *Tenuitella* either, for reasons explained above. It should be emphasized that members of the tenuitellid plexus may have been overlooked in previous studies because of their rarity and small size.

The phylogenetic ancestor of *Praetenuitella* also remains uncertain. However, several authors have proposed that microperforate taxa originated from one or more benthic foraminiferal ancestors (Brinkhuis and Zachariasse, 1988; Li and Radford, 1991; Li et al., 1992; Liu and Olsson, 1992; D'Hondt et al., 1994; Huber et al., 2006; Darling et al., 2009; Leckie, 2009). As noted below, this might be supported by carbon isotope data, which indicate affinity to benthic foraminifers.

***Praetenuitella antica* Leon-Rodriguez, Leckie, and Dickens, new species**

Holotype: “*Tenuitella*” sp., Leon-Rodriguez and Dickens (Fig. 3V, 2010),

Reillustration in Pl. 1, Figs 1-3; Paratypes: Pl. 1, Figs. 4-12; Pl. 2, Figs. 1-12;

Pl. 3, 1-20

Description

Type of wall: Monolamellar, radial calcite wall. Test is finely macroperforate (1.2 – 2.0 μm pores) and moderately pustulose wall on the earliest chambers that progresses into microperforate (<1 μm pores) and sparsely pustulose in later chambers.

Test morphology: Subquadrate, lobate test of small size (~100 μm), moderate trochospiral, axial periphery subrounded, chambers globular to ovate, chambers compressed in edge view; 12 - 13 chambers in a trochospiral arrangement, 4-5 chambers in the final whorl, which increase slowly in size as added; sutures depressed, radial and slightly curved to straight on both sides. Dextral coiling more common than sinistral. Narrow to closed umbilicus. Aperture extraumbilical-umbilical low arch with a thin lip. Pustules are less than 2 μm of diameter. Sometimes last chamber is aberrant and more ovate (kummerform), in such cases aperture is smaller and half-rimmed by a flap-like lip. Apertural lip may or not have pustules.

Distinguishing features

Small and subquadrate test with typically 4 chambers in the final whorl. Moderate density of fine pustules on the initial chambers becoming weakly pustulose on later formed chambers. *P. antica* n.sp. differs from *T. insolita*, (Jenkins), *T. praegemma*, (Li), and *T. patefacta*, Li in having a low arch extraumbilical aperture and having fewer chambers in the last whorl. *P. antica* n.sp. shows fine macroperforations and a more densely pustulose wall on the earlier chambers that later change to a microperforate and sparsely pustulose wall in the final chambers, while *Tenuitella* spp. is characterized by a microperforate wall on all chambers. Dissolution may have artificially enlarged the pores on some specimens of *P. antica* illustrated here (e.g., Pl. 1, fig. 9; Pl. 2, fig. 10).

Praetenuitella antica also differs from other tenuitellids by having a tighter coiling showing a higher trochospiral arrangement.

Species within the *Dipsidripella* genus are somewhat similar to *P. antica*, but *Dipsidripella* spp. have bigger pustules, and their wall texture is often hispid and displays a wider range of pore sizes. Particularly, *Dipsidripella danvillensis* has bigger blunt to hispid pustules and bigger size pores (Pl. 16.8 in Huber et al. 2006). *D. liqianyui* has blunt pustules that have a tendency to coalesce and also has a greater number of chambers in the last whorl than *P. antica* (Pl. 16.9 in Huber et al. 2006). *P. antica* n.sp. is distinguished from *Turborotalita* spp. by having a monolamellar wall rather than the bilamellar spinose, ruber-type reticulated wall of *Turborotalita*.

Li (1992; Plate 3, Figs. 8 and 9) illustrated the umbilical side and the side view of *Tenuitella clemenciae* (Bermudez) from the Kerguelen Plateau (Hole 747A). This species strongly resembles the morphology of *P. antica* n.sp. In fact, at Hole 747A, *T. clemenciae* has four chambers in the final whorl and is found with a diameter of about 100 μm (Li et al., 1992). However, the stratigraphic range of *T. clemenciae* ranges from the lower to middle Miocene, covering Zones N7-N10 (Li et al., 1992). (Kennett and Srinivasan) (1983; Plate 40, Figure 1-6) consider that *T. clemenciae* is characterized by 5 chambers in the last whorl, which in that case would be a reasonable characteristic to distinguish this species from *P. antica* n.sp. In spite of this, it would be desirable to have more illustrations of the *T. clemenciae* specimens from the Kerguelen Plateau to establish distinctive morphological characteristics between the two species, although it is clear that the two species are stratigraphically separated by more than 20 Myr.

Type Sample

Leg 199, ODP Site 1215 Hole A, 5H, 5, 18.5-20.5 (35.89 mbsf), Biozone E3-E4 (lower Eocene) following biozonation by Berggren and Pearson (2005).

Type Locality

ODP Hole 1215A, equatorial Pacific Ocean, 26°01.77'N, 147°55.99'W

Etymology

Latin “antica”= old, ancient; aged

Repository

Holotype and 31 paratype specimens will be deposited in the collections of the National Museum of Natural History, Smithsonian Institution, Washington, D.C.

4.3.2. Morphometrics

We have followed a similar strategy to that used by Pearson et al. (2001) for the morphometrics of *Mutabella variabilis*, which is thought to be a descendant of the tenuitellids (Pearson et al., 2001). Histograms show that about 70% of the specimens have dextral coiling and 4 chambers in the last whorl (**Figure 4.3**). The sample population shows an approximately normal distribution of the maximum diameter, Chamber Expansion Index (CEI), and the Dorsal Chamber View Index (DCVI). Maximum diameter ranges between 80 and 131 μm (**Figure 4.3**). The CEI is an estimate for areal increase in chamber size of the last whorl (Pearson et al., 2001). In the case of *P. antica* this index fluctuates from 1.06 to 1.46 (**Figure 4.3**); these numbers are lower than

those reported for *Mutabella variabilis* (CEI averages between 1.55 and 1.62). This means that chambers in *P. antica* do not enlarge as greatly as in *M. variabilis*. The DCVI in *P. antica* averages 2.2, which implies that the length of the penultimate chamber is more or less double the height. This index also serves as indirect indicator of test trochospirality (Pearson et al., 2001). The more trochospiral the coiling is, the more involute the test is, and also the more closed the umbilicus is. In tests with high trochospirality, DCVI values are high. For example, *Mutabella variabilis* that is somewhat planispiral (Pearson et al., 2001) exhibits DCVI values that range between 1.51 and 1.88. On the other hand, our specimens of *P. antica* show greater DCVI values (between 1.63 and 3.36; **Figure 4.3**). Therefore, *P. antica* has a higher trochospiral coil than *M. variabilis*. This can be confirmed by a close examination of SEM images of both species.

4.3.3. Stable Isotope Composition

Stable isotopes were measured on 6 samples containing multiple specimens of *P. antica* n.sp. but reliable data came from only 3 of these samples (**Table 4.1 and Figure 4.4**). The $\delta^{18}\text{O}$ values range from -2.64 to -1.5 ‰, and the $\delta^{13}\text{C}$ values range from -0.63 to -0.47 ‰.

The stable isotope compositions can be compared to those of other foraminifera in the same samples (**Table 4.1 and Figure 4.4**). The $\delta^{18}\text{O}$ values of *P. antica* n. sp. are somewhat similar to mixed-water dwelling planktic foraminifera *Acarinina* (from -2.95 to -0.70‰) and *Morozovella* (from -2.35 to -1.20‰), and slightly more negative than the benthic *Nuttallides* spp. (from -0.99 to 0.62‰). However, the $\delta^{13}\text{C}$ values of *P. antica* n.

sp. are significantly less than coexistent acarininids (from 1.41. to 3.26‰) and morozovellids (from 2.01 to 3.05‰). Instead, $\delta^{13}\text{C}$ values are more similar to the planktic *Chiloguembelina* spp. (-0.32‰) and *Nuttallides* spp. (from 0.00 to 0.67‰).

The temperature of carbonate precipitation can be estimated for *P. antica* n. sp. from the $\delta^{18}\text{O}$ values. We calculate between 18.3 and 23.6°C using an established temperature equation (Erez and Luz, 1983), with a $\delta^{18}\text{O}_{\text{SMOW}}$ of -0.96‰ that implies no permanent ice caps during the late Paleocene and early Eocene (Zachos et al., 1994).

4.3.4. Stratigraphic Distribution

The species was found in multiple samples of uppermost Paleocene and lower Eocene sediment (Biozones P5-E5) at Site 1215 (**Figure 4.5**). Some specimens identified as *P. antica* n. sp. were also found in a single sample of middle Eocene sediment at Site U1333..This sample is definitely older than biozone E12, and possibly occur within biozone E8. The stratigraphic range of *P. antica* n. sp. is poorly constrained.

4.3.5. Geographic Distribution

The geographic range of this species cannot be traced without additional work. Most likely, the taxon can be found in other Eocene sections deposited at low latitudes in the Pacific.

4.3.6. Abundance

Praetenuitella antica n. sp. is not particularly abundant throughout the upper Paleocene and lowermost Eocene section (Unit II) at IODP Site 1215. However, it becomes more abundant in the uppermost part of the lower Eocene section at this site.

In the uppermost Paleocene (57.81 - 54.11 mccsf), the absolute abundance of *P. antica* n. sp. does not exceed 20 individuals per ~3 g sediment sample. However, this can represent up to ~71% of the total planktic foraminiferal assemblage (**Figure 4.6**). The interval that corresponds to the Paleocene-Eocene boundary is marked by strong carbonate dissolution (54.11 - 53.34 mccsf); this dissolution greatly affected all the foraminiferal taxa during this interval including *P. antica* n. sp. (0-2 specimens per ~3 g of sediment). For several meters above the PETM, the abundance of planktic foraminifers increases significantly; in the case of *P. antica* n. sp., the abundance at 51.6 mccsf exceeds (29 specimens per ~3 g of sediment) that in the upper Paleocene. This post-PETM interval is thought to be a deep-sea carbonate recovery phase, when carbonate preservation increased (Leon-Rodriguez and Dickens, 2010; Leon-Rodriguez et al., Submitted). Between 52.07 and 35.60 mccsf, the number specimens of *P. antica* n. sp. fluctuates from 0 to 35 individuals per ~3g of sediment. In some cases, however, this species completely dominates and accounts for 75-100% of the planktic foraminiferal assemblage (**Figure 4.6**). The depth horizon of the H1 event (~35.1 mccsf) is characterized by strong carbonate dissolution (Leon-Rodriguez and Dickens, 2010; Leon-Rodriguez et al., Submitted), where only a few praetenuitellids are preserved (<6 individuals per ~3g of sediment). The recovery phase that follows H1 (~35.2 mccsf) is

marked by a greater improvement in the absolute abundances of *P. antica* n. sp (>20 specimens per ~3 g of sediment). (**Figure 4.6**). Abundance of this species steadily increases from the H1 to just before the I1 event and reach reach a maximum of 115 individuals per ~3 g of sediment sample at 31.83 mccsf (**Figure 4.6**). These higher abundances abruptly terminate at the I1 event at 29.90 mccsf, which is characterized by strong carbonate dissolution where not foraminifers are preserved (Leon-Rodriguez and Dickens, 2010; Leon-Rodriguez et al., Submitted). Above this horizon numbers of *P. antica* n. sp. slightly recover to <3 specimens per ~3 g of sediment sample. However, by 28.06 mccsf, neither planktic nor benthic foraminifers are no longer found in the record as result of carbonate dissolution (Leon-Rodriguez and Dickens, 2010).

Overall, the abundance of *P. antica* n. sp. at ODP Site 1215 displays a peculiar stratigraphic distribution suggesting a trend of higher abundances of this species through out the accumulation of Unit II (**Figure 4.6**). It is noted that this roughly coincides with a slight cooling trend inferred in the $\delta^{18}\text{O}_{\text{bulk}}$ record (Leon-Rodriguez et al., Submitted;**Figure 4.6**).

4.3.7. Solution Susceptibility and Temperature Control

In samples from Site 1215 where carbonate content is low (<50%), foraminifera assemblages are dominated by *Acarinina* and *Praetenuitella antica* n. sp. (Leon-Rodriguez et al., Submitted). Both genera are probably especially resistant to carbonate dissolution. Crossplots of the relative abundance of *Praetenuitella antica* n. sp and *Acarinina* spp. vs. carbonate content from sediment samples from Site 1215 show that *Acarinina* is more abundant than *Praetenuitella* in sediment samples where carbonate

content is less 50% (**Figure 4.7**). Likewise, when the carbonate content is higher than 50%, *Acarinina* have a tendency to dominate the assemblages although *Praetenuitella* is an important component of the assemblage.

Relative abundances of both genera might also be controlled by the temperature of shallow water. This inference comes from a comparison to bulk carbonate $\delta^{18}\text{O}$ (**Figure 4.7**). Crossplots show that samples dominated by *Acarinina* spp. generally occur when $\delta^{18}\text{O}_{\text{bulk}}$ is lower (from -2.2 to -1.4‰), and samples dominated by *P. antica* n. sp. generally occur when $\delta^{18}\text{O}_{\text{bulk}}$ is higher (from -2.2 to -0.62‰).

4.4. Discussion

4.4.1. Phylogenetic Importance

The finding of *P. antica* n. sp. forces a re-evaluation of this branch of microperforate planktic foraminifera. The astonishing morphological similarities of *P. antica* n. sp. with tenuitellids (i.e., *T. insolita*, *T. praegemma*, and *T. gemma*, illustrations in Huber et al., 2006), and the fact that they all share monolamellar wall structure, support a phylogenetic connection. Isotopic data also provide evidence to link these taxa, as the tests of all are characterized by anomalously low $\delta^{13}\text{C}$ (Berger et al., 1978; Liu et al., 1997; Pearson and Wade, 2009).

Relatively few studies have focused on tenuitellids (Li, 1987; Li et al., 1992; Li et al., 1995; Huber et al., 2006). This may reflect their small size and relatively low abundance. Nevertheless, the documentation of *Praetenuitella* in upper Paleocene-middle

Eocene sediment implies a richer history for this plexus than previously believed. In particular, there is currently a significant stratigraphic gap, perhaps 12 Myr, between the youngest occurrence of *Praetenuitella* and the oldest occurrence of *Tenuitella* (Huber et al., 2006). It is possible that small and rare transitional species between these two genera might have been overlooked in the middle Eocene sedimentary record in other marine sites.

A provocative idea is that microperforate planktic species like the tenuitellids s.l. could have originated from benthic ancestors (Brinkhuis and Zachariasse, 1988; Li and Radford, 1991; Li et al., 1992; Liu and Olsson, 1992; D'Hondt et al., 1994; Huber et al., 2006; Darling et al., 2009; Leckie, 2009). Thus, it is possible that a common benthic ancestor gave rise to praetenuitellids and to tenuitellids one or more times during the early Paleogene. Leckie (2009) suggests that oceanographic changes (e.g., drop in oxygen) could cause some benthic foraminifers to switch to a planktic mode of life. It is yet to unknown when and from what foraminiferal branch praetenuitellids appear in geological record.

4.4.2. Inferred Paleobiology

Oxygen isotope values on *P. antica* (from -2.64 to -1.5‰) suggest that this species lived in water between 18 and 24°C. These temperatures fall within the range of those for planktic foraminifers that live within the mixed layer to upper thermocline zone. Therefore, the planktic character of this previously undocumented species is almost certain (**Figure 4.4**).

The considerably depleted $\delta^{13}\text{C}$ values of *Praetenuitella* support the postulated phylogenetic link with tenuitellids and other microperforate taxa (Liu et al., 1997)(Liu et al., 1997; Huber et al., 2006). The low values may indicate rapid growth rates (Berger et al., 1978; Pearson and Wade, 2009), where metabolic carbon contributes to shell material. Huber et al. (2006) have also suggested that ^{13}C -depleted values in *Tenuitella* indicate that this genus lived within the Oxygen Minimum Zone (OMZ). This also might be the case for *Praetenuitella*.

Praetenuitella antica n. sp. is present throughout Unit II at ODP Site 1215 (**Figure 4.6**), despite major oceanographic changes that occurred from the late Paleocene through the early Eocene (Zachos et al., 2008). It is first found in low abundance during the late Paleocene, when sea surface temperatures were relatively cool. However, it is also present during the early Eocene, when sea surface temperatures were much warmer. In fact, *P. antica* n. sp. has a peak abundance between the H1 and I1 hyperthermal events. Likely, *P. antica* n. sp. could thrive under a wide range of sea surface temperatures. This view is corroborated by crossplots showing the relative abundances of *Acarinina* spp. and *P. antica* n. sp. compared to $\delta^{18}\text{O}_{\text{bulk}}$ (**Figure 4.7**). Samples with high abundances of *P. antica* n. sp. exhibit a wider range in $\delta^{18}\text{O}_{\text{bulk}}$ than samples with high abundances of *Acarinina* spp.

Moreover, the concurrence of a long-term gentle cooling in the record (Leon-Rodriguez et al., Submitted) and an overall trend of greater abundances of *P. antica* from the late Paleocene to the early Eocene may reflect a long-term change in surface water temperatures, nutrient levels, or both that could have been caused seasonal upwelling and

productivity. This is specially striking at the peak of abundance of *P. antica* n.sp., where benthic foraminiferal and fish debris accumulation rates increase as well (Leon-Rodriguez et al., Submitted). These changes may be related to northward tectonic migration of the site from 10 to 14°N (Leon-Rodriguez and Dickens, 2010) to a region of higher the influence of cooler-surface waters and seasonal-upwelling (Leon-Rodriguez et al., Submitted).

4.4.3. Susceptibility to Dissolution

We have studied carbonate dissolution throughout Unit II at Site 1215 (Leon-Rodriguez and Dickens, 2010; Leon-Rodriguez et al., Submitted). This work suggests that differential dissolution occurs among planktic foraminifera. Specifically *Acarinina* and *Praetenuitella* appear the most resistant to dissolution; these are followed by *Morozovella*, *Subbotina*, *Globanomalina*, and *Igorina* (Leon-Rodriguez et al., Submitted). In examining planktic foraminiferal assemblages from ODP Site 1209 (Shatsky Rise), Petrizzo et al. (2008) suggested that *Acarinina* and *Morozovella* were more resistant to carbonate dissolution than *Subbotina*. A dissolution experiment on late Paleocene-early Eocene age sediment samples (Nguyen et al., 2009) further shows that corrosiveness of seawater sequentially affects *Acarinina* (the least) and *Morozovella*, *Subbotina*, *Globanomalina* and *Zeauvigerina* (the most). One might think that *Praetenuitella* would behave similarly to the small microperforate *Zeauvigerina*, but this is not the case at Site 1215. Interestingly, if praetenuitellids were descendants from benthic foraminifers, they might have some taphonomic characteristics that make them more resistant to carbonate dissolution.

4.5. Conclusions

We describe a previously unknown planktic foraminiferal species of the late Paleocene to middle Eocene of the Equatorial Pacific Ocean. We formally describe this species as *Praetenuitella antica* n.sp. Three important points make *P. antica* n. sp. a taxonomically and paleoceanographically important species:

1. Supporting evidence shows that this species that is likely phylogenetically related to the late Eocene tenuitellids. Therefore, this study places the tenuitellid “lineage” ~20 Myr older than previously documented;
2. The record at Site 1215 indicates that this species was probably tolerant to a wide range of temperatures; it became more abundant when tropical-subtropical sea surface temperatures were slightly cooler.
3. This is a species that although its small size is moderately resistant to dissolution as it is found in pelagic sediments that have less than 50% of carbonate content.

4.6. Acknowledgements

Isotope data were generated by David Finkelstein at the Geosciences Stable Isotope Laboratory, University of Massachusetts, Amherst. Samples were collected at the Gulf Coast Repository, College Station. Paul Pearson, Bill Berggren, Richard Olsson, Isabella Premoli Silva, Bridget Wade, and Michal Kucera offered critical and valuable comments on the genus assignment that should be used for *P. antica*.

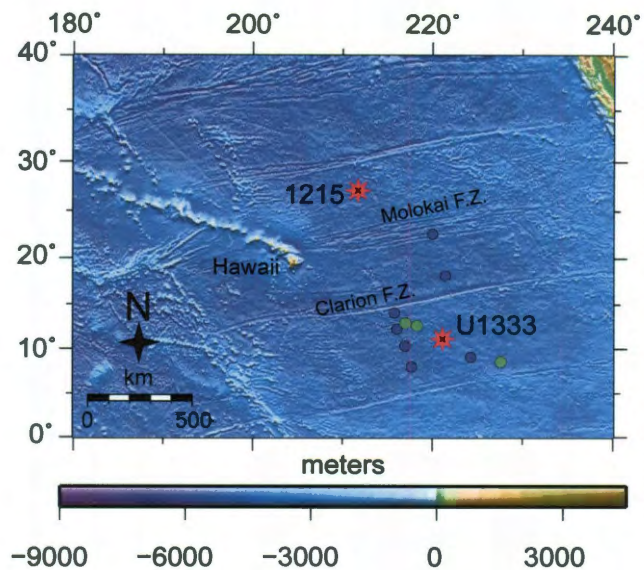


Figure 4.1 – Location of ODP Site 1215 and IODP Site U1333 in the eastern Pacific. Blue dots correspond to sites drilled by Leg 199, and green dots correspond to sites drilled by Expedition 320 (Lyle and Wilson, 2002; Pālike et al., 2010). Bathymetry and topography from Smith and Sandwell (1997).

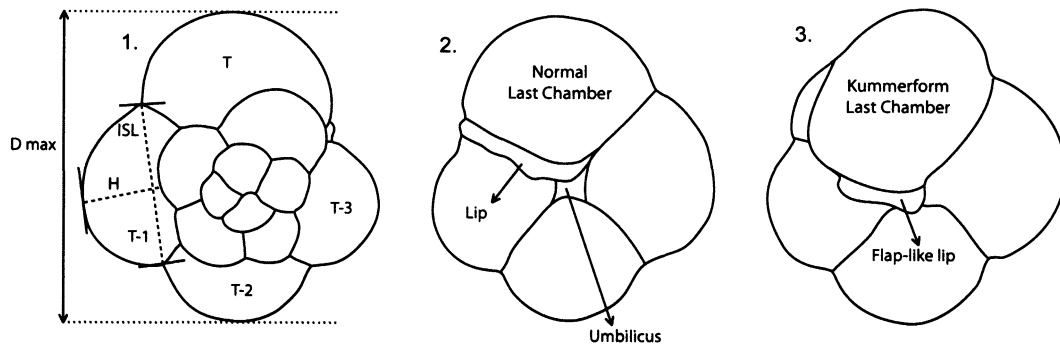


Figure 4.2 – General morphology of *Praetenuitella antica* n. sp.. 1. Spiral view with measurements taken for morphometrics (see Methods). 2. Umbilical view with normal last chamber. 3. Umbilical view with kummerform last chamber.

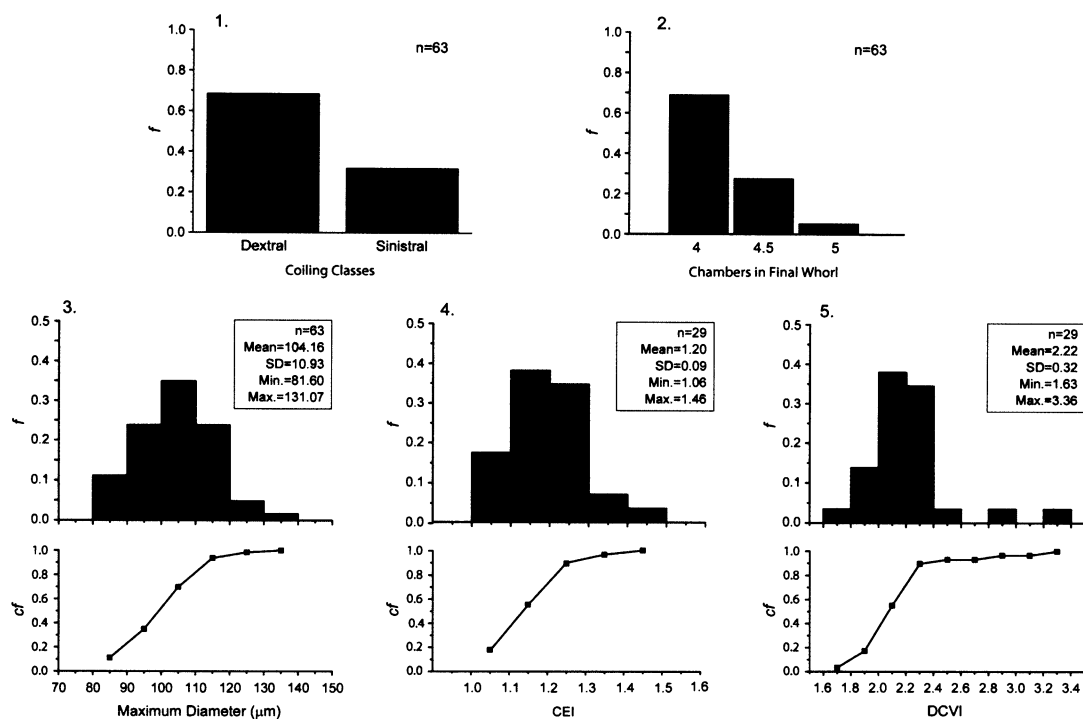


Figure 4.3 – Morphometrics and descriptive statistics of *Praetenuitella antica* n. sp.
1. Histogram of coiling direction. 2. Histogram of number of chamber in the final whorl. 3. Histogram of frequency and cumulative frequency of maximum diameter (D_{max}). 4. Histogram of frequency and cumulative frequency of Chamber Expansion Index (CEI). 5. Histogram of frequency and cumulative frequency of Dorsal Chamber View Index (DCVI).

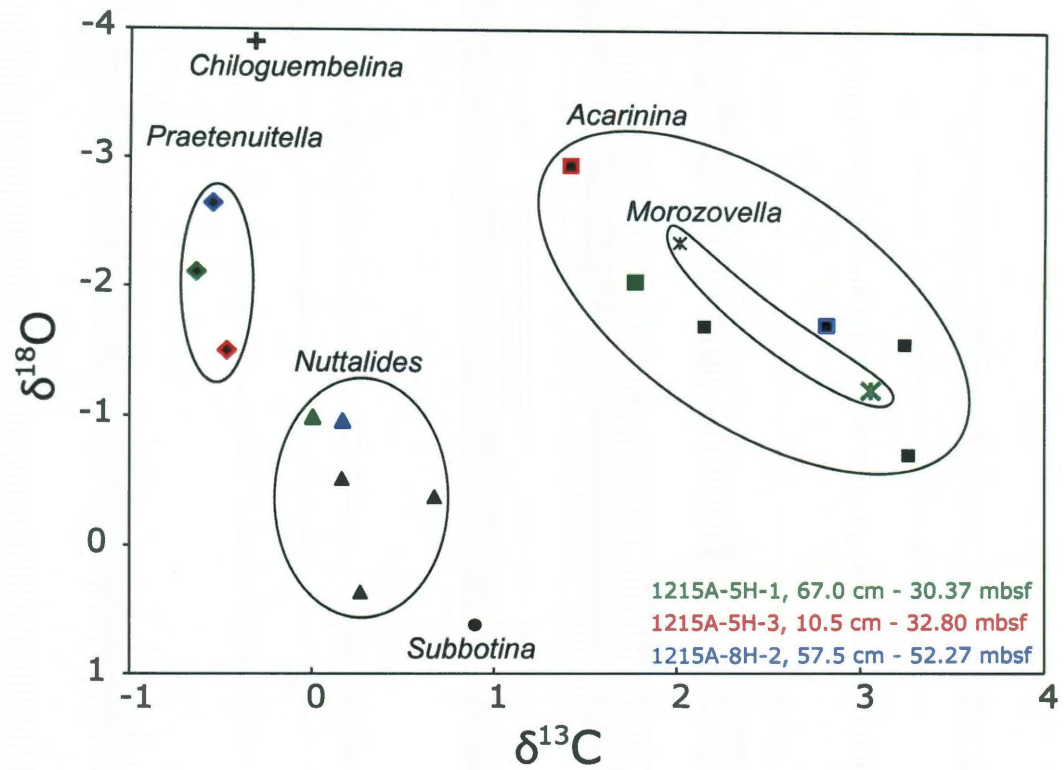


Figure 4.4 – Multispecies isotope data from selected samples of ODP Site 1215 and IODP Site U1333. Colors correspond to samples with reliable *Praetenuitella antica* n. sp.; black note other samples (Table 4.1).

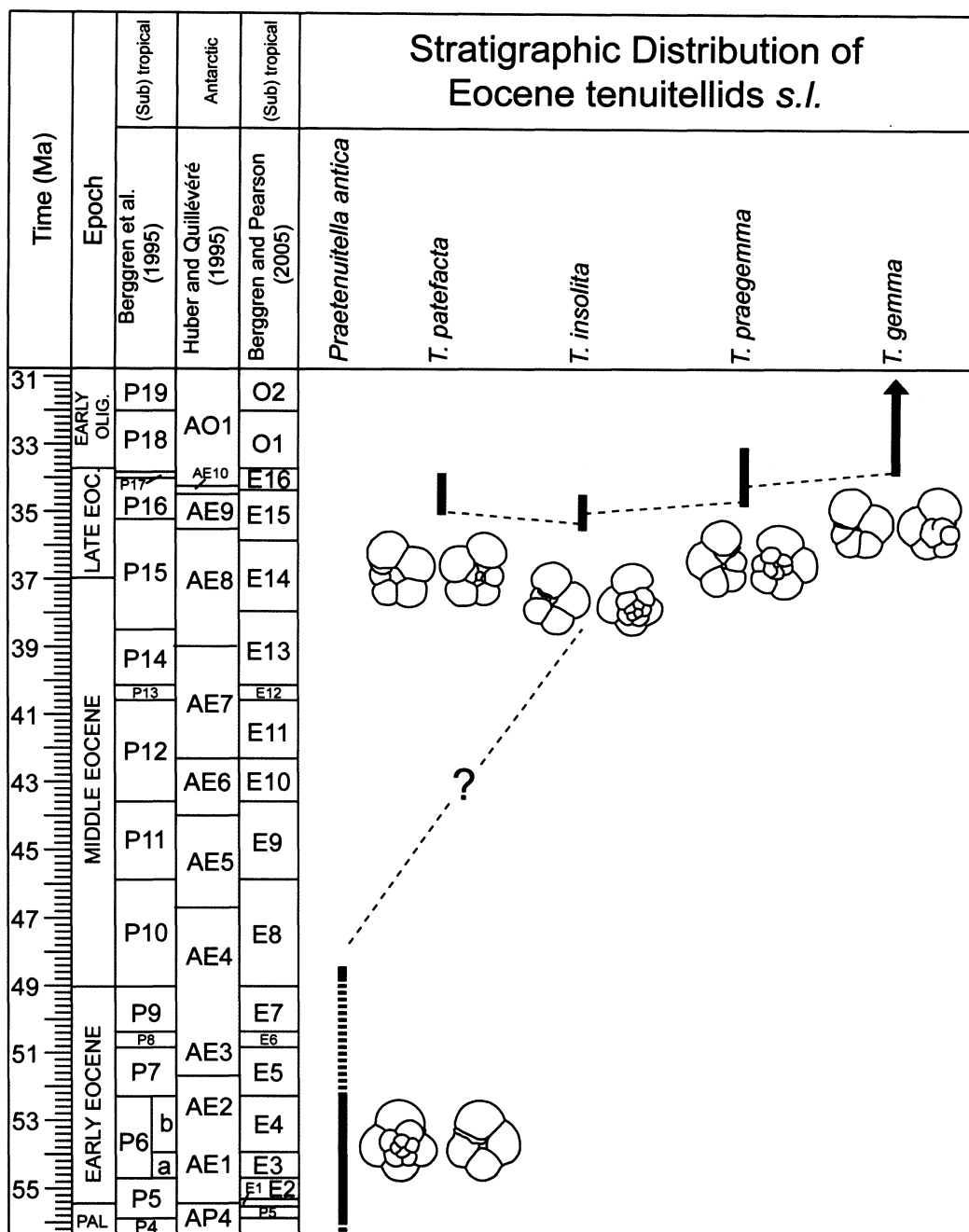


Figure 4.5 – Stratigraphic distribution of *Praetenuitella antica* n.sp. (this study) and other tenuitellids of the Eocene (Huber et al., 2006). Biostratigraphic biozonation taken from (Berggren and Pearson, 2005; Huber et al., 2006).

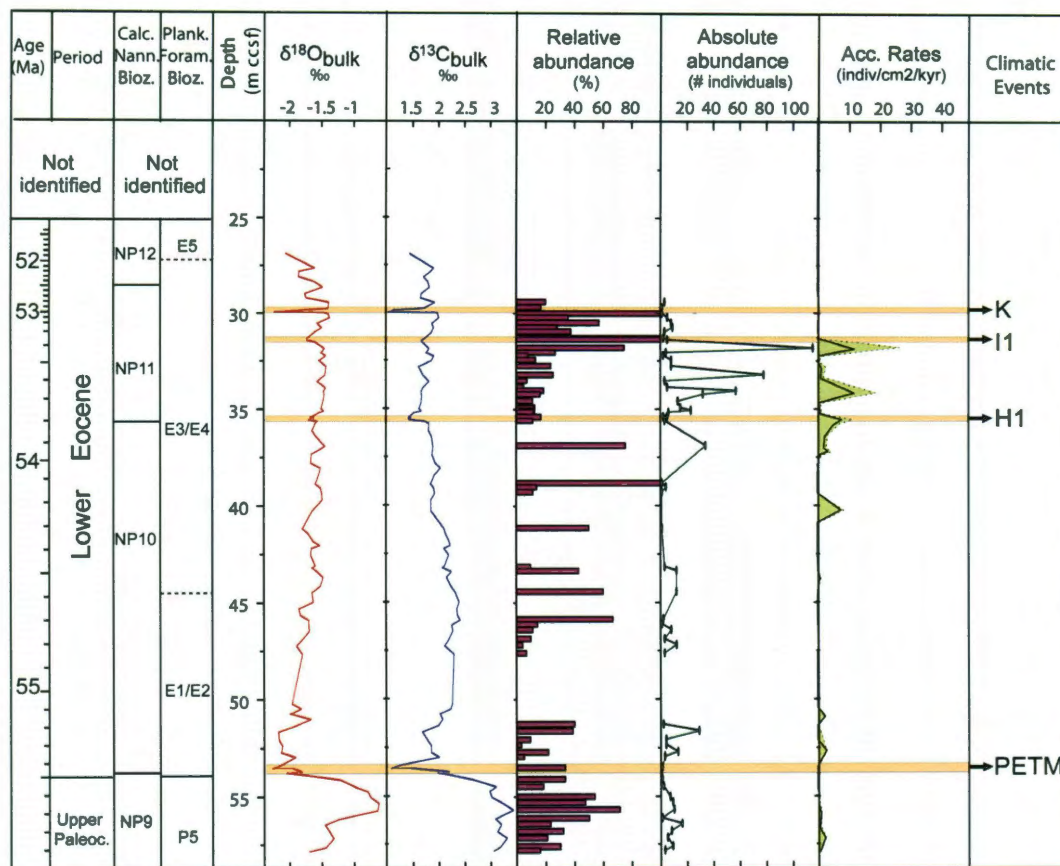


Figure 4.6 – Relative and absolute abundance of *Praetenuitella antica* n. sp. at ODP Site 1215. Absolute abundance is based on ~3 g of sediment sample. Bulk stable isotope data and climatic events taken from study by Leon-Rodriguez and Dickens (2010).

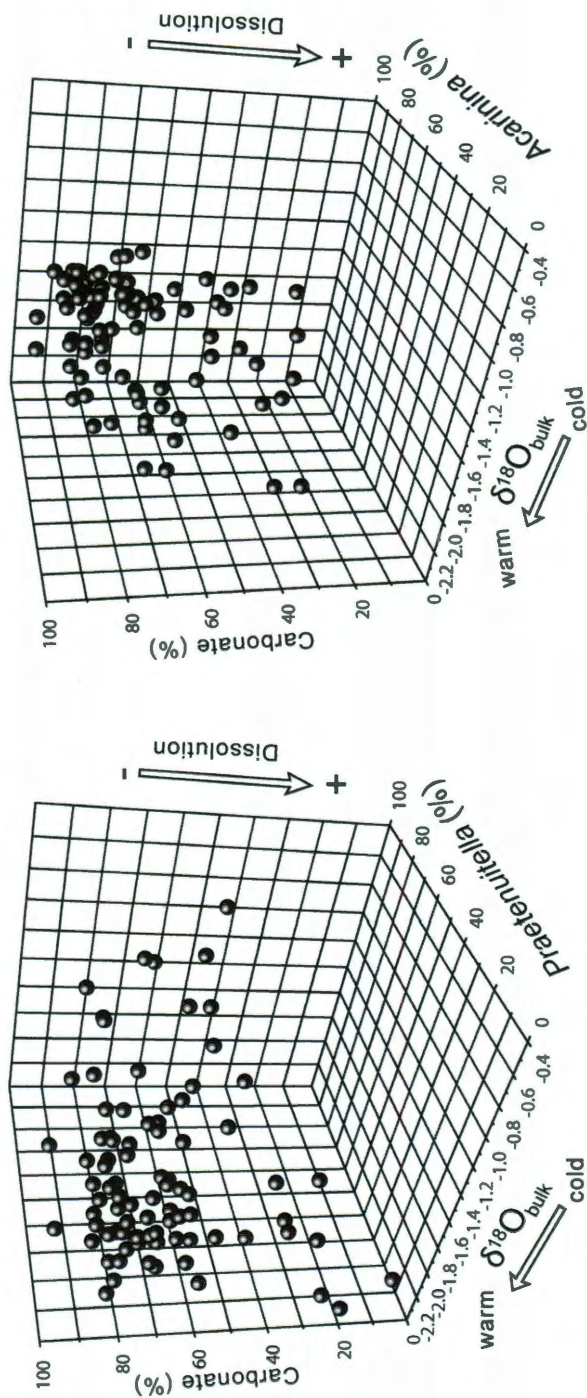


Figure 4.7

Figure 4.7 – Tridimensional crossplots showing the relative abundance of *Praetenuitella antica* n. sp., carbonate content, and bulk carbonate oxygen isotope values from samples at ODP Site 1215. Carbonate content (wt%) and isotope data were published by Leon-Rodriguez and Dickens (2010).

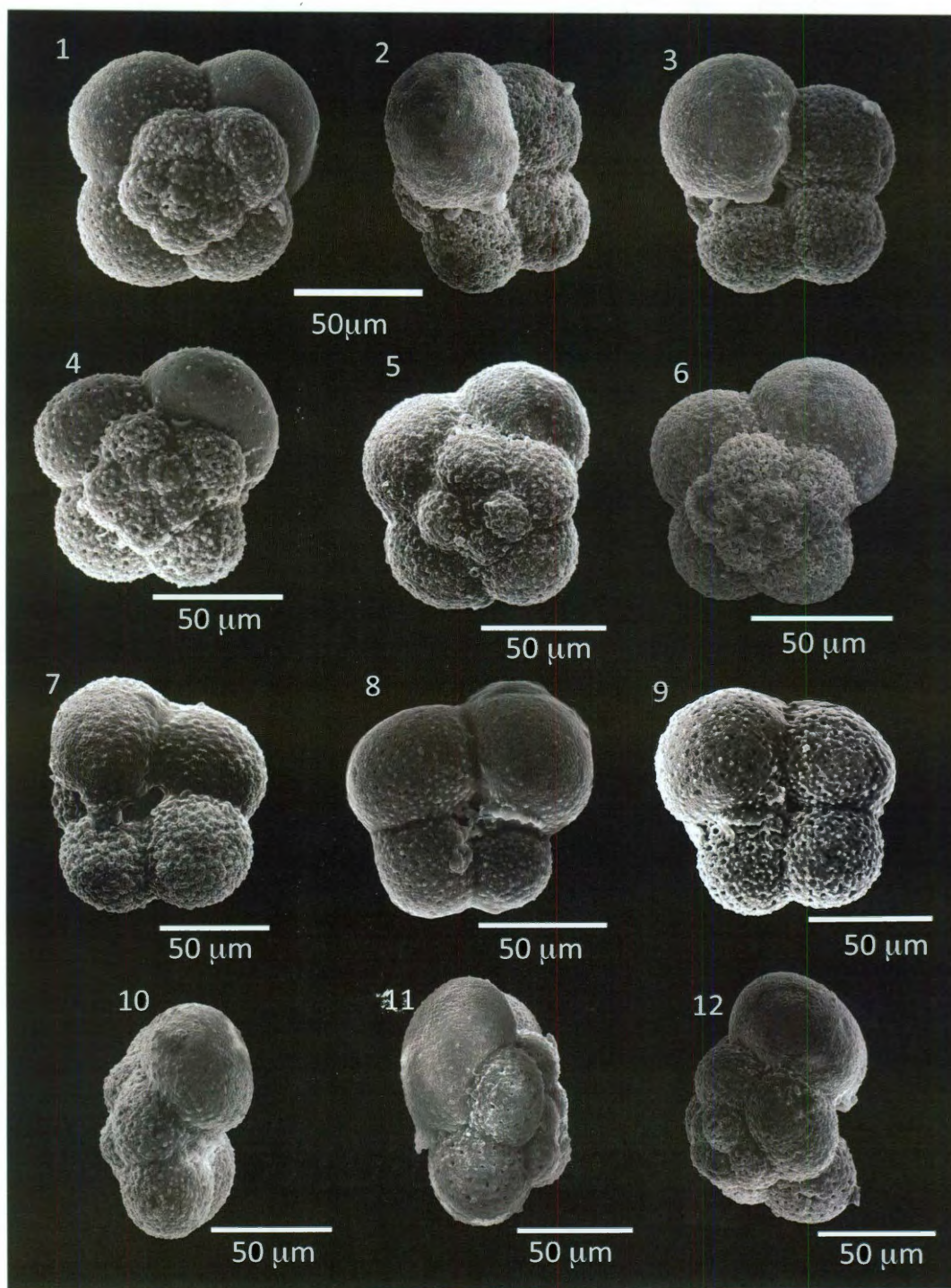


Plate 4.1

Plate 4.1 - *Praetenuitella antica* n.sp. Figure 1-3 Holotype, Biozone E4, spiral side reillustration of “*Tenuitella*” sp. Leon-Rodriguez and Dickens (Fig. 3V, 2010); Figure 4, Paratype, Spiral view, reillustration of “*Tenuitella*” sp. Leon-Rodriguez and Dickens (Fig. 3W, 2010); Figure 5, Paratype, Spiral view; Figure 6, Paratype, Spiral view; Figure 7, Paratype, Umbilical view; Figure 8, Paratype, Umbilical view, reillustration of “*Tenuitella*” sp. Leon-Rodriguez and Dickens (Fig. 3X, 2010); Figure 9, Paratype, Umbilical view, reillustration of “*Tenuitella*” sp. Leon-Rodriguez and Dickens (Fig. 3U, 2010); Figure 10 - 12, Paratypes, Peripheral views. Figure 1 - 3, 5, 10 - 11: ODP Hole 1215A, 5H, 5, 18.5-20.5 (35.89 mbsf); Figure 4, ODP Hole 1215A, 008H, 02, 57.5 - 59.5 cm (52.28 mbsf); Figure 6-7, 12 ODP Hole 1215A, 6H, 3, 128.5 - 130.5 cm (43.49 mbsf); Figure 8: ODP Hole 1215A, 8H, 6, 139.5 - 141.5 cm (59.1 mbsf); Figure 9: ODP Hole 1215A, 5H, 1, 67 - 69 cm (30.37 mbsf).

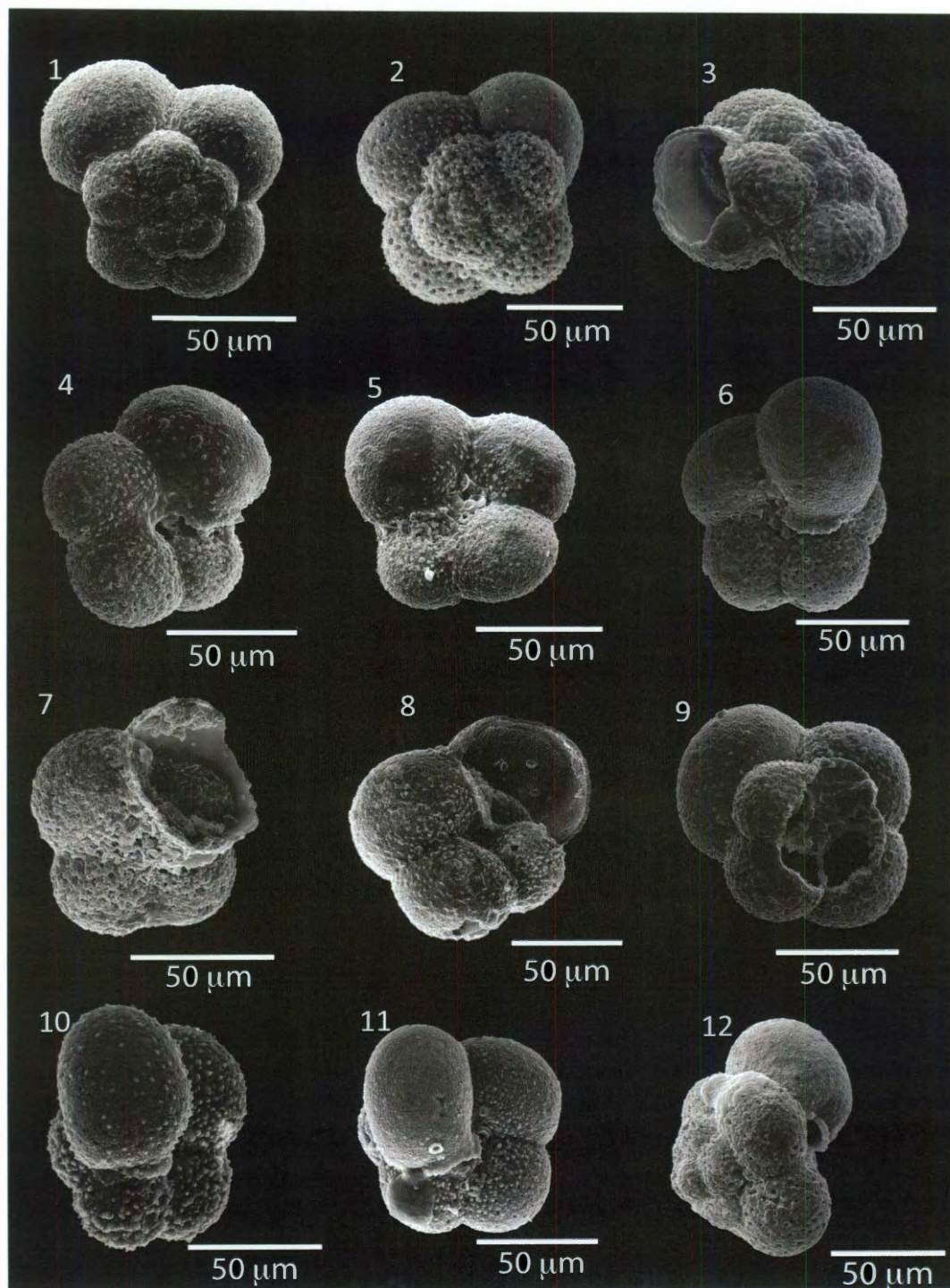


Plate 4.2

Plate 4.2 - *Praetenuitella antica* n.sp. Figure 1-2 Paratypes, spiral side; Figure 3 Paratype, peripheral and spiral view, broken last chamber; Figure 4-6, Paratypes, Umbilical view; Figure 7-9, Paratypes, broken specimens showing interior arrangement; Figure 10-11, Paratype umbilical view, kummerform last chamber. Figure 12 Paratype, Peripheral view. Figure 1,11: ODP Hole 1215A, 5H, 5, 18.5-20.5 (35.89 mbsf); Figure 2-3, 6: ODP Hole 1215A, 6H, 3, 128.5 – 130.5 cm (43.49 mbsf); Figure 4, 7-8, ODP Hole 1215A, 008H, 05, 130 – 132 cm (57.50 mbsf); Figure 5, ODP Hole 1215A, 5H, 1, 67 – 69 cm (30.37 mbsf); Figure 9-10: ODP Hole 1215A, 8H, 6, 57 – 59 cm (58.27 mbsf); Figure 12: ODP Hole 1215A, 8H, 2, 57.5 – 59.5 cm (52.28 mbsf).

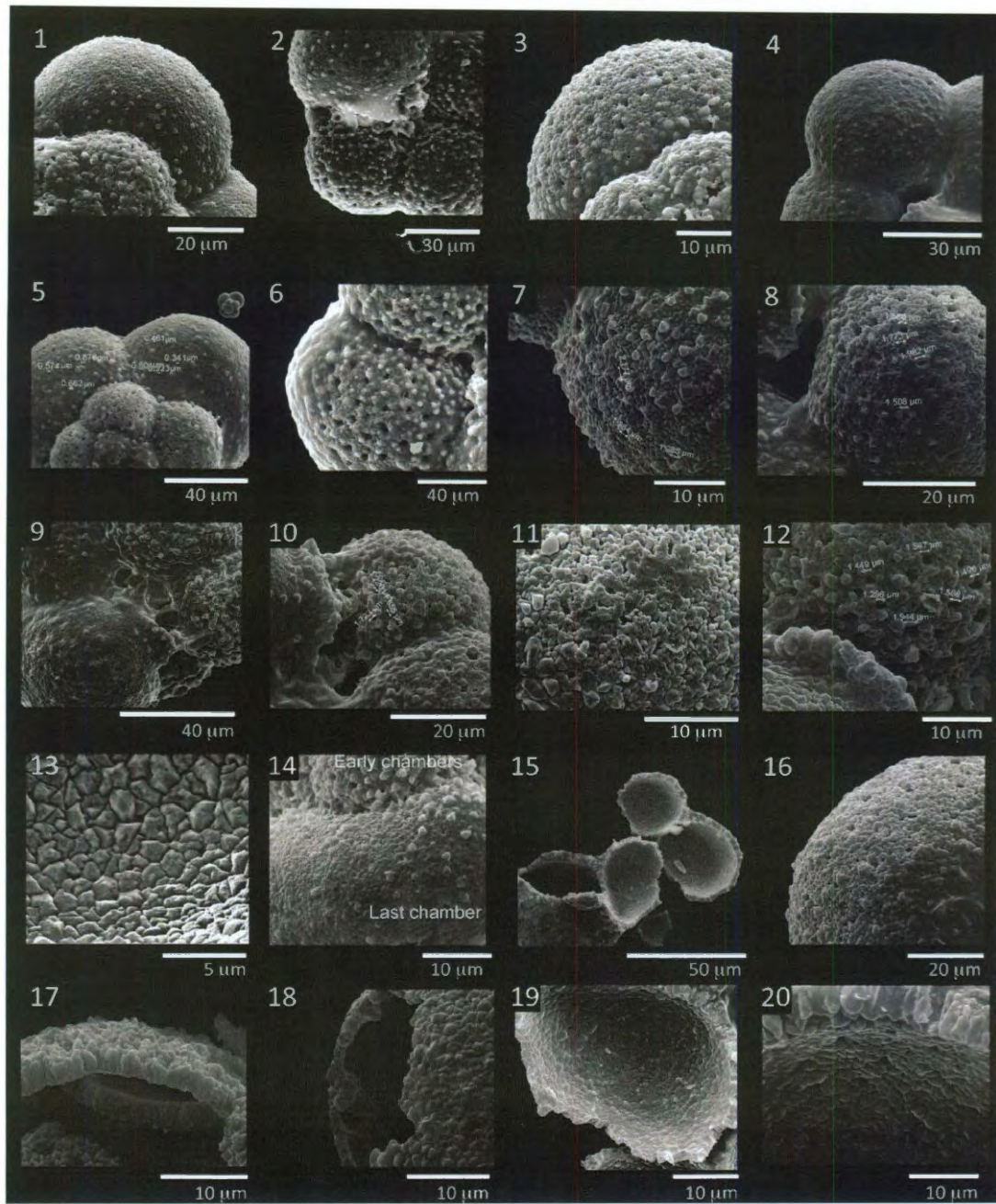


Plate 4.3

Plate 4.3 - *Praetenuitella antica* n.sp. Figure 1 Holotype in Pl.1, detail of wall spiral side, Figure 2 Paratype in Pl.1, 9. Detail of wall and lip, umbilical side, Figure 3 Paratype, detail of wall spiral side, Figure 4 Paratype, detail of wall umbilical side, Figure 5 Paratype, detail recrystallized chambers, spiral view, Figure 6 Paratype, macroperforate wall on umbilical side, Figure 7 Spiral view detail pores and pustules on spiral view, Figure 8 Paratype, Umbilical view detail pores. Figure 9 -10 Paratype, detail of umbilical are, lip on extraumbilical aperture, Figure 11 Paratype, recrystallized wall, penultimate chamber, Figure 12 Paratype, Detail of umbilical area, lip on extraumbilical aperture, Figure 13 Paratype, Detail interior of broken chamber with signs of recrystallization, Figure 14 Paratype, detail last chamber, microperforate and sparsely pustulose wall, Figure 15 Paratype, Purposely broken test to examine wall structure, Figure 16 Paratype, detail of microperforate wall penultimate chamber, Figure 17 – 20 Paratypes, monolamellar wall with visible signs of recrystallization. Figure 1, 5, 7, 16: ODP Hole 1215A, 5H, 5, 18.5-20.5 (35.89 mbsf); Figure 2, 8 – 9, 13 – 15, 19: ODP Hole 1215A, 5H, 1, 67 – 69 cm (30.37 mbsf); Figure 3: ODP Hole 1215A, 8H, 5, 130 – 132 cm (57.50 mbsf); Figure 4, 6, 12, 17, 20: ODP Hole 1215A, 6H, 3, 128.5 – 130.5 cm (43.49 mbsf); Figure 18: ODP Hole 1215A, 8H, 6, 107 – 109 cm (57.50 mbsf)

Sample	Sample ID	Species	Number of Specimens	$\delta^{13}\text{C}$ (‰)	$\delta^{18}\text{O}$ (‰)	Notes
1	U1333A-20X-2, 63	<i>Praetenuitella</i>	60	-6.20	-13.83	Discarded
2	1215A-5H-1, 67	<i>Praetenuitella</i>	50	-5.41	-11.76	Discarded
3	1215A-5H-2, 69	<i>Praetenuitella</i>	100	-0.64	-2.11	
4	1215A-5H-3, 10.5	<i>Praetenuitella</i>	100	-0.47	-1.50	
5	1215A-6H-3, 128.5	<i>Praetenuitella</i>	120	-9.80	-22.01	Discarded
6	1215A-8H-2, 57.5	<i>Praetenuitella</i>	60	-0.55	-2.64	
7	U1333A-20X-2, 63	<i>Subbotina</i>	8	0.90	0.62	
8	U1333A-20X-2, 63	<i>Nuttalides</i>	3	0.27	0.37	
9	1215A-5H-1, 67	<i>Nuttalides</i>	8	0.16	-0.51	
10	1215A-5H-2, 69	<i>Nuttalides</i>	5	0.00	-0.99	
11	1215A-6H-3, 128.5	<i>Nuttalides</i>	7	0.67	-0.37	
12	1215A-8H-2, 57.5	<i>Nuttalides</i>	11	0.17	-0.96	
13	1215A-5H-1, 67	<i>Morozovella</i>	4	2.01	-2.35	
14	1215A-5H-2, 69	<i>Morozovella</i>	5	3.05	-1.20	
15	1215A-5H-3, 10.5	<i>Morozovella</i>	3	0.58	-5.05	Discarded
16	1215A-8H-2, 57.5	<i>Morozovella</i>	2	-21.03	-44.26	Discarded
17	U1333A-20X-2, 63	<i>Chiloguembelina</i>	70	-0.32	-3.90	
18	U1333A-20X-2, 63	<i>Acarinina</i>	10	3.26	-0.70	
19	1215A-5H-1, 67	<i>Acarinina</i>	13	2.15	-1.70	
20	1215A-5H-2, 69	<i>Acarinina</i>	14	1.77	-2.04	
21	1215A-5H-3, 10.5	<i>Acarinina</i>	10	1.41	-2.95	
22	1215A-6H-3, 128.5	<i>Acarinina</i>	4	3.24	-1.56	
23	1215A-8H-2, 57.5	<i>Acarinina</i>	4	2.82	-1.68	

Table 4.1 – Stable isotope analysis of *Praetenuitella antica* n. sp. and other Eocene foraminifera from samples at ODP Site 1215 and IODP Site U1333.

Chapter 5

Conclusions

The sedimentary record at Site 1215 contains a 42 m thick interval of carbonate ooze. This lithologic unit was deposited between 57 and 51.5 Ma, during which the seafloor subsided and moved northwest away from the crest of the Eastern Pacific Rise. The section accumulated below the lysocline, and the termination of Unit II represents passage through the CCD. However, during this time, the depth of the lysocline varied significantly.

Overall, the carbonate content in this unit increased and the preservation of planktic and benthic foraminifera improved upcore through Unit II. This suggests that the lysocline (and CCD) generally deepened at this location from the late Paleocene through the early Eocene. Such an interpretation has been made at other locations, and may signify an increase in the flux of carbon to the ocean. This is important to models of early Paleogene carbon cycling and climate because it implies that one or more boundary conditions are changing during this time.

The carbonate ooze unit also has four relatively short intervals of pronounced carbonate dissolution, that are identified by very low carbonate MARs and strong decrease of planktic and benthic foraminiferal accumulation rates. These are interpreted as geologically brief rises in the lysocline, which correspond with four negative CIEs that have been documented at other locations. The combined dissolution and carbon isotope records at Site 1215 strongly suggest that there were at least four intervals of fairly rapid and massive injection of ^{13}C -depleted carbon that led to ocean acidification. These events are the PETM (55.5 Ma), H1/ETM-2 (53.7 Ma), I1 (53.2 Ma) and K/X (52.5 Ma). Moreover, it is observed that immediately after the hyperthermals and within 200 kyr, carbonate, planktic and benthic foraminiferal accumulation rates improve. These are known as carbonate “overshoots” that likely indicate short-term drops in the lysocline. The mechanism to increase carbonate accumulation immediately after dissolution probably comes from weathering that likely removed CO_2 from the atmosphere and supplied excess Ca^{2+} and HCO_3^- to the ocean.

The record at Site 1215 also indicates that the amount of ^{13}C -depleted carbon input associated to each hyperthermal directly influenced the amount of carbonate dissolution and subsequent accumulation at each time. The greater the ^{13}C -depleted carbon input (CIE event) the lesser the carbonate MARs observed. The same rationality applies for the increase of carbonate MARs after each event. The higher the carbon masses involved, the higher the overcompensation observed immediately after. Carbon cycle modeling and handful observations at other marine sites previously suggested this behavior.

The record at Site 1215 also indicates that planktic foraminifers follow a predictable pattern for selective dissolution. Species of *Acarinina* are preferentially preserved over

Morozovella, which are preferentially preserved over *Subbotina*, *Igorina*, and *Globanomalina*. A tiny and previously overlooked genus, *Praetenuitella*, also appears resistant to dissolution. Despite the imprint of dissolution, changes in the oxygen isotope record and in foraminiferal assemblages suggest that the hyperthermal events at Site 1215 were superimposed on a slight long-term cooling between 55.3 and 52.6 Ma. Thus, warm-water dwellers (*Acarinina* and *Morozovella*) appear soon after the hyperthermals, but cooler-water dwellers (*Praetenuitella*) prevail over the long-term. This long-term cooling differs from most locations, and may reflect northward tectonic migration of the site towards cooler regions with higher influence of seasonal upwelling during this time.

At last, this dissertation documents the finding of a new planktic foraminiferal species, *Praetenuitella antica*, that lived during the latest Paleocene to middle Eocene. Morphological analysis and stable isotope data from this species give supporting evidence to phylogenetically link it to the late Eocene tenuitellids. This means that the tenuitellid “lineage” is roughly 20 myr older than previously documented. *P. antica* n.sp. was probably tolerant to a wide range of temperatures but most likely had preference for cooler temperatures. Moreover, despite that this species had a small size, it was moderately resistant to dissolution as it is found in pelagic sediments that have less than 50% of carbonate content.

References

- Agnini, C., Fornaciari, E., Rio, D., Tateo, F., Backman, J., Giusberti, L., 2007. Responses of calcareous nannofossil assemblages, mineralogy and geochemistry to the environmental perturbations across the Paleocene/Eocene boundary in the Venetian Pre-Alps. *Marine Micropaleontology* 63, 19-38.
- Agnini, C., Macrì, P., Backman, J., Brinkhuis, H., Fornaciari, E., Giusberti, L., Luciani, V., Rio, D., Sluijs, A., Speranza, F., 2009. An early Eocene carbon cycle perturbation at ~52.5 Ma in the Southern Alps: Chronology and biotic response. *Paleoceanography* 24, PA2209.
- Alegret, L., Ortiz, S., Orue-Etxebarria, X., Bernaola, G., Baceta, J.I., Monechi, S., Apellaniz, E., Pujalte, V., 2009. the Paleocene-Eocene Thermal Maximum: New Data on Microfossil Turnover At the Zumaia Section, Spain. *Palaios* 24, 318-328.
- Archer, D., 1996. An atlas of the distribution of calcium carbonate in sediments of the deep sea. *Global Biogeochemical Cycles* 10, 159-174.
- Bé, A.W.H., Morse, J., Harrison, S., 1975. Progressive dissolution and ultrastructural breakdown in planktonic foraminifera, *Dissolution of deep-sea carbonates*, 13 ed. Cushman Foundation Special Publication, Washington, DC, pp. 27-55.
- Berger, W.H., 1968. Planktonic Foraminifera: selective solution and paleoclimatic interpretation. *Deep Sea Research and Oceanographic Abstracts* 15, 31-43.
- Berger, W.H., 1970. Biogenous Deep-Sea Sediments: Fractionation by Deep-Sea Circulation. *Geological Society of America Bulletin* 81, 1385-1402.
- Berger, W.H., 1973. Deep-sea carbonates; Pleistocene dissolution cycles. *The Journal of Foraminiferal Research* 3, 187-195.
- Berger, W.H., Killingley, J., Vincent, E., 1978. Stable isotopes in deep-sea carbonates: Box Core ERDC-92, West Equatorial Pacific. *Oceanologica Acta* 1, 203-216.
- Berggren, W.A., 1977. Atlas of Palaeogene Planktonic Foraminifera, *Oceanic micropalaeontology*. Academic Press, London, pp. 205-300.
- Berggren, W.A., Pearson, P.N., 2005. A revised tropical to subtropical Paleogene planktonic foraminiferal zonation. *The Journal of Foraminiferal Research* 35, 279-298.
- Berggren, W.A., Pearson, P.N., 2006. Tropical to subtropical planktonic foraminiferal zonation of the Eocene, *Atlas of Eocene Planktonic Foraminifera*, 41 ed. Cushman Foundation Special Publication, Fredericksburg, VA, pp. 29-40.

- Birch, G., 1981. The Karbonat-Bombe: A Precise, Rapid and Cheap Instrument for Determining Calcium Carbonate in Sediments and Rocks. *Transactions - Geological Society of South Africa* 84, 199-203.
- Blow, W.H., 1979. The Cainozoic Globigerinida: a study of the morphology, taxonomy, evolutionary relationships and the stratigraphical distribution of some Globigerinida (mainly Globigerinacea), The Netherlands.
- Boersma, A., Premoli-Silva, I., 1983. Paleocene Planktonic Foraminiferal Biogeography and the Paleooceanography of the Atlantic Ocean. *Micropaleontology* 29, 355.
- Boudreau, B.P., Middelburg, J.J., Meysman, F.J.R., 2010. Carbonate compensation dynamics. *Geophysical Research Letters*, 37, L03603.
- Bowen, G., Koch, P., Gingerich, P., Norris, R., 2001. Refined isotope stratigraphy across the continental Paleocene-Eocene boundary on Polecat Bench in the northern Bighorn Basin, Paleocene-Eocene Stratigraphy and Biotic Change in the Bighorn and Clarks Fork Basins, Wyoming, Michigan Papers on Paleontology No. 33. University of Museum of Paleontology, The University of Michigan, Ann Arbor, MI, pp. 73–88.
- Bowen, G.J., Bralower, T.J., Delaney, M.L., Dickens, G.R., Kelly, D.C., Koch, P.L., Kump, L.R., Meng, J., Sloan, L.C., Thomas, E., Wing, S.L., Zachos, J.C., 2006. Eocene Hyperthermal Event Offers Insight Into Greenhouse Warming. *Eos Trans. AGU* 87, 165-169.
- Bowles, J., 2006. Data report: revised magnetostratigraphy and magnetic mineralogy of sediments from Walvis Ridge, Leg 208, in: Kroon, D., Zachos, J.C., Richter, C. (Eds.), *Proceedings of the Ocean Drilling Program, Scientific Results Volume 208*. Ocean Drilling Program, College Station, TX, pp. 1-24.
- Bralower, T.J., 2002. Evidence of surface water oligotrophy during the Paleocene-Eocene thermal maximum: Nannofossil assemblage data from Ocean Drilling Program Site 690, Maud Rise, Weddell Sea. *Paleoceanography* 17, 13-1–13-9.
- Bralower, T.J., Thomas, D.J., Zachos, J.C., Hirschmann, M.M., Röhl, U., Sigurdsson, H., Thomas, E., Whitney, D.L., 1997. High-resolution records of the late Paleocene thermal maximum and circum-Caribbean volcanism: Is there a causal link? *Geology* 25, 963-966.
- Bralower, T.J., Zachos, J.C., Thomas, E., Parrow, M., Paull, C.K., Kelly, D.C., Premoli-Silva, I., Sliter, W.V., Lohmann, K.C., 1995. Late Paleocene to Eocene paleoceanography of the equatorial Pacific Ocean: Stable isotopes recorded at Ocean Drilling Program Site 865, Allison Guyot. *Paleoceanography* 10, 841.

- Bramlette, M., 1961. Pelagic sediments, *Oceanography*. Am. Assoc. Adv. Sci. Pub., Washington, DC, pp. 345-366.
- Brewer, P., Hester, K., 2009. Ocean acidification and the increasing transparency of the ocean to low frequency sound. *Oceanography* 22, 86-93.
- Brinkhuis, H., Zachariasse, W., 1988. Dinoflagellate cysts, sea level changes and planktonic foraminifers across the Cretaceous-Tertiary boundary at El Haria, northwest Tunisia. *Marine Micropaleontology* 13, 153-191.
- Broecker, W.S., Broecker, S., 1974. Carbonate dissolution on the western flank of the East Pacific Rise, *Studies in Paleo-Oceanography*. SEPM (Society for Sedimentary Geology), pp. 44-57.
- Caldeira, K., Wickett, M.E., 2003. Oceanography: anthropogenic carbon and ocean pH. *Nature* 425, 365.
- Cande, S., Kent, D., 1995. Revised calibration of the geomagnetic polarity timescale for the Late Cretaceous and Cenozoic. *Journal of Geophysical Research - Solid Earth* 100, 6093-6095.
- Chaisson, W.P., Leckie, R.M., 1993. High-resolution Neogene planktonic foraminifer biostratigraphy of Site 806, Ontong Java Plateau (western equatorial Pacific). In Berger, W.H., Kroenke, L.W., Mayer, L.A., et al., (Eds.). *Proceedings of the Ocean Drilling Program, Scientific Results 130*. Ocean Drilling Program, College Station, TX, 137-178.
- Colosimo, A., Bralower, T., Zachos, J., 2006. Evidence for lysocline shoaling at the Paleocene/Eocene Thermal Maximum on Shatsky Rise, *Proceedings of the Ocean Drilling Program, Scientific Results Volume 198*. IODP publications.
- Cramer, B., Kent, D.V., 2005. Bolide summer: The Paleocene/Eocene thermal maximum as a response to an extraterrestrial trigger. *Palaeogeography, Palaeoclimatology, Palaeoecology* 224, 144-166.
- Cramer, B.S., Wright, J.D., Kent, D.V., Aubry, M.P., 2003. Orbital climate forcing of $\delta^{13}\text{C}$ excursions in the late Paleocene-early Eocene (chrons C24n-C25n). *Paleoceanography* 18, 1097.
- Cui, Y., Kump, L.R., Ridgwell, A.J., Charles, A.J., Junium, C.K., Diefendorf, A.F., Freeman, K.H., Urban, N.M., Harding, I.C., 2011. Slow release of fossil carbon during the Palaeocene-Eocene Thermal Maximum. *Nature Geoscience* 4, 481-485.
- Darling, K.F., Thomas, E., Kasemann, S.a., Sears, H.a., Smart, C.W., Wade, C.M., 2009. Surviving mass extinction by bridging the benthic/planktic divide.

- Proceedings of the National Academy of Sciences of the United States of America 106, 12629-12633.
- Demicco, R.V., Lowenstein, T.K., Hardie, L.A., 2003. Atmospheric pCO₂ since 60 Ma from records of seawater pH, calcium, and primary carbonate mineralogy. *Society*, 793-796.
- Denman, K.L., Brasseur, G., Chidthaisong, A., Ciais, P., Cox, P.M., Dickinson, R.E., Hauglustaine, D., Heinze, C., Holland, E., Jacob, D., U.Lohmann, Ramachandran, S., Dias, P.L.d.S., Wofsy, S.C., Zhang, X., 2007. Couplings Between Changes in the Climate System and Biogeochemistry., in: Solomon, S., D. Qin, M.M., Z. Chen, M.M., Averyt, K.B., M.Tignor, Miller, H.L. (Eds.), *Climate Change 2007: The Physical Science Basis. Contribution of Working Group I to the Fourth Assessment Report of the Intergovernmental Panel on Climate Change*. Cambridge University Press, Cambridge, United Kingdom and New York, NY, USA.
- D'Hondt, S., Zachos, J.C., Schultz, G., 1994. Stable Isotopic Signals and Photosymbiosis in Late Paleocene Planktic Foraminifera. *Paleobiology* 20, 391-406.
- Dickens, G.R., 2000. Methane oxidation during the late Palaeocene thermal maximum. *Bulletin de la Société géologique de France* 171, 37-49.
- Dickens, G.R., 2011. Methane release from gas hydrate systems during the Paleocene-Eocene thermal maximum and other past hyperthermal events: setting appropriate parameters for discussion. *Climate of the Past Discussions* 7, 1139-1174.
- Dickens, G.R., Castillo, M.M., Walker, J.C.G., 1997. A blast of gas in the latest Paleocene: Simulating first-order effects of massive dissociation of oceanic methane hydrate. *Geology* 25, 259-262.
- Doney, S.C., Balch, W.M., Fabry, V.J., Feely, R.A., 2009. Ocean acidification: a critical emerging problem for the ocean sciences. *Oceanography* 22, 16-25.
- Erez, J., Luz, B., 1983. Experimental paleotemperature equation for planktonic foraminifera. *Geochimica et Cosmochimica Acta* 47, 1025-1031.
- Expedition 320/321 Scientists, 2010a. Methods, in: Pälike, H., Lyle, M., Nishi, H., Raffi, I., Gamage, K., Klaus, A., and the Expedition 320/321 Scientists (Eds.), *Proceedings of the Integrated Ocean Drilling Program, Volume 320/321*, pp. 1-80.
- Expedition 320/321 Scientists, 2010b. Site U1333, in: Pälike, H., Nishi, H., Lyle, M., Raffi, I., Gamage, K., Expedition 320/321 Scientists (Eds.), *Proceedings of the Integrated Ocean Drilling Program, Volume 320/321*, pp. 1-93.

- Farley, K.A., Eltgroth, S.F., 2003. An alternative age model for the Paleocene–Eocene thermal maximum using extraterrestrial ^3He . *Earth and Planetary Science Letters* 208, 135-148.
- Feely, R.A., Doney, S.C., Cooley, S.R., 2009. Ocean Acidification. *Oceanography* 22, 36-47.
- Forster, P., Ramaswamy, V., Artaxo, P., Bernsten, T., Betts, R., Fahey, D.W., Haywood, J., Lean, J., Lowe, D.C., Myhre, G., others, 2007. Changes in atmospheric constituents and in radiative forcing, in: Solomon, S., Qin, D., Manning, M., Chen, Z., Marquis, M., Averyt, K.B., M.Tignor, Miller, H.L. (Eds.), *Climate Change 2007: The Physical Science Basis. Contribution of Working Group I to the Fourth Assessment Report of the Intergovernmental Panel on Climate Change*. Cambridge University Press, Cambridge, United Kingdom and New York, NY, USA., pp. 129-234.
- Galeotti, S., Krishnan, S., Pagani, M., Lanci, L., Gaudio, A., Zachos, J.C., Monechi, S., Morelli, G., Lourens, L., 2010. Orbital chronology of Early Eocene hyperthermals from the Contessa Road section, central Italy. *Earth and Planetary Science Letters* 290, 192-200.
- Hancock, H.J.L., Dickens, G.R., 2005. Carbonate dissolution episodes in Paleocene and Eocene sediment, Shatsky Rise, west-central Pacific, *Proceedings of the Ocean Drilling Program, Scientific Results Volume* 198.
- Hancock, H.J.L., Dickens, G.R., Thomas, E., Blake, K.L., 2007. Reappraisal of early Paleogene CCD curves: foraminiferal assemblages and stable carbon isotopes across the carbonate facies of Perth Abyssal Plain. *International Journal of Earth Sciences* 96, 925-946.
- Hecht, A., Eslinger, E., Garmon, L., 1975. Experimental studies on the dissolution of planktonic foraminifera, in: Sliter, W.V., Bé, A.W.H., Berger, W.H. (Eds.), *Dissolution of Deep-Sea Carbonates*. Cushman Foundation Special Publication 13, Washington, DC, pp. 56-69.
- Herguera, J., 1992. Deep-sea benthic foraminifera and biogenic opal: Glacial to postglacial productivity changes in the western equatorial Pacific. *Marine Micropaleontology* 19, 79-98.
- Herguera, J.C., Berger, W., 1991. Paleoproductivity from benthic foraminifera abundance: Glacial to postglacial change in the west-equatorial Pacific. *Geology* 19, 1173.

- Hilting, A.K., Kump, L.R., Bralower, T.J., 2008. Variations in the oceanic vertical carbon isotope gradient and their implications for the Paleocene-Eocene biological pump. *Paleoceanography* 23, 1-15.
- Hollis, C.J., Dickens, G.R., Field, B.D., Jones, C.M., Percy Strong, C., 2005. The Paleocene–Eocene transition at Mead Stream, New Zealand: a southern Pacific record of early Cenozoic global change. *Palaeogeography, Palaeoclimatology, Palaeoecology* 215, 313-343.
- Huber, B.T., 1991. Paleogene and Early Neogene Planktonic Foraminiferal Biostratigraphy of Sites 738 AND 744, Kerguelen Plateau (Southern Indian Ocean), in: Barron, J., Larsen, B., et al. (Ed.), *Proceedings of the Ocean Drilling Program, Scientific Results 119*. College Station, pp. 427-449.
- Huber, B.T., Olsson, R., Pearson, P., 2006. Taxonomy, biostratigraphy, and phylogeny of Eocene microporiferate planktonic foraminifera (*Jenkinsina*, *Cassigerinelloita*, *Chiloguembelina*, *Streptochilus*, *Zeauvigerina*, *Tenuitella*, and *Cassigerinella*) and problematica (*Dipsidripella*), in: Pearson PN, O.R., Huber BT, Hemleben C, Berggren WA (Ed.), *Atlas of Eocene planktonic Foraminifera*. Cushman Foundation for Foraminiferal Research Special Publication, pp. 461-508.
- Huber, M., 2002. Straw man 1: A preliminary view of the tropical Pacific from a global coupled climate model simulation of the early Paleogene., in: Lyle, M., Wilson, P.A., Janecek, T.R., et al. (Ed.), *Proceedings of the Ocean Drilling Program, Initial Reports Volume 199*, pp. 1-30.
- Jones, S., Maclennan, J., 2006. Regional uplift, gas hydrate dissociation and the origins of the Paleocene–Eocene Thermal Maximum. *Earth and Planetary Science Letters* 245, 65-80.
- Kelly, D.C., 2002. Response of Antarctic (ODP Site 690) planktonic foraminifera to the Paleocene–Eocene thermal maximum: Faunal evidence for ocean/climate change. *Paleoceanography* 17, 101029/.
- Kelly, D.C., Bralower, T.J., Zachos, J.C., 1998. Evolutionary consequences of the latests Paleocene thermal maximum for tropical planktonic foraminifera. *Palaeogeography, Palaeoclimatology, Palaeoecology* 141, 139-161.
- Kelly, D.C., Bralower, T.J., Zachos, J.C., Premoli-Silva, I., Thomas, E., 1996. Rapid diversification of planktonic foraminifera in the tropical Pacific (ODP Site 865) during the late Paleocene thermal maximum. *Geology* 24, 423.
- Kelly, D.C., Nielsen, T.M.J., McCarren, H.K., Zachos, J.C., Röhl, U., 2010. Spatiotemporal patterns of carbonate sedimentation in the South Atlantic:

- Implications for carbon cycling during the Paleocene–Eocene thermal maximum. *Palaeogeography, Palaeoclimatology, Palaeoecology* 293, 30-40.
- Kelly, D.C., Zachos, J.C., Bralower, T.J., Schellenberg, S.A., 2005. Enhanced terrestrial weathering/runoff and surface ocean carbonate production during the recovery stages of the Paleocene-Eocene thermal maximum. *Paleoceanography* 20, 101029/.
- Kennett, J.P., Srinivasan, M., 1983. *Neogene Planktonic Foraminifera: A Phylogenetic Atlas*. Hutchinson Ross Publishing Company, Stroudsburg, United States (USA).
- Kennett, J.P., Stott, L.D., 1991. Abrupt deep-sea warming, palaeoceanographic changes and benthic extinctions at the end of the Palaeocene. *Nature* 353, 225-229.
- Kent, D.V., Cramer, B.S., Lanci, L., Wang, D., Wright, J.D., Van der Voo, R., 2003. A case for a comet impact trigger for the Paleocene/Eocene thermal maximum and carbon isotope excursion. *Earth and Planetary Science Letters* 211, 13-26.
- Kleypas, J., Buddemeier, R., Archer, D., Gattuso, J., 1999. Geochemical consequences of increased atmospheric carbon dioxide on coral reefs. *Science* 284: 118-120.
- Kleypas, J.A., Yates, K.K., 2009. *Coral Reefs and Ocean Acidification*. *Oceanography* 22, 108-117.
- Koch, P.L., Zachos, J.C., Gingerich, P.D., 1992. Correlation between isotope records in marine and continental carbon reservoirs near the Palaeocene/Eocene boundary. *Nature* 358, 319-322.
- Kump, L.R., Bralower, T.J., Ridgwell, A., 2009. *Ocean Acidification in Deep Time*. *Oceanography* 22, 94-107.
- Leckie, R.M., 2009. Seeking a better life in the plankton. *Proceedings of the National Academy of Sciences of the United States of America* 106, 14183-14184.
- Leckie, R.M., Farnham, C., Schmidt, M.G., 1993. Oligocene planktonic foraminifer biostratigraphy of hole 803d (ontong java plateau) and hole 628a (little bahama bank), and comparison with the southern high latitudes, in: Berger, W.H., Kroenke, L.W., Mayer, L.A. (Eds.), *Proceedings of the Ocean Drilling Program, Scientific Results 130*. Ocean Drilling Program, College Station, TX, pp. 113-136.
- Leon-Rodriguez, L., Dickens, G.R., 2010. Constraints on ocean acidification associated with rapid and massive carbon injections : The early Paleogene record at ocean drilling program site 1215 , Equatorial Pacific Ocean. *Palaeogeography, Palaeoclimatology, Palaeoecology* 298, 409-420.

- Leon-Rodriguez, L., Dickens, G.R., Leckie, R.M., Submitted. Carbonate and Foraminiferal Accumulation across the Lower Paleogene record at ODP Site 1215, eastern Equatorial Pacific Ocean Marine Micropaleontology.
- Li, Q., 1987. Origin, phylogenetic development and systematic taxonomy of the *Tenuitella plexus* (Globigerinitidae Globigerininina). *The Journal of Foraminiferal Research* 17, 298-320.
- Li, Q., Jian, Z., Li, B., 2004. Oligocene–Miocene planktonic foraminifer biostratigraphy, Site 1148, northern South China Sea., in: Prell, W.L., Wang, P., Blum, P., Rea, D.K., and Clemens, S.C (Ed.), *Proceeding of the Ocean Drilling Program, Initial Reports ODP, Scientific Results*, 184, pp. 1-26.
- Li, Q., McGowran, B., Boersma, A., 1995. Early Palaeocene *Parvularugoglobigerina* and late Eocene *Praetenuitella*: does evolutionary convergence imply similar habitat? *Journal of Micropalaeontology* 14, 119-134.
- Li, Q., McGowran, B., James, N.P., 2003. Eocene–Oligocene planktonic foraminiferal biostratigraphy of Sites 1126, 1130, 1132, and 1134, ODP Leg 182, Great Australian Bight, in: Hine, A.C., Feary, D.A., and Malone, M.J. (Ed.), *Proceedings of the Ocean Drilling Program, Scientific Results* 182, pp. 1-28.
- Li, Q., Radford, S.S., 1991. Evolution and biogeography of Paleogene microperforate planktonic foraminifera. *Palaeogeography, Palaeoclimatology, Palaeoecology* 83, 87-115.
- Li, Q., Radford, S.S., Banner, F.T., 1992. Distribution of Microperforate Tenuitellid Planktonic Foraminifera in Holes 747A and 749B, Kerguelen Plateau, in: Wise, S.W., Schlich, R. (Eds.), *Proceeding of the Ocean Drilling Program, Scientific Results*, 120, pp. 569-594.
- Liu, C., Browning, J.V., Miller, K.G., Olsson, R.K., 1997. Upper Cretaceous to Miocene planktonic foraminiferal biostratigraphy: results of Leg 150X, the New Jersey Coastal Plain Drilling Project, pp. 111-128, in: Miller, K.G., Snyder, S.W. (Eds.), *Proceedings of the Ocean Drilling Program, Scientific Results* 150X, pp. 111-127.
- Liu, C., Olsson, R.K., 1992. Evolutionary radiation of microperforate planktonic Foraminifera following the K/T mass extinction event. *The Journal of Foraminiferal Research* 22, 328-346.
- Liu, C., Olsson, R.K., Hubert, B.T., 1998. A benthic paleohabitat for *Praepararotalia* gen. nov. and *Antarcticella* Loeblich and Tappan. *The Journal of Foraminiferal Research* 28, 3.

- Lourens, L.J., Sluijs, A., Kroon, D., Zachos, J.C., Thomas, E., Röhl, U., Bowles, J., Raffi, I., 2005. Astronomical pacing of late Palaeocene to early Eocene global warming events. *Nature* 435, 1083-1087.
- Lu, G., Keller, G., 1993. The Paleocene-Eocene transition in the Antarctic Indian Ocean: Inference from planktic foraminifera. *Marine Micropaleontology* 21, 101-142.
- Lu, G., Keller, G., 1995. Ecological stasis and saltation: species richness change in planktic foraminifera during the late Paleocene to early Eocene, DSDP Site 577, Palaeogeography, Palaeoclimatology, Palaeoecology, pp. 211-227.
- Luciani, V., Giusberti, L., Agnini, C., Backman, J., Fornaciari, E., Rio, D., 2007. The Paleocene–Eocene Thermal Maximum as recorded by Tethyan planktonic foraminifera in the Forada section (northern Italy). *Marine Micropaleontology* 64, 189-214.
- Lyle, M., 2003. Neogene carbonate burial in the Pacific Ocean. *Paleoceanography* 18.
- Lyle, M.W., Wilson, P.A., 2002. Leg 199 Summary. Proceedings of the Ocean Drilling Program, Initial Reports 199. Ocean Drilling Program. College Station, TX, pp. 1–87.
- Lyle, M.W., Wilson, P.A., 2006. Leg 199 synthesis: evolution of the equatorial Pacific in the early Cenozoic, Proceedings of the Ocean Drilling Program, Scientific Results, 199. Ocean Drilling Program, College Station, TX, pp. 1–39.
- Martini, E., 1971. Standard Tertiary and Quaternary calcareous nannoplankton zonation. Proceedings of the 2nd Planktonic Conference., 739–785.
- Mcgowran, B., 1989. Silica burp in the Eocene ocean. *Geology* 17, 857-860.
- McInerney, F.a., Wing, S.L., 2010. The Paleocene-Eocene Thermal Maximum—a Perturbation of Carbon Cycle, Climate, and Biosphere with Implications for the Future. *Annual Review of Earth and Planetary Sciences* 39, 110301095600077.
- Moore, T.C., 2004. Paleogene tropical Pacific: Clues to circulation, productivity, and plate motion. *Paleoceanography* 19.
- Müller, G., Gastner, M., 1971. The "Karbonat-Bombe"TM, a simple device for the determination of the calcium carbonate content in sediments, soils and other minerals. *Neues Jahrbuch für Mineralogie* 10, 466-469.
- Murphy, B.H., Farley, K.a., Zachos, J.C., 2010. An extraterrestrial ³He-based timescale for the Paleocene–Eocene thermal maximum (PETM) from Walvis Ridge, IODP Site 1266. *Geochimica et Cosmochimica Acta* 74, 5098-5108.

- Nguyen, T.M.P., Petrizzo, M.R., Speijer, R.P., 2009. Experimental dissolution of a fossil foraminiferal assemblage (Paleocene–Eocene Thermal Maximum, Dababiya, Egypt): Implications for paleoenvironmental reconstructions. *Marine Micropaleontology* 73, 241-258.
- Nicolo, M.J., Dickens, G.R., Hollis, C.J., 2010. South Pacific intermediate water oxygen depletion at the onset of the Paleocene - Eocene thermal maximum as depicted in New Zealand margin sections. 25, 1-12.
- Nicolo, M.J., Dickens, G.R., Hollis, C.J., Zachos, J.C., 2007. Multiple early Eocene hyperthermals: Their sedimentary expression on the New Zealand continental margin and in the deep sea. *Geology* 35, 699.
- Nomura, R., Takata, H., 2005. Data report: Paleocene/Eocene benthic foraminifers, ODP Leg 199 Sites 1215, 1220, and 1221, equatorial central Pacific Ocean, in: Wilson, P.A., Lyle, M., Firth, J.V. (Eds.), *Proceedings of the Ocean Drilling Program, Scientific Results 199*, College Station, TX, pp. 1-34.
- Norris, R.D., 1996. Symbiosis as an Evolutionary Innovation in the Radiation of Paleocene Planktic Foraminifera. *Paleobiology* 22, 461-480.
- O'Connor, J.M., Duncan, R.a., 1990. Evolution of the Walvis Ridge-Rio Grande Rise Hot Spot System: Implications for African and South American Plate Motions Over Plumes. *Journal of Geophysical Research* 95, 17475-17502.
- Olsson, R., K., Hemleben, C., Berggren, W.A., Huber, B.T., 1999. *Atlas of Paleocene planktonic Foraminifera.*, 85 Edition. Smithsonian Contributions to Paleobiology, Washington, DC.
- Orr, J.C., Caldeira, K., Fabry, V.J., Gattuso, J., Haugan, P., Lehodey, P., Pantoja, S., Portner, H.-O., Riebesell, U., Trull, T., Urban, E., Hood, M., Broadgate, W., 2009. research priorities for understanding Ocean acidification. *Oceanography* 22, 182-189.
- Orr, J.C., Fabry, V.J., Aumont, O., Bopp, L., Doney, S.C., Feely, R.A., Gnanadesikan, A., Gruber, N., Ishida, A., Joos, F., Key, R.M., Lindsay, K., Maier-Reimer, E., Matear, R., Monfray, P., Mouchet, A., Najjar, R.G., Plattner, G.-K., Rodgers, K.B., Sabine, C.L., Sarmiento, J.L., Schlitzer, R., Slater, R.D., Totterdell, I.J., Weirig, M.-F., Yamanaka, Y., Yool, A., 2005. Anthropogenic ocean acidification over the twenty-first century and its impact on calcifying organisms. *Nature* 437, 681-686.
- Pagani, M., Pedentchouk, N., Huber, M., Sluijs, A., Schouten, S., Brinkhuis, H., {Sinninghe Damsté}, J.S., Dickens, G.R., Backman, J., Clemens, S., Cronin, T., Eynaud, F., Gattacceca, J., Jakobsson, M., Jordan, R., Kaminski, M., King, J.,

- Koc, N., Martinez, N.C., McInroy, D., {Moore Jr}, T.C., O'Regan, M., Onodera, J., Pälike, H., Rea, B., Rio, D., Sakamoto, T., Smith, D.C., {St John}, K.E.K., Suto, I., Suzuki, N., Takahashi, K., Watanabe, M., Yamamoto, M., 2006. Arctic hydrology during global warming at the Palaeocene/Eocene thermal maximum. *Nature* 442, 671-675.
- Pälike, H., Nishi, H., Lyle, M., Raffi, I., Gamage, K., Klaus, A., 2010. Expedition 320/321 Summary, Proceedings of the Integrated Ocean Drilling Program, Volume 320/321. Integrated Ocean Drilling Program Management International, Inc., pp. 1-141.
- Panchuk, K., Ridgwell, A., Kump, L.R., 2008. Sedimentary response to Paleocene-Eocene Thermal Maximum carbon release: A model-data comparison. *Geology* 36, 315.
- Parsons, B., Sclater, J.G., 1977. An analysis of the variation of ocean floor bathymetry and heat flow with age. *Journal of Geophysical Research* 82, 803-827.
- Pearson, P.N., Ditchfield, P.W., Singano, J., Harcourt-Brown, K.G., Nicholas, C.J., Olsson, R.K., Shackleton, N.J., Hall, M.a., 2001. Warm tropical sea surface temperatures in the Late Cretaceous and Eocene epochs. *Nature* 413, 481-487.
- Pearson, P.N., Norris, R.N., J., E.A., 2001. *Mutabella mirabilis* gen. et sp nov., a Miocene microperforate planktonic foraminifer with an extreme level of intraspecific variability. *The Journal of Foraminiferal Research* 31, 120-132.
- Pearson, P.N., Olsson, R.K., Huber, B.T., Hemleben, C., Berggren, W.A., 2006. Atlas of Eocene planktonic foraminifera, 41 ed. Cushman Foundation Special Publication, Fredericksburg, VA.
- Pearson, P.N., Wade, B.S., 2009. Taxonomy and Stable Isotope Paleoecology of Well-Preserved Planktonic Foraminifera From the Uppermost Oligocene of Trinidad. *The Journal of Foraminiferal Research* 39, 191-217.
- Peterson, M.R., 1966. Calcite: Rates of Dissolution in a Vertical Profile in the Central Pacific. *Science* 154, 1542.
- Petrizzo, M.R., 2007. The onset of the Paleocene–Eocene Thermal Maximum (PETM) at Sites 1209 and 1210 (Shatsky Rise, Pacific Ocean) as recorded by planktonic foraminifera. *Marine Micropaleontology* 63, 187-200.
- Petrizzo, M.R., Leoni, G., Speijer, R.P., {De Bernardi}, B., Felletti, F., 2008. Dissolution Susceptibility of Some Paleogene Planktonic Foraminifera From ODP Site 1209 (Shatsky Rise, Pacific Ocean). *The Journal of Foraminiferal Research* 38, 357-371.

- Poag, C.W., Commeau, J.a., 1995. Paleocene to middle Miocene planktic foraminifera of the southwestern Salisbury Embayment, Virginia and Maryland; biostratigraphy, allostratigraphy, and sequence stratigraphy. *The Journal of Foraminiferal Research* 25, 134-155.
- Raffi, I., Backman, J., Palike, H., 2005. Changes in calcareous nannofossil assemblages across the Paleocene/Eocene transition from the paleo-equatorial Pacific Ocean. *Palaeogeography, Palaeoclimatology, Palaeoecology* 226, 93-126.
- Rea, D.K., Lyle, M., 2005. Paleogene calcite compensation depth in the eastern subtropical Pacific: Answers and questions. *Paleoceanography* 20, PA1012.
- Ridgwell, A., Schmidt, D.N., 2010. Past constraints on the vulnerability of marine calcifiers to massive carbon dioxide release. *Nature Geoscience* 3, 196-200.
- Ridgwell, A., Zeebe, R., 2005. The role of the global carbonate cycle in the regulation and evolution of the Earth system. *Earth and Planetary Science Letters* 234, 299-315.
- Ries, J.B., Cohen, A.L., McCorkle, D.C., 2009. Marine calcifiers exhibit mixed responses to CO₂-induced ocean acidification. *Geology* 37, 1131-1134.
- Röhl, U., Westerhold, T., Monechi, S., Thomas, E., Zachos, J.C., Donner, B., 2006. The third Early Eocene Thermal Maximum: Characteristics, Timing, and Mechanisms of the "X" Event. *Geophysical Research Abstracts* 8, 8-9.
- Sexton, P., 2005. Foraminiferal taphonomy, palaeoecology and palaeoceanography of the Eocene. University of Southampton & Southampton Oceanography Centre, Southampton, UK.
- Shipboard Scientific Party, 2002a. Leg 199 Summary, in: Lyle, M., Wilson, P.A., Janecek, T.R., et al. (Ed.), *Proceedings of the Ocean Drilling Program, 199, Initial Reports*, Ocean Drilling Program, College Station, TX, pp. 1-87.
- Shipboard Scientific Party, 2002b. Site 1215, in: Lyle, M., Wilson, P.A., Janecek, T.R., et al. (Ed.), *Proceedings of the Ocean Drilling Program, Initial Reports 199, Ocean Drilling Program*, College Station, TX, pp. 1-60.
- Shipboard Scientific Party, 2002c. Explanatory Notes, in: Lyle, M., Wilson, P.A., Janecek, T.R., et al. (Ed.), *Proceedings of the Ocean Drilling Program, Initial Reports 199*, pp. 1-70.
- Shipboard Scientific Party, 2002d. Leg 198 Summary, in: Bralower, T.J., Premoli-Silva, I., Malone, M.J. et al. (Ed.), *Proceedings of the Ocean Drilling Program, Initial Reports 198*, pp. 1-148.

- Shipboard Scientific Party, 2004. Site 1262, in: Zachos, J.C, Kroon, D., Blum, P. et al. (Eds.), *Proceedings of the Ocean Drilling Program, Initial Reports 208*, Ocean Drilling Program, College Station, TX pp. 1-92.
- Sluijs, A., Bowen, G., Brinkhuis, H., Lourens, L., Thomas, E., 2007a. The Palaeocene-Eocene Thermal Maximum super greenhouse: biotic and geochemical signatures. age models and mechanisms of global change, *Deep-Time Perspectives on Climate Change: Marrying the Signal from Computer Models and Biological Proxies*. The Micropaleontological Society, Special Publications, London, pp. 323-349.
- Sluijs, A., Brinkhuis, H., Schouten, S., Bohaty, S.M., John, C.M., Zachos, J.C., Reichart, G.-J., Sinninghe Damsté, J.S., Crouch, E.M., Dickens, G.R., 2007b. Environmental precursors to rapid light carbon injection at the Palaeocene/Eocene boundary. *Nature* 450, 1218-1221.
- Sluijs, A., Schouten, S., Donders, T.H., Schoon, P.L., Röhl, U., Reichart, G.-J., Sangiorgi, F., Kim, J.-H., Sinninghe Damsté, J.S., Brinkhuis, H., 2009. Warm and wet conditions in the Arctic region during Eocene Thermal Maximum 2. *Nature Geoscience* 2, 777-780.
- Sluijs, A., Schouten, S., Pagani, M., Woltering, M., Brinkhuis, H., Sinninghe Damsté, J.S., Dickens, G.R., Huber, M., Reichert, G.-J., Stein, R., Matthiessen, J., Lourens, L.J., Pedentchouk, N., Backman, J., Moran, K., 2006. Subtropical Arctic Ocean temperatures during the Palaeocene/Eocene thermal maximum. *Nature* 441, 610-613.
- Smith, W.H., Sandwell, D.T., 1997. Global Sea Floor Topography from Satellite Altimetry and Ship Depth Soundings. *Science* 277, 1956-1962.
- Stap, L., Lourens, L.J., Thomas, E., Sluijs, A., Bohaty, S., Zachos, J.C., 2010. High-resolution deep-sea carbon and oxygen isotope records of Eocene Thermal Maximum 2 and H2. *Geology* 38, 607-610.
- Stap, L., Sluijs, A., Lourens, L.J., Thomas, E., 2009. Patterns and magnitude of deep sea carbonate dissolution during Eocene Thermal Maximum 2 and H2, Walvis Ridge, southeastern Atlantic Ocean. *Paleoceanography* 24, PA1211.
- Svensen, H., Planke, S., Malthe-Sørenssen, A., Jamtveit, B., Myklebust, R., Rasmussen Eidem, T., Rey, S.S., 2004. Release of methane from a volcanic basin as a mechanism for initial Eocene global warming. *Nature* 429, 542-545.
- Takahashi, T., Broecker, W., 1977. Mechanisms for calcite dissolution on the sea floor, in: Andersen, N.R., Malahoff, A. (Eds.), *The Fate of Fossil Fuel CO₂ in the Oceans*. Plenum Press, New York, N.Y., United States (USA), pp. 455-477.

- Tans, P., 2009. An accounting of the observed increase in oceanic and atmospheric CO₂ and an Outlook for the Future. *Oceanography* 22, 26-35.
- Thomas, E., 1998. Biogeography of the late Paleocene benthic foraminiferal extinction, in: Aubry, M.P., Lucas, S., Berggren, W.A. (Eds.), Late Paleocene-early Eocene climatic and biotic events in the marine and terrestrial records. Columbia University Press, New York, pp. 214-243.
- Thomas, E., 2007. Cenozoic mass extinctions in the deep sea: What perturbs the largest habitat on Earth? *GSA Special Papers* 424, 1-23.
- Thomas, E., Shackleton, N.J., 1996. The Paleocene-Eocene benthic foraminiferal extinction and stable isotope anomalies. *Geological Society, London, Special Publications* 101, 401-441.
- Thunell, R., Honjo, S., 1981. Calcite dissolution and the modification of planktonic foraminiferal assemblages. *Marine Micropaleontology* 6, 169-182.
- Van Andel, T., 1975. Mesozoic/cenozoic calcite compensation depth and the global distribution of calcareous sediments. *Earth and Planetary Science Letters* 26, 187-194.
- Walker, J.C.G., Hays, P.B., Kasting, J.F., 1981. A negative feedback mechanism for the long-term stabilization of Earth's surface temperature. *Journal of Geophysical Research* 86, 9776-9782.
- Walker, J.C.G., Kasting, J.F., 1992. Effects of fuel and forest conservation on future levels of atmospheric carbon dioxide. *Palaeogeography, Palaeoclimatology, Palaeoecology* 97, 151-189.
- Westerhold, T., Röhl, U., 2009. High resolution cyclostratigraphy of the early Eocene – new insights into the origin of the Cenozoic cooling trend. *Climate of the Past* 5, 309-327.
- Westerhold, T., Röhl, U., Laskar, J., Raffi, I., Bowles, J., Lourens, L.J., Zachos, J.C., 2007. On the duration of magnetochrons C24r and C25n and the timing of early Eocene global warming events: Implications from the Ocean Drilling Program Leg 208 Walvis Ridge depth transect. *Paleoceanography* 22, 1-19.
- Westerhold, T., Röhl, U., Raffi, I., Fornaciari, E., Monechi, S., Reale, V., Bowles, J., Evans, H.F., 2008. Astronomical calibration of the Paleocene time. *Palaeogeography, Palaeoclimatology, Palaeoecology* 257, 377-403.
- Wing, S.L., Harrington, G.J., Smith, F.a., Bloch, J.I., Boyer, D.M., Freeman, K.H., 2005. Transient floral change and rapid global warming at the Paleocene-Eocene boundary. *Science* 310, 993-996.

- Zachos, J.C., Bohaty, S., John, C., McCarren, H., 2007. The Paleocene-Eocene carbon isotope excursion: Constraints from individual shell planktonic foraminifera records. *Philosophical Transactions of the Royal Society A*, 365: 1829-1842.
- Zachos, J.C., Dickens, G.R., Zeebe, R.E., 2008. An early Cenozoic perspective on greenhouse warming and carbon-cycle dynamics. *Nature* 451, 279-283.
- Zachos, J.C., McCarren, H., Murphy, B., Röhl, U., Westerhold, T., 2010. Tempo and scale of late Paleocene and early Eocene carbon isotope cycles : Implications for the origin of hyperthermals. *Earth and Planetary Science Letters* 299, 242-249.
- Zachos, J.C., Pagani, M., Sloan, L., Thomas, E., Billups, K., 2001. Trends, rhythms, and aberrations in global climate 65 Ma to present. *Science* 292, 686-693.
- Zachos, J.C., Röhl, U., Schellenberg, S.A., Sluijs, A., Hodell, D.A., Kelly, D.C., Thomas, E., Nicolo, M., Raffi, I., Lourens, L.J., McCarren, H., Kroon, D., 2005. Rapid acidification of the ocean during the Paleocene-Eocene thermal maximum. *Science* 308, 1611-1615.
- Zachos, J.C., Schellenberg, S.A., Röhl, U., Hodell, D.A., Sluijs, A., Kelly, D.C., Thomas, E., Nicolo, M.J., Lourens, L.J., Raffi, I., McCarren, H., Kroon, D., 2005. Rapid acidification of the ocean during the Paleocene-Eocene thermal maximum. *Science* 308, 1611-1615.
- Zachos, J.C., Stott, L.D., Lohmann, K.C., 1994. Evolution of Early Cenozoic marine temperatures. *Paleoceanography* 9, 353.
- Zachos, J.C., Wara, M.W., Bohaty, S., Delaney, M.L., Petrizzo, M.R., Brill, A., Bralower, T.J., Premoli-Silva, I., 2003. A transient rise in tropical sea surface temperature during the Paleocene-Eocene thermal maximum. *Science* 302, 1551-1554.
- Zeebe, R.E., 2011. Where are you heading Earth? *Nature Geoscience* 4, 416-417.
- Zeebe, R.E., Zachos, J.C., 2007. Reversed deep-sea carbonate ion basin gradient during Paleocene-Eocene thermal maximum. *Paleoceanography* 22, PA3201.
- Zeebe, R.E., Zachos, J.C., Caldeira, K., Tyrrell, T., 2008. Carbon emissions and acidification. *Science* 321, 51-52.
- Zeebe, R.E., Zachos, J.C., Dickens, G.R., 2009. Carbon dioxide forcing alone insufficient to explain Palaeocene–Eocene Thermal Maximum warming. *Nature Geoscience* 2, 576-580.

Appendix A

DATA REPORT: Stable Isotope and Carbonate Content Analyses of the Middle to Upper Eocene Sediments at IODP Sites U1332 and U1333.

ABSTRACT

Stable isotope and carbonate content analyses were conducted on bulk sediment from the Integrated Ocean Drilling Program (IODP) Sites U1332 and U1333. We generated records from three of the holes (U1332 A and B, and U1333 A), which sampled marine pelagic sediments dominated by alternations of nannofossil and radiolarian oozes that accumulated from the middle to the late Eocene. These data are necessary to investigate short-term and long-term variations in the carbon cycle and their effect on pelagic carbonate accumulation. Carbonate-rich horizons found in the middle to upper Eocene likely correspond to previously documented CAE's 2-7. Bulk $\delta^{18}\text{O}$ in Site U1332 fluctuates between -3.60 and 2.25‰ while in Site U1333 fluctuates between -1.85 and 0.28‰. Bulk $\delta^{13}\text{C}$ in Site U1332 fluctuates between -1.02 and 5.06‰ while in Site U1333 fluctuates between 1.41 and 3.49 ‰. This detailed stable isotope stratigraphy provides a high-resolution record that improves the current reference curves available from the middle Eocene to lower Oligocene in the equatorial Pacific Ocean.

A.1. Introduction

Profound changes in the global carbon cycle occurred during the Paleogene, which are evidenced by a series of shifts in the stable carbon isotope composition of carbonate and organic carbon (Zachos et al., 2001; Zachos et al., 2008). The most prominent $\delta^{13}\text{C}$ high of the Cenozoic occurred during the late Paleocene (~59-56 Ma), a time of transition from relatively cool to relatively warm conditions and presumably massive deposition of organic carbon (Shackleton and Hall, 1984). This was followed by a long-term decline in global $\delta^{13}\text{C}$ records. Although the nature of this change remains an open issue, it was punctuated by several brief events characterized by extreme depletion in $\delta^{13}\text{C}$ (Cramer et al., 2003; Lourens et al., 2005; Thomas and Zachos, 2000; Thomas et al., 2000). The most pronounced of these events occurred across the Paleocene/Eocene thermal maximum (PETM) which began at ~55.5 Ma (Bowen and others, 2006; Kennett and Stott, 1991; Sluijs et al., 2007). For this <200 kyr aberration, the negative $\delta^{13}\text{C}$ excursion clearly signifies a massive injection of ^{13}C -depleted carbon to the ocean and atmosphere (Dickens et al., 1997; Katz et al., 1999). After the PETM and several other carbon isotope anomalies, $\delta^{13}\text{C}$ records of carbonate plunge to a minimum centered at ~52 Ma. This interval of very low $\delta^{13}\text{C}$ may include additional carbon events, each associated with a negative $\delta^{13}\text{C}$ excursion. It also ushers in the early Eocene Climatic Optimum (EECO), the time of peak Cenozoic global temperatures. All proxy indicators suggest high atmospheric pCO_2 for much of the early Paleogene, particularly around the EECO, although the amount is a contentious issue (Pearson and Palmer, 2000; Yapp, 2004).

The PETM and other carbon injection events may represent possible analogs to understand and estimate Earth's responses to anthropogenic carbon input. The source, cause, nature, mass, and number of carbon injections occurred in early Paleogene remain uncertain ((Dickens, 2011; Sluijs et al., 2007). One of the biggest problems is that the community lacks detailed records of the early Paleogene lysocline and calcite compensation depth (CCD). These markers of carbonate saturation in the ocean are linked to the global carbon cycle (Archer and Maier-Reimer, 1994). Moreover, massive injections of carbon in the Paleogene should have caused calcium carbonate dissolution on the seafloor. The magnitude and location of these carbon inputs also dictate the extent of this dissolution observed in the pelagic records (Dickens et al., 1997; Zeebe et al., 2009). Although carbonate dissolution clearly occurred during the PETM, even the best records of this dissolution (e.g., on Walvis Ridge, (Zachos et al., 2005)) provide only loose constraints on carbon input (Panchuk et al., 2008; Zeebe et al., 2009). This is because detailed records of the lysocline and CCD are needed before, during, and after each event from different ocean basins.

CCD curves of low temporal resolution have been generated for the early Paleogene (Rea and Lyle, 2005; Van Andel, 1975). These curves have been constructed by establishing the depth and time of carbonate-clay horizons. Low-resolution records of lysocline behavior have also been published from Shatsky Rise in the western Equatorial Pacific (Hancock and Dickens, 2005). In this case, dissolution proxies, particularly benthic foraminiferal abundance and foraminiferal fragmentation, are tracked over depth and time. Although the available records indicate some generalities of carbonate

saturation of the early Paleogene oceans, they are fairly incomplete, especially for the late Paleocene and early Eocene.

In order to improve predictions for Earth's response to major changes in carbon cycling, a better understanding of past analogs is needed, especially examples from warm climates like those experienced during the Eocene (Zeebe et al., 2009). Recently, early Paleogene high-resolution CCD and lysocline reconstruction in the Equatorial Pacific Ocean at the ODP Site 1215 (Leon-Rodriguez and Dickens, 2010) has shown the dynamic and close relationship between carbon input and pelagic carbonate accumulation. Short-term ($<10^5$ years) or rapid ^{13}C -depleted carbon input results in relative fast rises of the lysocline, while long-term ($>10^5$ years) input of carbon results in an overall improvement or deepening of the lysocline. This type of investigation and the techniques used in this work can be the basis to extend our knowledge of the Eocene ocean/atmosphere dynamics. The IODP expedition 320 successfully recovered an age transect that covers the last 53 millions of years of the Pacific Ocean history (Pälike et al., 2010). The Sites U1332 and U1333 recovered marine sediments deposited on the seafloor just above of the productivity zone of the Equatorial region during the Eocene (Pälike et al., 2010). Previous investigations in the early Paleogene have already shown that ocean acidification occurred during major and rapid inputs of carbon into the atmosphere/ocean system, and responses were different from one ocean basin to another (Leon-Rodriguez and Dickens, 2010; Stap et al., 2009; Zachos et al., 2005; Zeebe and Zachos, 2007). From the preliminary results of Expedition 320, it appears that at least seven Carbonate Accumulation Events (CAE's) or periods of greater carbonate accumulation during the middle Eocene (Pälike et al., 2009). These events were not shown in other CCD

reconstructions (Lyle and Wilson, 2006; Rea and Lyle, 2005) most likely because of the lack of high-resolution sampling. The links between these events and global climatic changes is still unknown, and a detailed study is necessary to elucidate why and how the lysocline/CCD fluctuated during the Eocene. How many dissolution intervals exist in these new records? How do they relate to the CAE's? And in overall, How pelagic carbonate sedimentation is related to the carbon cycle during the Eocene?

These changes of the lysocline/CCD can be investigated using the IODP sites from Expedition 320, which provide a very complete composite section of the Eocene with the possibility of carrying out high-resolution analyses that could lead us towards a better understanding of the oceans response to climatic changes. We are particularly interested in establishing the relationship between changes of the carbonate ocean chemistry and carbonate preservation (CAE's), and the climatic events that followed the K/"X" event and preceded the Eocene/Oligocene boundary in the Equatorial Pacific Ocean (e.g. the EECO and the Middle Eocene Climatic Optimum, MECO). For that purpose, we have focused on the record from the sites U1332 and U1333, which provide high-quality and continuous record of pelagic sediments. These sites have been chosen because their relatively well-constrained age models and the completeness of their sedimentary record that varies from radiolarian oozes to nannofossil oozes. We present high-resolution stable isotope geochemistry ($\delta^{13}\text{C}$ and $\delta^{18}\text{O}$) and carbonate content analyses from these two sites, specifically from U1332 Hole A and B, and U1333 Hole A. These chemical proxies provide the most fundamental data to establish relationships among ^{13}C -depleted carbon input, changes in ocean temperature, and accumulation of

pelagic carbonate throughout the middle to the late Eocene in the Equatorial Pacific Ocean.

A.2. Sites and Samples

IODP Sites U1332 and U1333 (**Figure A.1**) are located Southeast of Hawaii in the central Pacific. More specifically the location and water depths of the studied holes were: U1332A: 11°54.7095'N 141°02.7428'W at 4,935.1 m, U1332B: 11°54.7209'N 141°02.7427'W at 4,936.9 m, U1333A: 10° 30.9953'N 138°25.1728'W at 4,865.0 m. Site U1332 lies on the oceanic crust of the Pacific Plate formed during the magnetic polarity C21r, while the U1333 site lies on chron C20r (Pälike et al., 2010). This assures the collection of sediments younger than 49 Ma (Cande and Kent, 1995). Shipboard stratigraphy from these sites indicates lower Miocene to middle Eocene deposition for the recovered sediment sections. The studied sections (**Figure A.2 and A.3**) comprise ~70 - 80 m of sediment that, in both sites, corresponds specifically to the middle to upper Eocene. Originally, the section from Site U1332 was subdivided in 6 sedimentary units from which we studied Units IV and V (Expedition 320/321 Scientists, 2010b). Unit IV corresponds to clayey radiolarian ooze, radiolarian ooze, radiolarian nannofossil ooze, nannofossil radiolarian ooze, nannofossil ooze, and porcellanite, as well as underlying basalt pebbles. Unit V corresponds to clay, zeolite clay, and chert that overlie the basalts of Unit VI (Expedition 320/321 Scientists, 2010b). The section from Site U1333 included 5 sedimentary units. We studied Units III and IV of this site (Expedition 320/321 Scientists, 2010c). Unit III corresponds to clayey radiolarian ooze, clayey

nannofossil ooze, nannofossil radiolarian ooze, nannofossil ooze, radiolarian nannofossil ooze, radiolarian ooze, nannofossil ooze, and porcellanite. Unit IV includes nannofossil ooze and limestone that overlie the basalts of Unit V of this site (Expedition 320/321 Scientists, 2010c). We rely on the age models presented on the Proceedings of the Expedition that give age constraints of ~1myr or less (Pälike et al., 2010). The magnetostratigraphy for the studied units is relatively well constrained and easily correlatable (Pälike et al., 2010). Site-to-site correlation and composite depth scales resulted from the integration of high resolution XRF (X-ray fluorescence) records along with paleomagnetic and biostratigraphic frameworks constructed from Equatorial Pacific ODP and IODP sites of Leg 199 and Expedition 320/321 (Westerhold et al., 2011).

We collected ca. 370 samples of 10-cc “tubes” of sediment. Hole A was analyzed between 74 and 161 mccsf-a, Hole U1332B between 76 and 158 mccsf-a, Hole U1332A between 131 and 203 mccsf-a. The term mccsf-a refers to meters core composite depth below seafloor that result from aligning cores from one hole or multiple adjacent holes (Expedition 320/321 Scientists, 2010a). Samples were taken every ~10 - 15 cm resolution with higher density of sampling in the most calcareous horizons. Samples were selected to avoid any disturbed intervals caused by drilling and coring.

A.3. Methodology

A.3.1. Sample Processing

About 370 samples from holes U1332A, U1332B, and U1333 were cleaned with 18 M Ω deionized water to eliminate salts that precipitated from interstitial water. After

freeze-drying, two aliquots were taken from each sample: ~0.5 g for stable isotope and carbonate content analyses, and 2–5 g were kept for future biostratigraphic and/or dissolution proxy analyses. Those samples for bulk stable isotope and carbonate content analyses were powdered and homogenized in glass mortars.

A.3.2. Geochemistry

Stable isotope analyses were carried out at Stable Isotope Laboratory at the University of California Santa Cruz using Autocarb acid reaction devices coupled with Dual-Inlet instruments Prism, Optima, and Kiel-253 mass spectrometers (a complete list of data is shown in **Tables A.1, A.2, and A.3**). Based on several replicate analyses of the Carrara Marble (CMO5) and NBS-19 standards, analytical precision is better than ± 0.05 ‰. Corrected delta values are expressed relative to international standards PDB (PeeDee Belemnite) for $\delta^{13}\text{C}$ and $\delta^{18}\text{O}$. Samples with suspected very low carbonate content were run using the Kiel device with as much as 20 mg of bulk material and increased the amount of acid added to the sample to generate enough signal to measure. The Kiel-253 generates a measurement of the CaCO_3 equivalent weight in the sample that can be divided by the total sample weight to calculate carbonate content. For the Prism instrument, carbonate content was generated from the Prism Transducer Carbonate Calibration ($R^2 = 0.98722$) that calibrates the autocarb device pressure transducer to calcium carbonate mass in the sample. This is later divided by the sample weight used for the run.

A.3.3. Composite Depths and Age Models

Revised composite depth (ccsf) scales and integration of IODP Sites from the Equatorial Pacific including sites U1332 and U1333 have been used to correct core depth below seafloor (csf) for expansion or contraction of the relative depth scale within any core (Westerhold et al., 2011). These revised depths were used to build a preliminary age model that includes biostratigraphic and magnetostratigraphic datums published in the Proceedings of Expedition 320/321 (Expedition 320/321 Scientists, 2010b, c). Future high-resolution biostratigraphy is expected to improve the current age control on sediment sections of the Eocene and Oligocene at Sites U1332 and U1333.

A.4. Results

A.4.1. Bulk Oxygen Isotope Record

A.4.1.1. Site U1332

Oxygen isotope values fluctuate between -2.00 and 2.25‰ (Kiel) and between -3.60 and -0.22‰ (Prism). The lower middle Eocene section (**Figure A.2**) between 120 and 150 m ccsf-a presents $\delta^{18}\text{O}$ values that are relatively more negative (from -0.03 to -2.09‰) than in the rest of the middle to late Eocene. The upper-middle to upper Eocene, between 80 and 120 mcsf, is characterized by a positive trend that ranges between 0.03 and 2.25‰. Between ~ 74 and 80 m ccsf-a (lower Oligocene), the oxygen isotope record has negative trend. $\delta^{18}\text{O}$ record declines to -2.33‰, this value is only comparable to those of the lowest middle Eocene.

A.4.1.2. Site U1333

Oxygen isotope values vary between -1.16 and 0.22‰ (Kiel), and between -1.85 and 0.28 (Prism). The $\delta^{18}\text{O}$ values (**Figure A.3**) in the interval between ~175 -and 200 m ccsf-a (lower middle Eocene section) fluctuate from -1.41 to 0.28‰, but usually stay within the order of ~-1.00‰. This contrasts with slightly more depleted values between ~163 and 175 m ccsf-a that go as low as -1.85‰. The upper middle to upper Eocene section (136-163 m ccsf-a) is characterized by “cyclic” fluctuations in the $\delta^{18}\text{O}$ record. Values in this interval generally range from -1.74 to 0.22‰ but remained slightly more positive than in the lower middle Eocene. The upper most section corresponds to the lower Oligocene (between ~131 and 136 m ccsf-a) and it is characterized by strong $\delta^{18}\text{O}$ shifts (**Figure A.3**). The first shift goes from a relatively positive to a very depleted value (from -0.70‰ to -1.74‰), and the second shifts from a depleted more positive values (from 1.74‰ to 0.29‰).

A.4.2. Bulk Carbon Isotope Record

A.4.2.1. Site U1332

Carbon isotope values fluctuate between -1.02 and 5.06‰ (Kiel) and between 1.22 and 4.83‰ (Prism). The lower middle Eocene section (**Figure A.2**) between 120 and 150 m ccsf-a shows relatively steady pattern, where $\delta^{13}\text{C}$ values average 2.14‰. Major fluctuations in the $\delta^{13}\text{C}$ record are observed in the upper middle Eocene and Oligocene (from 80 to 120 m ccsf-a). At least four distinctive negative excursions are

observed within this interval, which correspond to more than 2‰ depletions coupled with one positive excursions of $\delta^{18}\text{O}$.

A.4.2.2. Site U1333

Carbon isotope values vary between 1.80 and 3.49‰ (Kiel) and between 1.41 and 3.49‰ (Prism). The lower section that corresponds to the lower middle Eocene (between ~175 and 200 m ccsf-a) is characterized by relatively steady values of $\delta^{13}\text{C}$ that range from 1.58 to 2.23 ‰ (**Figure A.3**); later the record have a positive trend (between ~163 and 175 m ccsf-a) where values reach a maximum of 3.49‰. In the upper middle to upper Eocene (between 136 and 163 m ccsf-a), the $\delta^{13}\text{C}$ record shows a depleted trend and has more “cyclic” variations. This interval is characterized by $\delta^{13}\text{C}$ values that range from 1.41 to 2.49‰. The uppermost interval of the studied section that corresponds to the lower Oligocene (between ~131 and 136 m ccsf-a) is enclosed by two strong shifts in the $\delta^{13}\text{C}$ record (**Figure A.3**). The first shift goes from relatively positive to very depleted values (from -2.45‰ to -1.41‰). The second, goes from 1.41‰ to 1.96‰ (**Figure A.3**).

A.4.3. Carbonate Content

A.4.3.1. Site U1332

Carbonate content in Site U1332 fluctuates between 0.00 and 61.25% (**Figure A.2**). In general, carbonate-rich intervals observed throughout the record correspond to the CAE's initially observed during Expedition 320 (Pälike et al., 2010). The carbonate content in the lowest section (between ~135 and 150 m ccsf-a) is low with values that range between 0.00 and 18.29%. The carbonate content increases between 118 and 135 m

ccsf-a (CAE 3; **Figure A.2**) reaching a maximum of 50.33% in this interval. The overlying section, between 106 and 118 m ccsf-a (upper middle Eocene), is characterized by very low carbonate content, which ranges from 0.00 to 9.80%. This is followed by a carbonate-rich interval that occurs between ~100 and 106 m ccsf-a, and it likely corresponds to the CAE4. Thinner intervals with relatively higher carbonate content occur between 80-100 m ccsf-a (upper Eocene) and they probably correspond to CAE's 5-7. These carbonate-rich intervals are less obvious (ranging from ~3.00 to 23.71%) than those observed in the lower part of the section. The carbonate content increases dramatically between 74 and 80 m ccsf where values range from 34.64 to 61.25%. This part of the section shows the highest carbonate content in the record and corresponds to the lower Oligocene.

A.4.3.2. Site U1333

Carbonate content in Site U1333 fluctuates between 0.00 and 100% (**Figure A.3**). Carbonate-rich intervals observed throughout the studied section correspond to the CAE's initially observed during the Expedition 320 (Pälike et al., 2010). The carbonate content in the lowest section (between 192 and 205 m ccsf-a) is relatively high with values ranging from 0.34 to 100% and average 41.27%. Overlying this interval there is a low carbonate content horizon (<10.6%) that lies between 188 and 192 m ccsf-a. Carbonate content picks up again between ~172 and 188 m ccsf-a; these values range from 1.70 to 100% and average 56.63%. This interval likely corresponds to the CAE3 that occurs in the lower middle Eocene (Pälike et al., 2010). Immediately above (between 161 and 172 m ccsf-a) carbonate content decreases to values that range from 0.00 to

23.95%. This is followed by another carbonate-rich interval, most likely corresponding to the CAE4 (**Figure A.3**) that occurs in the upper middle Eocene (between 155 to 161 m ccsf-a). Carbonate content in this interval is relatively high with values that range from 10.44 to 56.60% with an average of 32.02%. The upper part of the section (between 135 and 155 m ccsf-a) corresponds to the rest of the middle Eocene to the upper Eocene and it is characterized by numerous fluctuations in the carbonate content, which result in alternations of thin packages of low carbonate and carbonate-rich intervals. The high carbonate content horizons likely correspond to the CAE's 5-7 (**Figure A.3**). Within these intervals carbonate is usually lower than 50% with just one exception where carbonate content reaches 83.87%. The lower Oligocene that lies between ~132 and 135 m ccsf-a is characterized by less than 30% carbonate content. Unfortunately, three of the samples that were taken at the topmost part of the studied interval display odd "negative" values. This is likely related to laboratory processing problems. Therefore, these values have been dismissed and are not shown in the **Figure A.3**.

A.5. Summary and Future Work

The detailed stable isotope stratigraphy covering the middle Eocene to the lower Oligocene provides a high-resolution record of this interval at IODP Sites U1332 and U1333. These records will likely improve the Pacific reference curves available for this interval.

Carbonate record from both sites nicely depict the CAE's observed in the Pacific Ocean (Lyle and Wilson, 2002; Pälike et al., 2010). These preliminary results have great

potential for investigating fluctuations of the lysocline and CCD. To better address this topic, it is necessary to analyze in detail the oxygen and carbon isotope records in order to investigate whether they are coupled or not with minima and maxima of carbonate content in both sites. Ultimately, we will use these data to understand the short-term ($<10^5$) and long-term ($<10^5$) variations in the carbon cycle, as well as the effect that these changes might have had on the pelagic carbonate accumulation in the equatorial Pacific Ocean during the middle to late Eocene.

A.6. Acknowledgments

We are grateful to Isabel Rodriguez-Hernandez and Glenn Snyder for their help with sample preparation. Jen Lehman and Dyke Andreasen from the Stable Isotope Lab at the University of California in Santa Cruz (UCSC) run the stable isotope and carbonate content analyses. They also kindly rerun numerous samples to assure reliable data points in the records, especially where carbonate content was extremely low. Many thanks to Brandon Murphy and James Zachos for their hospitality during my visit to UCSC. Heiko Pälike and Thomas Westerhold provided guidelines for calculations and corrections of the composite depths for the studied sites. This research was funded and used samples provided by the Integrated Ocean Drilling Program (IODP). These initial results are part of the Post-Expedition Activities of Expedition 320/321.

A.7. References

- Archer, D., Maier-Reimer, E., 1994. Effect of deep-sea sedimentary calcite preservation on atmospheric CO₂ concentration. *Nature* 367, 260-263.
- Bowen, G., others, 2006. Eocene Hyperthermal Event Offers Insight Into Greenhouse Warming. *Eos Transactions AGU* 87, 165-169.
- Cande, S., Kent, D., 1995. Revised calibration of the geomagnetic polarity timescale for the Late Cretaceous and Cenozoic. *Journal of Geophysical Research - Solid Earth* 100, 6093-6095.
- Cramer, B.S., Wright, A.A., Kent, D.V., Aubry, M.P., 2003. Orbital climate forcing of $\delta^{13}\text{C}$ excursions in the late Paleocene-early Eocene (chrons C24n-C25n). *Paleoceanography* 18.
- Dickens, G.R., 2011. Methane release from gas hydrate systems during the Paleocene-Eocene thermal maximum and other past hyperthermal events: setting appropriate parameters for discussion. *Climate of the Past Discussions* 7, 1139-1174.
- Dickens, G.R., Castillo, M.M., Walker, J.C.G., 1997. A blast of gas in the latest Paleocene: Simulating first-order effects of massive dissociation of oceanic methane hydrate. *Geology* 25, 259.
- Expedition 320/321 Scientists, 2010a. Methods, in: Pälike, H., Lyle, M., Nishi, H., Raffi, I., Gamage, K., Klaus, A., and the Expedition 320/321 Scientists (Ed.), *Proceedings of the Integrated Ocean Drilling Program, Volume 320/321*, pp. 1-80.
- Expedition 320/321 Scientists, 2010b. Site U1332, in: Pälike, H., Nishi, H., Lyle, M., Raffi, I., Gamage, K., Expedition 320/321 Scientists (Eds.), *Proceedings of the Integrated Ocean Drilling Program, Volume 320/321. Integrated Ocean Drilling Program Management International, Inc., Tokyo*.
- Expedition 320/321 Scientists, 2010c. Site U1333, in: Pälike, H., Nishi, H., Lyle, M., Raffi, I., Gamage, K., Expedition 320/321 Scientists (Eds.), *Proceedings of the Integrated Ocean Drilling Program, Volume 320/321. Integrated Ocean Drilling Program Management International, Inc., Tokyo*, pp. 1-93.
- Hancock, H.J.L., Dickens, G.R., 2005. Carbonate dissolution episodes in Paleocene and Eocene sediment, Shatsky Rise, west-central Pacific, *Proceedings of the Ocean Drilling Program, Scientific Results Volume 198*.
- Katz, M.E., Pak, D.K., Dickens, G.R., Miller, K.G., 1999. The source and fate of massive carbon input during the latest Paleocene thermal maximum. *Science* 286, 1531-1533.

- Kennett, J.P., Stott, L.D., 1991. Abrupt deep-sea warming, palaeoceanographic changes and benthic extinctions at the end of the Palaeocene. *Nature* 353, 225-229.
- Leon-Rodriguez, L., Dickens, G.R., 2010. Constraints on ocean acidification associated with rapid and massive carbon injections: The early Paleogene record at ocean drilling program site 1215, Equatorial Pacific Ocean. *Palaeogeography, Palaeoclimatology, Palaeoecology* 298, 409-420.
- Lourens, L., Sluijs, A., Kroon, D., Zachos, J.C., Thomas, E., Roehl, U., Bowles, J., Raffi, I., 2005. Astronomical modulation of late Palaeocene to early Eocene global warming events. *Nature* 435, 1083-1087.
- Lyle, M., Wilson, P., 2002. Proceedings of the Ocean Drilling Program, 199 Initial Reports. Ocean Drilling Program.
- Lyle, M., Wilson, P.A., 2006. Leg 199 synthesis: evolution of the equatorial Pacific in the early Cenozoic, Proc. ODP, Sci. Results, 199. Ocean Drilling Program, College Station, TX, pp. 1-39.
- Pälike, H., Nishi, H., Lyle, M., Raffi, I., Gamage, K., Klaus, A., 2010. Expedition 320/321 Summary, Proceedings of the Integrated Ocean Drilling Program, Volume 320/321. Integrated Ocean Drilling Program Management International, Inc., pp. 1-141.
- Pälike, H., Nishi, H., Lyle, M., Raffi, I., Klaus, A., Gamage, K., 2009. Integrated Ocean Drilling Program Expedition 320 Preliminary Report Pacific Equatorial Age Transect. Integrated Ocean Drilling Program Management International, Inc.
- Panchuk, K., Ridgwell, A., Kump, L.R., 2008. Sedimentary response to Paleocene-Eocene Thermal Maximum carbon release: A model-data comparison. *Geology* 36, 315.
- Pearson, P.N., Palmer, M.R., 2000. Atmospheric carbon dioxide concentrations over the past 60 million years. *Nature* 406, 695-699.
- Rea, D.K., Lyle, M., 2005. Paleogene calcite compensation depth in the eastern subtropical Pacific: Answers and questions. *Paleoceanography* 20, PA1012.
- Shackleton, N.J., Hall, M.A., 1984. Carbon isotope data from Leg 74 sediments, in: Moore, J., T. C., Rabinowitz, P.D., Boersma, A., Borella, P.E., Chave, A.D. (Eds.), Initial Reports. DSDP. US Government Printing Office, Washington, pp. 613-619.
- Sluijs, A., Bowen, G., Brinkhuis, H., Lourens, L., Thomas, E., 2007. The Palaeocene-Eocene Thermal Maximum super greenhouse: biotic and geochemical signatures, age models and mechanisms of global change, Deep-Time Perspectives on Climate Change: Marrying the Signal from Computer Models and Biological

- Proxies. The Micropaleontological Society, Special Publications, London, pp. 323-349.
- Stap, L., Sluijs, A., Lourens, L.J., Thomas, E., 2009. Patterns and magnitude of deep sea carbonate dissolution during Eocene Thermal Maximum 2 and H2, Walvis Ridge, southeastern Atlantic Ocean. *Paleoceanography* 24, PA1211.
- Thomas, E., Zachos, J.C., 2000. Was the late Paleocene thermal maximum a unique event? *GFF* 122, 169-170.
- Thomas, E., Zachos, J.C., Bralower, T.J., 2000. Deep-sea environments on a warm earth: latest Paleocene - early Eocene, in: Huber, B.T., MacLeod, K., Wing, S.L. (Eds.), *Warm climates in Earth history*. Cambridge University Press, pp. 132-160.
- Van Andel, T., 1975. Mesozoic/cenozoic calcite compensation depth and the global distribution of calcareous sediments. *Earth and Planetary Science Letters* 26, 187-194.
- Westerhold, T., Wilkens, R., Pälike, H., Lyle, M., Jones, T.D., Bown, P., Moore, T., Kamikuri, S.-i., 2011. Revised composite depth scales and integration of IODP Sites U1331, U1332, U1333, U1334 and ODP Sites 1218, 1219, 1220. Submitted.
- Yapp, C.J., 2004. Fe(CO₃)OH in goethite from a mid-latitude North American Oxisol: estimate of atmospheric CO₂ concentration in the Early Eocene "climatic optimum". *Geochimica et Cosmochimica Acta* 68, 935-947.
- Zachos, J., Pagani, M., Sloan, L., Thomas, E., Billups, K., 2001. Trends, rhythms, and aberrations in global climate 65 Ma to present. *Science* 292, 686-693.
- Zachos, J.C., Dickens, G.R., Zeebe, R.E., 2008. An early Cenozoic perspective on greenhouse warming and carbon-cycle dynamics. *Nature* 451, 279-283.
- Zachos, J.C., Schellenberg, S.A., Röhl, U., Hodell, D.A., Sluijs, A., Kelly, C.D., Thomas, E., Nicolo, M.J., Lourens, L.J., Raffi, I., McCarren, H., Kroon, D., 2005. Rapid acidification of the ocean during the Paleocene-Eocene thermal maximum. *Science (New York, N.Y.)* 308, 1611-1615.
- Zeebe, R.E., Zachos, J.C., 2007. Reversed deep-sea carbonate ion basin gradient during Paleocene-Eocene thermal maximum. *Paleoceanography* 22, PA3201.
- Zeebe, R.E., Zachos, J.C., Dickens, G.R., 2009. Carbon dioxide forcing alone insufficient to explain Palaeocene–Eocene Thermal Maximum warming. *Nature Geoscience* 2, 576-580.



Figure A.1 – IODP Sites U1332 and 1333 location map.

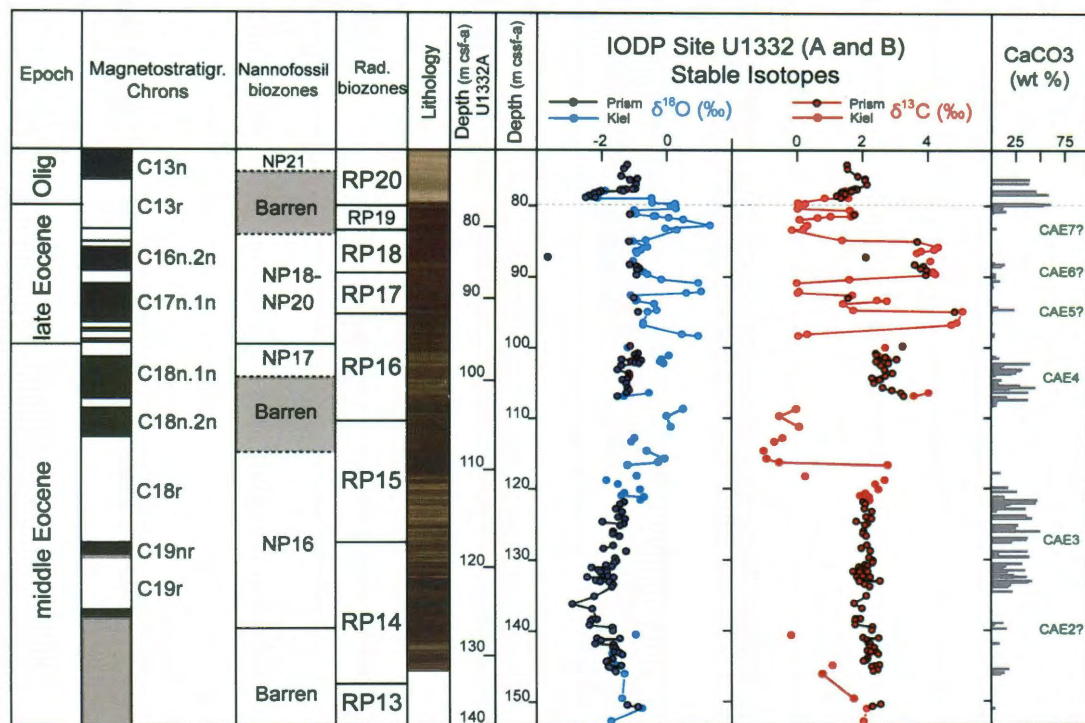


Figure A.2 – IODP Site U1332 (hole A and B) stable isotopes and carbonate content profiles.

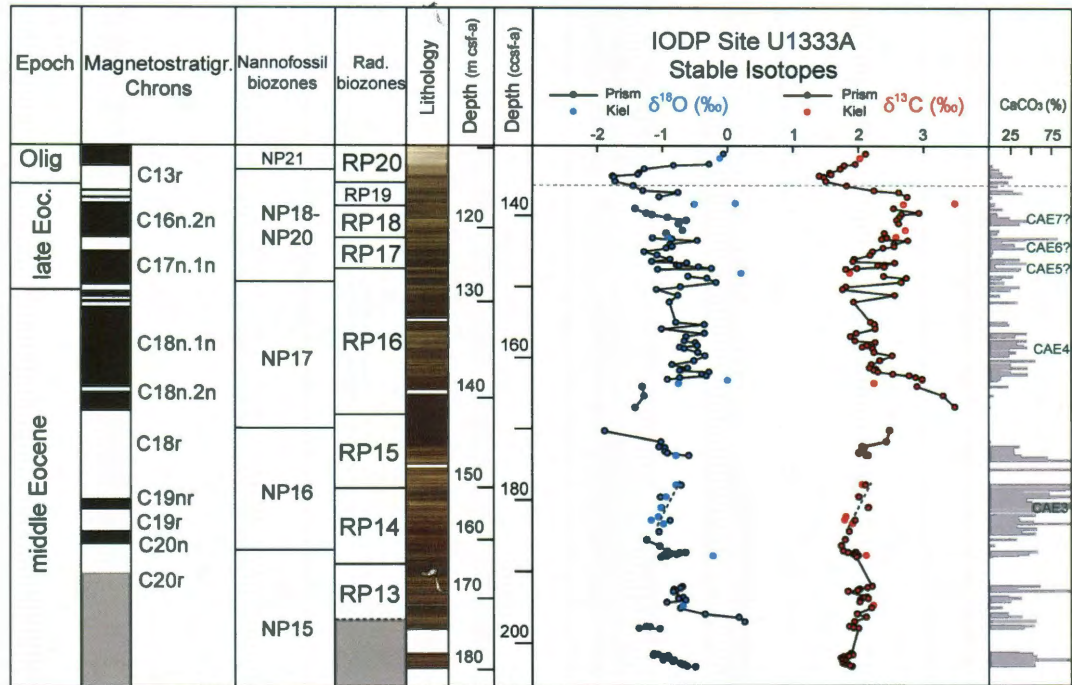


Figure A.3 – IODP Site U1333A stable isotopes and carbonate content profiles.

Site	Core	Section	Interval (m)	Depth CSF-A (m)	Depth CCSF-A (m)	Prism %CaCO ₃	Kiel %CaCO ₃	Prism δ ¹³ C	Kiel δ ¹³ C	Prism δ ¹⁸ O	Kiel δ ¹⁸ O
U1332A	9H	3W	0.57- 0.59	73.97	76.29	-9.98		2.04		-0.49	
U1332A	9H	3W	1.1- 1.12	74.50	77.01	40.53		2.07		-0.56	
U1332A	9H	4W	0.14- 0.16	75.04	77.71	27.87		1.69		-0.62	
U1332A	9H	4W	0.24- 0.26	75.14	77.84				1.73		-0.84
U1332A	9H	4W	0.39- 0.41	75.29	78.02				1.46		-1.54
U1332A	9H	4W	0.49- 0.51	75.39	78.14	0.47		1.24		-1.96	
U1332A	9H	4W	1.09- 1.11	75.99	78.85	5.83	15.38		1.36		-2.01
U1332A	9H	4W	1.28- 1.3	76.18	79.06		0.28		0.83		0.14
U1332A	9H	5W	0.44- 0.46	76.84	79.79		0.10		0.23		1.00
U1332A	9H	5W	1.36- 1.38	77.76	80.75		0.62		1.60		-0.49
U1332A	9H	6W	0.7- 0.72	78.60	81.59		0.54		1.64		0.22
U1332A	9H	7W	0.5- 0.52	79.90	82.84		0.12		0.30		2.25
U1332A	10H	1W	0.7- 0.72	80.60	83.51		0.11		-0.17		1.06
U1332A	10H	2W	0.7- 0.72	82.10	84.93		0.34		1.37		-0.06
U1332A	10H	3W	0.22- 0.24	83.12	85.91		0.70		4.31		-0.01
U1332A	10H	3W	0.6- 0.62	83.50	86.28		3.76		4.19		-0.23
U1332A	10H	3W	0.8- 0.82	83.70	86.47		13.99		3.79		-0.42
U1332A	10H	3W	1.1- 1.12	84.00	86.77		11.20		3.66		-0.39
U1332A	10H	4W	0.7- 0.72	85.10	87.85		5.08		4.07		-0.52
U1332A	10H	5W	0.7- 0.72	86.60	89.38		1.89		4.15		-0.14
U1332A	10H	6W	0.7- 0.72	88.10	90.95		0.09		-0.02		1.83
U1332A	10H	7W	0.31- 0.33	89.21	92.14		0.02		0.05		1.94
U1332A	11H	1W	0.28- 0.3	89.68	92.65		6.80		1.68		-0.61
U1332A	11H	1W	0.92- 0.94	90.32	93.35		1.33		2.44		-0.38
U1332A	11H	1W	1.05- 1.07	90.45	93.49		0.99		2.74		-0.42
U1332A	11H	1W	1.4- 1.42	90.80	93.88		0.19		1.40		0.24
U1332A	11H	2W	0.7- 0.72	91.60	94.77		0.18		1.71		0.33
U1332A	11H	3W	0.76- 0.78	93.16	96.54		3.85		4.89		-0.15
U1332A	11H	4W	0.7- 0.72	94.60	98.20		0.09		0.30		1.24
U1332A	11H	5W	0.77- 0.79	96.17	100.03		8.31		2.70		-0.72
U1332A	11H	6W	0.24- 0.26	97.14	101.18		0.34		2.47		0.77
U1332A	11H	6W	0.7- 0.72	97.60	101.72		17.84		2.76		0.51
U1332A	11H	6W	0.94- 0.96	97.84	102.01		16.68		2.52		0.46
U1332A	11H	6W	1.16- 1.18	98.06	102.27		21.02		2.51		0.58
U1332A	12H	1W	1.08- 1.1	99.98	104.58	2.13		2.43		-0.87	

Table A.1 – IODP Site U1332A stable isotope and carbonate content data.

Site	Core	Section	Interval (m)	Depth CSF-A (m)	Depth CCSF-A (m)	Prism %CaCO3	Kiel %CaCO3	Prism $\delta^{13}C$	Kiel $\delta^{13}C$	Prism $\delta^{18}O$	Kiel $\delta^{18}O$
U1332A	12H	1W	1.2- 1.22	100.10	104.73	10.55		2.68		-0.27	
U1332A	12H	1W	1.43- 1.45	100.33	105.01	12.32		2.66		-0.34	
U1332A	12H	2W	0.12- 0.14	100.52	105.24	6.53		2.90		-0.89	
U1332A	12H	2W	1.14- 1.16	101.54	106.49		0.95		4.02		0.05
U1332A	12H	3W	0.55- 0.57	102.45	107.61		0.10				
U1332A	12H	4W	0.77- 0.79	104.17	109.75		0.05		-0.55		0.69
U1332A	12H	5W	0.48- 0.5	105.38	111.28		0.07		0.06		0.84
U1332A	12H	6W	0.65- 0.67	107.05	113.43		0.04		-0.70		-0.58
U1332A	12H	7W	0.36- 0.38	108.06	114.74		0.05		-1.03		-0.03
U1332A	13H	1W	0.5- 0.52	108.90	115.84		0.05		-0.94		0.62
U1332A	13H	1W	1.18- 1.2	109.58	116.74	-2.59	9.84		2.77		-0.72
U1332A	13H	2W	0.18- 0.2	110.08	117.41	12.55		2.17		-0.36	
U1332A	13H	2W	1- 1.02	110.90	118.51	7.05		2.15		-0.07	
U1332A	13H	2W	1.35- 1.37	111.25	118.98	23.12		2.12		0.09	
U1332A	13H	3W	0.1- 0.12	111.50	119.31	31.09		1.90		-0.14	
U1332A	13H	3W	0.33- 0.35	111.73	119.62	42.02		1.85		-0.14	
U1332A	13H	3W	0.91- 0.93	112.31	120.41	16.18		2.03		-0.19	
U1332A	13H	3W	1.3- 1.32	112.70	120.94	8.46		2.06		-0.08	
U1332A	13H	4W	0.8- 0.82	113.70	122.31	9.60		1.79		-0.44	
U1332A	13H	4W	1.02- 1.04	113.92	122.61	-3.48		1.86		-0.74	
U1332A	13H	4W	1.28- 1.3	114.18	122.96	30.73		1.98		-0.42	
U1332A	13H	5W	0.62- 0.64	115.02	124.12	26.02		2.17		-0.33	
U1332A	13H	5W	1.06- 1.08	115.46	124.72	21.36		2.04		-0.61	
U1332A	13H	6W	0.28- 0.3	116.18	125.72	34.95		1.96		-0.72	
U1332A	13H	6W	0.55- 0.57	116.45	126.09	9.72		1.89		-0.75	
U1332A	13H	6W	1.04- 1.06	116.94	126.76	0.72		2.04		-1.03	
U1332A	13H	6W	1.38- 1.4	117.28	127.23	29.91		2.02		-0.84	
U1332A	13H	7W	0.38- 0.4	117.78	127.92	7.58		2.07		-0.87	
U1332A	14X	1W	0.52- 0.54	118.42	128.80	13.81		1.93		-0.91	
U1332A	14X	1W	0.85- 0.87	118.75	129.25	9.79		1.86		-0.98	
U1332A	14X	2W	0.36- 0.38	119.76	130.63	14.47		1.92		-1.68	
U1332A	14X	2W	0.74- 0.76	120.14	131.15	30.49		1.91		-2.04	
U1332A	14X	2W	0.97- 0.99	120.37	131.46	7.02		2.13		-1.78	
U1332A	14X	2W	1.2- 1.22	120.60	131.77	-1.52		2.18		-1.71	
U1332A	14X	3W	0.7- 0.72	121.60	133.11	-3.57		2.55		-1.72	

Table A.1 – (Continued) IODP Site U1332A stable isotope and carbonate content data.

Site	Core	Section	Interval (m)	Depth CSF-A (m)	Depth CCSF-A (m)	Prism %CaCO ₃	Kiel %CaCO ₃	Prism δ ¹³ C	Kiel δ ¹³ C	Prism δ ¹⁸ O	Kiel δ ¹⁸ O
U1332A	14X	4W	0.75- 0.77	123.15	135.16	8.03		2.13		-1.94	
U1332A	14X	5W	0.65- 0.67	124.55	136.96	-2.23		2.00		-2.00	
U1332A	14X	6W	0.32- 0.34	125.72	138.42	19.27		1.95		-1.83	
U1332A	15X	1W	0.78- 0.8	126.68	139.59			2.33		-1.27	
U1332A	15X	1W	1.16- 1.18	127.06	140.05	11.65		2.30		-1.25	
U1332A	15X	1W	1.3- 1.32	127.20	140.21	-3.07		1.98		-1.54	
U1332A	15X	2W	0.58- 0.6	127.98	141.13	0.40		2.51		-0.99	
U1332A	15X	2W	1.35- 1.37	128.75	142.02	27.88		2.25		-1.23	
U1332A	15X	3W	0.17- 0.19	129.07	142.38	27.34		2.23		-1.24	
U1332A	15X	3W	0.3- 0.32	129.20	142.52	36.36		2.38		-1.15	
U1332A	15X	3W	0.66- 0.68	129.56	142.93	41.91		2.16		-1.11	
U1332A	15X	3W	0.78- 0.8	129.68	143.06	3.61		2.26		-1.18	
U1332A	15X	3W	0.87- 0.89	129.77	143.16	4.08		2.44		-0.99	
U1332A	15X	3W	1.02- 1.04	129.92	143.32		0.81		2.20		-1.28
U1332A	15X	3W	1.13- 1.15	130.03	143.44	12.05		2.49		-0.88	
U1332A	15X	3W	1.24- 1.26	130.14	143.56	-3.26		2.29		-0.92	
U1332A	15X	4W	0.18- 0.2	130.58	144.04	26.53		2.15		-1.24	
U1332A	15X	4W	0.42- 0.44	130.82	144.30	18.25		2.10		-1.38	
U1332A	15X	4W	0.52- 0.54	130.92	144.40	18.96		2.03		-1.45	
U1332A	15X	4W	0.7- 0.72	131.10	144.59	-3.16		2.52		-0.91	
U1332A	15X	4W	1.03- 1.05	131.43	144.94		0.20		1.08		-1.13
U1332A	15X	4W	1.15- 1.17	131.55	145.07	18.29		2.38		-1.38	
U1332A	15X	4W	1.27- 1.29	131.67	145.19	1.19		2.28		-1.33	
U1332A	15X	5W	0.16- 0.18	132.06	145.59	13.58		2.47		-1.14	
U1332A	15X	5W	0.34- 0.36	132.24	145.78	9.99		2.33		-1.10	
U1332A	15X	5W	0.7- 0.72	132.60	146.14		0.13		0.77		-0.83
U1332A	16X	1W	0.7- 0.72	136.20	149.62		0.06		1.73		-0.92
U1332A	16X	2W	0.12- 0.14	137.12	150.47	-1.00		2.56		-0.78	
U1332A	16X	2W	0.45- 0.47	137.45	150.78	3.99		2.31		-0.39	
U1332A	16X	2W	0.74- 0.76	137.74	151.04		0.98		2.12		-0.20
U1332A	17X	1W	0.7- 0.72	145.20	158.13						

Table A.1 – (Continued) IODP Site U1332A stable isotope and carbonate content data.

Site	Core	Section	Interval (m)	Depth CSF-A (m)	Depth CCSF-A (m)	Prism %CaCO3	Kiel %CaCO3	Prism $\delta^{13}C$	Kiel $\delta^{13}C$	Prism $\delta^{18}O$	Kiel $\delta^{18}O$
U1332B	9H	3W	0.45- 0.47	70.55	74.28	39.54		1.53		-0.72	
U1332B	9H	3W	1- 1.02	71.10	74.84	39.01		1.54		-0.84	
U1332B	9H	4W	0.58- 0.6	72.18	75.94	46.24		1.85		-0.93	
U1332B	9H	4W	1.03- 1.05	72.63	76.40	59.03		2.07		-0.63	
U1332B	9H	5W	0.8- 0.82	73.90	77.73	47.40		1.83		-0.51	
U1332B	9H	5W	0.88- 0.9	73.98	77.81	61.25		1.72		-0.75	
U1332B	9H	5W	0.95- 0.97	74.05	77.88	49.73		1.64		-0.95	
U1332B	9H	5W	1.04- 1.06	74.14	77.98	53.67		1.66		-0.84	
U1332B	9H	5W	1.22- 1.24	74.32	78.17	0.67		1.38		-1.76	
U1332B	9H	5W	1.36- 1.38	74.46	78.32	12.16		1.45		-1.89	
U1332B	9H	6W	0.19- 0.21	74.79	78.67	10.32		1.20		-2.08	
U1332B	9H	6W	0.4- 0.42	75.00	78.90	4.67	8.36		1.37		-1.82
U1332B	9H	6W	0.54- 0.56	75.14	79.05		3.19		1.56		-1.81
U1332B	9H	6W	1.14- 1.16	75.74	79.70		0.16		0.01		0.17
U1332B	9H	7W	0.07- 0.09	76.17	80.17		0.09		0.15		0.83
U1332B	9H	7W	0.4- 0.42	76.50	80.53		0.09		0.00		1.03
U1332B	10H	1W	0.58- 0.6	77.18	81.29	5.74			1.76		-0.42
U1332B	10H	1W	0.85- 0.87	77.45	81.60		0.31		1.01		0.29
U1332B	10H	1W	1- 1.02	77.60	81.77		0.20		0.62		0.76
U1332B	10H	1W	1.22- 1.24	77.82	82.02		0.15		0.06		1.29
U1332B	10H	2W	0.85- 0.87	78.95	83.32		0.11		0.20		0.64
U1332B	10H	3W	0.85- 0.87	80.45	85.09		1.35		3.68		-0.53
U1332B	10H	4W	0.55- 0.57	81.65	86.54						
U1332B	10H	4W	1.14- 1.16	82.24	87.26	0.75		2.10		-3.63	
U1332B	10H	5W	0.5- 0.52	83.10	88.32	4.75		3.60		-0.67	
U1332B	10H	5W	0.7- 0.72	83.30	88.57	-0.77		3.87		-0.42	
U1332B	10H	5W	0.93- 0.95	83.53	88.86	8.88		3.78		-0.32	
U1332B	10H	5W	1.1- 1.12	83.70	89.07	0.27		3.96		-0.39	
U1332B	10H	6W	0.14- 0.16	84.24	89.75		2.55		4.23		0.00
U1332B	10H	6W	0.7- 0.72	84.80	90.46		0.13		1.59		0.50
U1332B	10H	7W	0.7- 0.72	86.30	92.36		0.11		0.01		1.40
U1332B	11H	1W	0.7- 0.72	86.80	93.00	23.71		1.57		-0.50	
U1332B	11H	2W	0.75- 0.77	88.35	94.99		1.27		5.06		0.01
U1332B	11H	3W	0.7- 0.72	89.80	96.86		3.36		4.72		-0.16
U1332B	11H	4W	0.44- 0.46	91.04	98.45		0.17		0.03		1.83
U1332B	12H	1W	1.02- 1.04	92.12	99.83	4.84		3.24		-0.61	

Table A.2 – IODP Site U1332B stable isotope and carbonate content data.

Site	Core	Section	Interval (m)	Depth CSF-A (m)	Depth CCSF-A (m)	Prism %CaCO3	Kiel %CaCO3	Prism $\delta^{13}C$	Kiel $\delta^{13}C$	Prism $\delta^{18}O$	Kiel $\delta^{18}O$
U1332B	12H	2W	0.3- 0.32	92.90	100.82	40.15		2.42		-0.32	
U1332B	12H	2W	0.49- 0.51	93.09	101.06	13.08		2.44		-0.43	
U1332B	12H	2W	0.75- 0.77	93.35	101.39	10.19		2.71		-0.36	
U1332B	12H	2W	0.98- 1	93.58	101.68	31.94		2.49		-0.35	
U1332B	12H	2W	1.1- 1.12	93.70	101.83	30.47		2.44		-0.19	
U1332B	12H	2W	1.25- 1.27	93.85	102.02	21.63		2.43		-0.56	
U1332B	12H	2W	1.36- 1.38	93.96	102.16	25.76		2.68		-0.42	
U1332B	12H	3W	0.18- 0.2	94.28	102.56	4.70		2.57		-0.91	
U1332B	12H	3W	0.68- 0.7	94.78	103.19	10.74		2.69		-1.05	
U1332B	12H	3W	1.08- 1.1	95.18	103.69	7.58		2.96		-0.57	
U1332B	12H	3W	1.35- 1.37	95.45	104.02	29.55		2.74		-0.54	
U1332B	12H	4W	0.09- 0.11	95.69	104.32	45.59		2.33		-0.55	
U1332B	12H	4W	0.21- 0.23	95.81	104.47	18.81		2.60		-0.58	
U1332B	12H	4W	0.66- 0.68	96.26	105.03	38.17		2.41		-0.59	
U1332B	12H	4W	1.2- 1.22	96.80	105.69	16.23		2.67		-0.52	
U1332B	12H	5W	0.03- 0.05	97.13	106.10	37.71		2.96		-0.45	
U1332B	12H	5W	0.3- 0.32	97.40	106.43	6.31		3.25		-0.52	
U1332B	12H	5W	0.7- 0.72	97.80	106.92		5.47		3.57		-0.85
U1332B	12H	6W	0.7- 0.72	99.30	108.73		0.44		-0.03		1.28
U1332B	13H	1W	1- 1.02	101.60	111.48		0.57				
U1332B	13H	2W	0.7- 0.72	102.80	112.90		0.06		-0.45		-0.47
U1332B	13H	3W	0.7- 0.72	104.30	114.67		0.54				
U1332B	13H	4W	0.6- 0.62	105.70	116.32		0.06		-0.55		0.38
U1332B	13H	5W	0.78- 0.8	107.38	118.31		0.12		0.24		-0.38
U1332B	13H	5W	1.24- 1.26	107.84	118.86		17.18		2.68		-1.48
U1332B	13H	6W	0.23- 0.25	108.33	119.44		26.37		2.39		-1.07
U1332B	13H	6W	0.87- 0.89	108.97	120.21		13.62		2.49		-0.27
U1332B	13H	6W	1.28- 1.3	109.38	120.71		47.38		2.09		-0.84
U1332B	13H	7W	0.07- 0.09	109.67	121.06		45.80		1.92		-0.94
U1332B	13H	7W	0.24- 0.26	109.84	121.27		19.33		2.20		-0.13
U1332B	13H	7W	0.58- 0.6	110.18	121.68		14.42		2.22		-0.25
U1332B	14X	1W	0.28- 0.3	110.38	121.92	35.27		2.04		-0.82	
U1332B	14X	1W	0.52- 0.54	110.62	122.22	5.62		2.10		-0.97	
U1332B	14X	1W	1.08- 1.1	111.18	122.91	36.17		2.07		-1.13	
U1332B	14X	1W	1.4- 1.42	111.50	123.31	41.90		2.30		-0.91	
U1332B	14X	2W	0.48- 0.5	112.08	124.03	-0.81		2.13		-1.04	

Table A.2 – (Continued) IODP Site U1332B stable isotope and carbonate content data.

Site	Core	Section	Interval (m)	Depth CSF-A (m)	Depth CCSF-A (m)	Prism %CaCO3	Kiel %CaCO3	Prism $\delta^{13}C$	Kiel $\delta^{13}C$	Prism $\delta^{18}O$	Kiel $\delta^{18}O$
U1332B	14X	2W	1.04- 1.06	112.64	124.73	24.89		1.83		-1.64	
U1332B	14X	2W	1.24- 1.26	112.84	124.99	21.57		2.17		-0.86	
U1332B	14X	2W	1.41- 1.43	113.01	125.20	50.33		2.09		-0.99	
U1332B	14X	3W	0.6- 0.62	113.70	126.08	37.53		2.05		-1.24	
U1332B	14X	3W	0.82- 0.84	113.92	126.37	36.27		2.03		-1.25	
U1332B	14X	3W	1.12- 1.14	114.22	126.75	21.20		2.12		-1.02	
U1332B	14X	4W	0.63- 0.65	115.23	128.07	37.38		2.15		-1.24	
U1332B	14X	4W	0.92- 0.94	115.52	128.45	7.75		1.98		-1.58	
U1332B	14X	4W	1.22- 1.24	115.82	128.85	39.16		2.25		-0.76	
U1332B	14X	5W	0.45- 0.47	116.55	129.82	31.83		2.22		-1.16	
U1332B	14X	5W	0.73- 0.75	116.83	130.20	15.37		2.33		-1.12	
U1332B	14X	5W	0.94- 0.96	117.04	130.48	12.05		2.31		-1.18	
U1332B	14X	5W	1.16- 1.18	117.26	130.78	34.69		2.08		-1.48	
U1332B	14X	5W	1.32- 1.34	117.42	131.00	17.08		2.15		-1.27	
U1332B	14X	6W	0.19- 0.21	117.79	131.50	23.30		1.94		-1.46	
U1332B	14X	6W	0.37- 0.39	117.97	131.75	36.43		1.72		-1.60	
U1332B	14X	6W	0.45- 0.47	118.05	131.86	22.99		1.93		-1.45	
U1332B	14X	6W	0.82- 0.84	118.42	132.37	42.01		2.02		-1.42	
U1332B	14X	6W	0.97- 0.99	118.51	132.49	17.05		2.23		-1.19	
U1332B	14X	6W	1.4- 1.42	118.57	132.57	37.98		1.92		-1.35	
U1332B	14X	7W	0.17- 0.19	118.86	132.97	20.22		2.08		-1.23	
U1332B	14X	7W	0.4- 0.42	119.00	133.17	17.65		2.23		-1.28	
U1332B	15X	2W	0.91- 0.93	119.27	133.54	1.36		1.84		-2.16	
U1332B	15X	2W	1.26- 1.28	119.50	133.86	22.12		1.90		-1.84	
U1332B	15X	4W	0.6- 0.62	121.20	136.24	-0.23		1.76		-2.71	
U1332B	15X	5W	0.64- 0.66	122.74	138.42	12.49		1.81		-1.96	
U1332B	15X	5W	0.83- 0.85	122.93	138.68	3.68		1.81		-2.01	
U1332B	15X	5W	1.22- 1.24	123.32	139.23	16.10		1.81		-2.06	
U1332B	15X	6W	0.7- 0.72	124.30	140.61		0.42		-0.19		-0.42
U1332B	15X	7W	0.1- 0.12	124.66	141.11	-1.52		2.21		-1.84	
U1332B	16X	1W	0.06- 0.08	124.85	141.38	8.53		2.06		-1.78	
U1332B	16X	1W	0.25- 0.27	125.20	141.87	-5.27		2.17		-1.63	
U1332B	17X	1W	0.12- 0.14	134.42	152.81		0.80		2.03		-1.32
U1332B	18X	1W	0.5- 0.52	144.40	159.94		0.36				
U1332B	18X	2W	0.21- 0.22	145.61	161.37		0.39				

Table A.2 – (Continued) IODP Site U1332B stable isotope and carbonate content data.

Site	Core	Section	Interval (m)	Depth CSF-A (m)	Depth CCSF-A (m)	Prism %CaCO ₃	Kiel %CaCO ₃	Prism δ ¹³ C	Kiel δ ¹³ C	Prism δ ¹⁸ O	Kiel δ ¹⁸ O
U1333A	13X	1W	0.4- 0.42	110.70	131.20	-8.41					
U1333A	13X	1W	0.88- 0.9	111.18	131.83	-15.30			2.03		-0.11
U1333A	13X	2W	0.02- 0.04	111.82	132.65	-12.93		1.96		-0.29	
U1333A	13X	2W	0.17- 0.19	111.97	132.84	4.71		1.78		-0.83	
U1333A	13X	2W	0.55- 0.57	112.35	133.31	12.70		1.73		-1.27	
U1333A	13X	2W	1.02- 1.04	112.82	133.88	16.48		1.57		-1.35	
U1333A	13X	2W	1.19- 1.21	112.99	134.09	4.74		1.59		-1.36	
U1333A	13X	2W	1.37- 1.39	113.17	134.30	28.67		1.41		-1.74	
U1333A	13X	3W	0.03- 0.05	113.33	134.49	-7.52		1.48		-1.72	
U1333A	13X	3W	0.55- 0.57	113.85	135.10	23.68		1.51		-1.69	
U1333A	13X	3W	1.08- 1.1	114.38	135.71	10.99		1.83		-1.40	
U1333A	13X	4W	0.17- 0.19	114.97	136.37	29.62		2.25		-1.25	
U1333A	13X	4W	0.45- 0.47	115.25	136.67	40.69		2.63		-0.70	
U1333A	13X	4W	1.02- 1.04	115.82	137.29	3.99		2.78		-0.98	
U1333A	13X	5W	0.35- 0.37	116.65	138.17		7.80		3.49		0.13
U1333A	13X	5W	0.5- 0.52	116.80	138.33		7.80		2.70		-0.50
U1333A	13X	5W	1.07- 1.09	117.37	138.92	17.20		2.57		-1.33	
U1333A	13X	6W	0.17- 0.19	117.97	139.54	9.85		2.96		-1.16	
U1333A	13X	6W	0.39- 0.41	118.19	139.76	10.99		2.69		-1.06	
U1333A	13X	6W	0.8- 0.82	118.60	140.17	25.44		2.67		-0.81	
U1333A	13X	6W	1.21- 1.23	119.01	140.58	46.98		2.62		-0.52	
U1333A	13X	7W	0.19- 0.21	119.49	141.06	37.70		2.66		-0.63	
U1333A	14X	1W	0.44- 0.46	120.44	141.99		12.89		2.73		-0.68
U1333A	14X	1W	0.85- 0.87	120.85	142.40	10.77		2.44		-0.82	
U1333A	14X	1W	1.08- 1.1	121.08	142.62		1.39				
U1333A	14X	1W	1.4- 1.42	121.40	142.93		3.69		2.59		-0.90
U1333A	14X	2W	0.04- 0.06	121.54	143.07	83.87		2.49		-1.01	
U1333A	14X	2W	0.22- 0.24	121.72	143.25	45.21		2.40		-0.70	
U1333A	14X	2W	0.42- 0.44	121.92	143.44	16.42		2.77		-0.40	
U1333A	14X	2W	0.95- 0.97	122.45	143.96	31.72		2.57		-0.81	
U1333A	14X	2W	1.28- 1.3	122.78	144.29	23.37		2.56		-0.78	
U1333A	14X	3W	0.02- 0.04	123.02	144.52	43.92		2.39		-0.87	
U1333A	14X	3W	0.5- 0.52	123.50	145.00	5.49		2.23		-1.20	
U1333A	14X	3W	1.03- 1.05	124.03	145.52	3.70		2.17		-1.15	
U1333A	14X	4W	0.1- 0.12	124.60	146.10	38.06		1.94		-0.95	

Table A.3 – IODP Site U1333A stable isotope and carbonate content data.

Site	Core	Section	Interval (m)	Depth CSF-A (m)	Depth CCSF-A (m)	Prism %CaCO ₃	Kiel %CaCO ₃	Prism δ ¹³ C	Kiel δ ¹³ C	Prism δ ¹⁸ O	Kiel δ ¹⁸ O
U1333A	14X	4W	0.41- 0.43	124.91	146.41	18.99		1.91		-1.22	
U1333A	14X	4W	0.63- 0.65	125.13	146.63	46.10		2.55		-0.67	
U1333A	14X	4W	0.88- 0.9	125.38	146.89	3.25		2.41		-0.83	
U1333A	14X	4W	0.97- 0.99	125.47	146.98	8.11		2.30		-0.78	
U1333A	14X	4W	1.13- 1.15	125.63	147.15	1.79		2.40		-0.48	
U1333A	14X	4W	1.38- 1.4	125.88	147.41	39.56		1.98		-0.27	
U1333A	14X	5W	0.02- 0.04	126.02	147.55	36.75		1.81		-1.10	
U1333A	14X	5W	0.54- 0.56	126.54	148.10		0.43		1.88		0.22
U1333A	14X	5W	0.94- 0.96	126.94	148.52	29.75		2.40		-0.61	
U1333A	14X	5W	1.2- 1.22	127.20	148.80	16.15		2.74		-0.31	
U1333A	14X	6W	0.21- 0.23	127.71	149.36	19.13		2.67		-0.17	
U1333A	14X	6W	0.78- 0.8	128.28	149.99	37.97		1.82		-0.71	
U1333A	14X	6W	1.12- 1.14	128.62	150.38	26.69		1.78		-1.07	
U1333A	14X	7W	0.36- 0.38	129.36	151.23	13.75		2.58		-0.72	
U1333A	15X	1W	0.54- 0.56	130.14	152.16	34.90		1.94		-0.85	
U1333A	15X	1W	0.81- 0.83	130.41	155.05	23.30		2.21		-0.75	
U1333A	15X	1W	1.09- 1.11	130.69	155.36	25.21		2.27		-0.30	
U1333A	15X	2W	0.13- 0.15	131.23	155.95	-2.92		2.28		-0.95	
U1333A	15X	2W	0.68- 0.7	131.78	156.55	46.26		1.98		-0.38	
U1333A	15X	2W	1.11- 1.13	132.21	157.02	32.44		1.89		-0.66	
U1333A	15X	3W	0.16- 0.18	132.76	157.62	46.60		1.96		-0.68	
U1333A	15X	3W	0.37- 0.39	132.97	157.85	34.41		2.26		-0.51	
U1333A	15X	3W	0.81- 0.83	133.41	158.33	42.93		2.14		-0.48	
U1333A	15X	3W	1.01- 1.03	133.61	158.54	46.91		2.07		-0.75	
U1333A	15X	3W	1.16- 1.18	133.76	158.71	25.51		2.22		-0.67	
U1333A	15X	4W	0.15- 0.17	134.25	159.24	33.24		2.25		-0.46	
U1333A	15X	4W	0.62- 0.64	134.72	159.76	25.28		2.53		-0.35	
U1333A	15X	4W	1.25- 1.27	135.35	160.44	56.60		2.34		-0.51	
U1333A	15X	5W	0.23- 0.25	135.83	160.97	27.09		2.21		-0.86	
U1333A	15X	5W	0.67- 0.69	136.27	161.45	47.43		2.17		-0.61	
U1333A	15X	5W	0.9- 0.92	136.50	161.70	14.32		2.28		-0.69	
U1333A	15X	5W	1- 1.02	136.60	161.81	10.44		2.25		-0.73	
U1333A	15X	5W	1.22- 1.24	136.82	162.05	26.96		2.31		-0.27	
U1333A	15X	6W	0.02- 0.04	137.12	162.38	47.74		2.54		-0.38	
U1333A	15X	6W	0.2- 0.22	137.30	162.57	14.81		2.79		-0.30	

Table A.3 – (Continued) IODP Site U1333A stable isotope and carbonate content data.

Site	Core	Section	Interval (m)	Depth CSF-A (m)	Depth CCSF-A (m)	Prism %CaCO3	Kiel %CaCO3	Prism $\delta^{13}C$	Kiel $\delta^{13}C$	Prism $\delta^{18}O$	Kiel $\delta^{18}O$
U1333A	15X	6W	0.44- 0.46	137.54	162.84	15.21		2.89		-0.71	
U1333A	15X	6W	0.66- 0.68	137.76	163.08	14.59		2.99		-0.90	
U1333A	15X	6W	0.82- 0.84	137.92	163.25		11.00		2.99		0.01
U1333A	15X	6W	1.2- 1.22	138.30	163.67		1.22		2.25		-0.74
U1333A	15X	7W	0.12- 0.14	138.72	164.12	23.95		2.91		-1.28	
U1333A	16X	1W	0.7- 0.72	139.90	165.41	6.43		3.31		-1.25	
U1333A	16X	2W	0.7- 0.72	141.40	167.05	1.74		3.49		-1.38	
U1333A	16X	3W	0.7- 0.72	142.90	168.69		0.22				
U1333A	16X	4W	0.7- 0.72	144.40	170.33	0.72		2.49		-1.85	
U1333A	16X	5W	0.64- 0.66	145.84	171.90	2.48		2.45		-0.98	
U1333A	16X	5W	1.3- 1.32	146.50	172.62	38.04		2.07		-1.01	
U1333A	16X	5W	1.4- 1.42	146.60	172.73	30.64		2.11		-0.91	
U1333A	16X	6W	0.36- 0.38	147.06	173.23	31.23		2.05		-0.91	
U1333A	16X	6W	0.59- 0.61	147.29	173.48	31.75		2.02		-0.87	
U1333A	16X	6W	0.91- 0.93	147.61	173.83	39.86			2.13		-0.78
U1333A	16X	6W	1.2- 1.22	147.90	174.15	71.66		2.02		-0.71	
U1333A	16X	7W	0.07- 0.09	148.27	174.55	166.54		1.95		-0.53	
U1333A	17X	1W	0.62- 0.64	149.42	175.81	143.63		2.20		-0.68	
U1333A	17X	1W	0.97- 0.99	149.77	177.94	220.03			2.07		-0.78
U1333A	17X	2W	0.08- 0.1	150.38	178.49	102.25		2.07		-0.74	
U1333A	17X	2W	0.24- 0.26	150.54	178.64	93.59		2.02		-0.93	
U1333A	17X	2W	0.51- 0.53	150.81	178.87	40.91		2.06		-0.83	
U1333A	17X	2W	0.91- 0.93	151.21	179.21	73.87		2.11		-1.02	
U1333A	17X	2W	1.14- 1.16	151.44	179.40	71.26		2.09		-0.92	
U1333A	17X	2W	1.38- 1.4	151.68	179.60	224.89			2.01		-0.93
U1333A	17X	3W	0.03- 0.05	151.83	179.72	82.64		1.95		-1.11	
U1333A	17X	3W	0.4- 0.42	152.20	180.01	46.41		2.22		-0.69	
U1333A	17X	3W	0.94- 0.96	152.74	180.43	53.14		2.06		-0.89	
U1333A	17X	3W	1.24- 1.26	153.04	180.66	105.63		2.04		-0.97	
U1333A	17X	4W	0.1- 0.12	153.40	180.93	88.42		2.15		-0.91	
U1333A	17X	4W	0.4- 0.42	153.70	181.15	137.58			2.17		-1.01
U1333A	17X	4W	1.1- 1.12	154.40	181.65	91.98		1.90		-1.22	
U1333A	17X	5W	0.4- 0.42	155.20	182.21	56.97		1.99		-1.18	
U1333A	18X	1W	0.25- 0.27	155.50	182.42	36.05			1.82		-1.05
U1333A	17X	5W	0.7- 0.72	155.90	182.69	32.91		2.01		-1.14	

Table A.3 – (Continued) IODP Site U1333A stable isotope and carbonate content data.

Site	Core	Section	Interval (m)	Depth CSF-A (m)	Depth CCSF-A (m)	Prism %CaCO3	Kiel %CaCO3	Prism $\delta^{13}C$	Kiel $\delta^{13}C$	Prism $\delta^{18}O$	Kiel $\delta^{18}O$
U1333A	18X	1W	0.7- 0.72	156.20	182.90	38.35			1.80		-1.16
U1333A	17X	5W	1.1- 1.12	156.66	183.21	54.95		1.58		-1.03	
U1333A	17X	5W	1.4- 1.42	157.00	183.44	143.75			1.92		-0.97
U1333A	17X	6W	0.36- 0.38	157.33	183.66	32.74		1.89		-1.40	
U1333A	18X	2W	0.33- 0.35	157.83	184.00	35.45		1.81		-1.23	
U1333A	17X	6W	0.7- 0.72	158.10	184.18	58.57		1.86		-1.29	
U1333A	17X	6W	1.03- 1.05	158.55	184.49	40.48		1.95		-1.41	
U1333A	17X	7W	0.03- 0.05	159.10	184.86	57.60		2.10		-1.29	
U1333A	17X	7W	0.25- 0.27	160.23	185.65	34.45		1.85		-1.13	
U1333A	18X	3W	0.7- 0.72	161.44	186.51	7.77		1.75		-1.04	
U1333A	18X	4W	0.15- 0.17	162.39	187.21	1.70		1.78		-0.90	
U1333A	18X	4W	0.38- 0.4	162.62	187.38	59.89		1.97		-0.62	
U1333A	18X	4W	0.48- 0.5	162.72	187.45	12.77		1.86		-0.70	
U1333A	18X	4W	0.72- 0.74	162.96	187.64	39.60		1.95		-0.85	
U1333A	18X	4W	0.78- 0.8	163.02	187.68	34.05		1.94		-0.75	
U1333A	18X	4W	0.87- 0.89	163.11	187.75	49.42		1.97		-0.94	
U1333A	18X	4W	1.03- 1.05	163.27	187.87	36.70		2.02		-0.90	
U1333A	18X	4W	1.12- 1.14	163.36	187.94		10.59		2.13		-0.21
U1333A	18X	4W	1.26- 1.28	163.50	188.05	5.52		1.99		-0.98	
U1333A	19X	1W	0.4- 0.42	168.40	192.20	62.85		2.23		-0.65	
U1333A	19X	1W	0.6- 0.62	168.60	192.39	22.35		2.16		-0.67	
U1333A	19X	1W	0.81- 0.83	168.81	192.58	34.90		2.05		-0.77	
U1333A	19X	1W	0.98- 1	168.98	192.74	14.25		2.00		-0.81	
U1333A	19X	1W	1.14- 1.16	169.14	192.89	105.16		1.85		-0.82	
U1333A	19X	2W	0.48- 0.5	169.98	193.69	24.83		2.14		-0.69	
U1333A	19X	2W	0.58- 0.6	170.08	193.78	12.95		2.10		-0.76	
U1333A	19X	2W	0.72- 0.74	170.22	193.92	39.92		2.16		-0.76	
U1333A	19X	2W	0.9- 0.92	170.40	194.09	21.46		2.04		-0.64	
U1333A	19X	2W	1.22- 1.24	170.72	194.41	27.44		2.03		-0.93	
U1333A	19X	3W	0.19- 0.21	171.19	194.87		1.74		2.24		-0.67
U1333A	19X	3W	0.52- 0.54	171.52	195.20	16.81		2.22		-0.71	
U1333A	19X	3W	1.4- 1.42	172.40	196.08	24.31		1.99		-0.34	
U1333A	19X	4W	0.33- 0.35	172.83	196.51	40.78		2.13		0.19	
U1333A	19X	4W	0.95- 0.97	173.45	197.14	57.98		1.95		0.28	
U1333A	19X	4W	1.25- 1.27	173.75	197.45		0.34				

Table A.3 – (Continued) IODP Site U1333A stable isotope and carbonate content data.

Site	Core	Section	Interval (m)	Depth CSF-A (m)	Depth CCSF-A (m)	Prism %CaCO ₃	Kiel %CaCO ₃	Prism δ ¹³ C	Kiel δ ¹³ C	Prism δ ¹⁸ O	Kiel δ ¹⁸ O
U1333A	19X	5W	0.07- 0.09	174.07	197.78	40.18		1.93		-1.24	
U1333A	19X	5W	0.12- 0.14	174.12	197.83	55.46		1.87		-1.17	
U1333A	19X	5W	0.27- 0.29	174.27	197.98	42.90		1.93		-1.34	
U1333A	19X	5W	0.36- 0.38	174.36	198.07	43.66		2.03		-1.06	
U1333A	20X	1W	0.2- 0.22	177.80	201.58	37.31		1.93		-1.15	
U1333A	20X	1W	0.3- 0.32	177.90	201.67	54.03		1.92		-1.09	
U1333A	20X	1W	0.43- 0.45	178.03	201.80	47.67		1.94		-1.15	
U1333A	20X	1W	0.54- 0.56	178.14	201.91	51.61		1.88		-0.93	
U1333A	20X	1W	0.61- 0.63	178.21	201.98	50.93		1.87		-1.01	
U1333A	20X	1W	0.72- 0.74	178.32	202.09	58.51		1.79		-0.94	
U1333A	20X	1W	0.91- 0.93	178.51	202.27	57.98		1.75		-0.90	
U1333A	20X	1W	1.08- 1.1	178.68	202.44	14.04		1.77		-1.00	
U1333A	20X	1W	1.14- 1.16	178.74	202.50	49.71		1.80		-0.83	
U1333A	20X	1W	1.22- 1.24	178.82	202.57	437.96		1.77		-0.83	
U1333A	20X	1W	1.33- 1.35	178.93	202.68	53.76		1.82		-0.84	
U1333A	20X	2W	0.16- 0.18	179.26	202.99	44.96		1.78		-0.72	
U1333A	20X	2W	0.28- 0.3	179.38	203.11	56.09		1.81		-0.66	
U1333A	20X	2W	0.36- 0.38	179.46	203.18	27.20		1.85		-0.67	
U1333A	20X	2W	0.52- 0.54	179.62	203.33	40.10		1.88		-0.61	
U1333A	20X	2W	0.63- 0.65	179.73	203.44	56.74		1.90		-0.47	

Table A.3 – (Continued) IODP Site U1333A stable isotope and carbonate content data.

Appendix B

Data Repository

Depth	$\delta^{13}\text{C}$	$\delta^{18}\text{O}$	CARBONATE CONTENT	Dry Weight	PLANKTIC	BENTHIC	TOTAL P+B	Planktonic/ Benthonic Ratio P/P+B
mbsl	‰	‰	wt %	gr	#	#	#	
20.30			0.00	1.640	0	0	0	0.000
20.79			0.00	1.503	0	0	0	0.000
21.17			0.00	1.426	0	0	0	0.000
21.51			0.00	1.515	0	0	0	0.000
21.88			0.00	1.448	0	0	0	0.000
22.33			0.00	1.874	0	0	0	0.000
22.74			0.00	1.528	0	0	0	0.000
23.07			0.00	1.609	0	0	0	0.000
23.33			0.00	1.553	0	0	0	0.000
23.63			0.00	1.784	0	0	0	0.000
24.05			0.00	1.677	0	1	1	0.000
24.48			0.00	1.857	0	0	0	0.000
24.87			0.00	1.020	0	0	0	0.000
25.28	1.44	-2.06	7.88	0.686	0	0	0	0.000
25.73			1.63	1.538	0	1	1	0.000
26.12	1.90	-1.61	61.05	2.053	0	25	25	0.000
26.29	1.84	-1.85	60.00	2.536	0	27	27	0.000
26.61	1.71	-1.86	16.62	1.470	0	0	0	0.000
26.85	1.79	-1.62	77.10	3.244	3	17	20	0.150
27.19	1.82	-1.49	78.62	2.847	5	32	37	0.135
27.56	1.66	-1.76	56.41	2.955	0	2	2	0.000
27.79	1.65	-1.74	62.00	2.352	0	23	23	0.000
28.06	1.92	-1.39	100.00	3.132	10	59	69	0.145
28.38	1.72	-1.40	81.49	2.661	6	40	46	0.130
28.42	1.60	-1.41	42.49	1.604	0	0	0	0.000
28.48	1.15	-1.73	25.64	1.505	0	0	0	0.000
28.56	1.10	-2.06	9.45	1.709	0	0	0	0.000
28.61	1.02	-2.23	1.42	1.696	0	0	0	0.000
28.65	1.96	-1.48	68.72	2.355	1	20	21	0.048
28.72	1.98	-1.40	60.82	3.128	1	16	17	0.059
28.95	2.00	-1.38	64.58	3.364	14	14	28	0.500
29.25	1.87	-1.57	83.46	2.893	14	109	123	0.114
29.51	1.90	-1.50	83.44	3.250	32	63	95	0.337
29.75	1.86	-1.61	49.83	2.017	8	21	29	0.276
29.80	1.73	-1.73	47.51	1.993	2	12	14	0.143
29.90	1.67	-1.73	40.65	1.532	5	26	31	0.161
30.00	1.68	-1.61	38.29	1.538	0	13	13	0.000
30.37	1.81	-1.46	78.90	2.948	214	497	711	0.301
30.62	1.76	-1.51	64.97	2.393	7	15	22	0.318
30.79	1.90	-1.44	86.69	3.540	26	69	95	0.274

Table B.1 – Carbon and oxygen isotopes carbonate content, sample dry weight, and foraminifera counts at ODP Site 1215A.

Depth	$\delta^{13}\text{C}$	$\delta^{18}\text{O}$	Carbonate Content	Dry Weight	Planktic	Benthic	Total P+B	Planktonic/Benthonic Ratio P/P+B
mbsl	‰	‰	wt %	gr	#	#	#	
31.06	1.86	-1.54	84.48	2.160	62	43	105	0.590
31.41	1.61	-1.43	83.96	2.885	35	15	50	0.700
31.89	1.70	-1.45	86.30	2.757	309	83	392	0.788
32.24	1.81	-1.57	84.09	2.309	43	27	70	0.614
32.59	1.69	-1.44	84.96	2.609	108	33	141	0.766
32.81	1.66	-1.47	90.67	3.447	306	93	399	0.767
33.07	1.67	-1.46	86.59	3.015	198	63	261	0.759
33.38	1.66	-1.48	84.75	2.762	119	67	186	0.640
33.76	1.62	-1.51	89.75	3.804	121	92	213	0.568
33.90	1.66	-1.47	73.32	3.602	187	61	248	0.754
34.01	1.52	-1.54	68.26	3.313	52	53	105	0.495
34.22	1.42	-1.67	41.44	2.244	35	21	56	0.625
34.27	1.46	-1.62	41.51	2.550	30	32	62	0.484
34.32	1.42	-1.63	42.50	2.246	9	13	22	0.409
34.38	1.43	-1.70	34.11	2.817	6	12	18	0.333
34.48	1.72	-1.57	65.92	4.324	27	24	51	0.529
34.61	1.81	-1.60	75.74	3.047	5	10	15	0.333
35.02	1.80	-1.65	70.48	2.057	10	40	50	0.200
35.31	1.86	-1.59	83.89	3.249	5	27	32	0.156
35.89	1.89	-1.45	79.18	2.690	45	18	63	0.714
36.32	1.87	-1.66	53.14	2.071	1	24	25	0.040
36.81	1.93	-1.67	79.65	3.389	16	28	44	0.364
37.11	2.03	-1.52	83.25	3.820	9	41	50	0.180
37.50	1.91	-1.55	100.00	2.946	2	41	43	0.047
37.97	1.84	-1.60	80.02	3.635	1	47	48	0.021
38.20	1.90	-1.52	71.00	2.889	29	43	72	0.403
38.50	1.92	-1.50	71.79	2.977	4	40	44	0.091
38.88	1.85	-1.49	70.89	3.272	2	1	3	0.667
39.50	1.85	-1.65	60.77	2.811	8	38	46	0.174
39.87	2.10	-1.80	65.27	2.029	2	60	62	0.032
40.16	2.13	-1.71	82.18	3.011	15	44	59	0.254
40.61	2.20	-1.63	80.58	2.911	8	63	71	0.113
40.82	2.22	-1.53	90.46	5.047	15	51	66	0.227
40.97	2.10	-1.66	67.04	2.598	3	20	23	0.130
41.32	2.19	-1.67	68.84	2.966	0	64	64	0.000
41.97	2.11	-1.60	87.10	3.479	19	72	91	0.209
42.08	2.07	-1.65	70.33	2.726	32	46	78	0.410
42.31	2.24	-1.57	82.16	3.612	28	27	55	0.509
42.61	2.15	-1.48	68.45	2.983	15	34	49	0.306

Table B.1 – (Continued) Carbon and oxygen isotopes, carbonate content, sample dry weight, and foraminifera counts at ODP Site 1215A.

Depth	$\delta^{13}\text{C}$	$\delta^{18}\text{O}$	Carbonate Content	Dry Weight	Planktic	Benthic	Total P+B	Planktonic/ Benthonic Ratio P/P+B
mbsl	‰	‰	wt %	gr	#	#	#	
43.12	2.23	-1.52	73.01	2.179	8	21	29	0.276
43.49	2.32	-1.65	88.74	3.035	20	186	206	0.097
43.99	2.39	-1.63	79.99	2.576	8	35	43	0.186
44.38	2.35	-1.85	74.12	2.780	5	96	101	0.050
44.76	2.36	-1.83	66.68	2.769	3	85	88	0.034
45.01	2.41	-1.70	68.95	2.682	3	127	130	0.023
45.31	2.25	-1.70	79.02	2.772	7	7	14	0.500
45.62	2.27	-1.69	88.80	5.060	73	92	165	0.442
46.12	2.19	-1.80	82.69	3.169	31	39	70	0.443
46.47	2.11	-1.89	82.17	3.569	307	47	354	0.867
46.93	2.29	-1.80	73.94	2.587	46	20	66	0.697
50.70	2.26	-1.96	78.30	1.635	0	1	1	0.000
50.99	2.23	-1.82	75.81	2.093	1	6	7	0.143
51.29	2.02	-1.99	62.19	2.751	1	37	38	0.026
51.58	2.07	-1.67	75.02	2.516	1	40	41	0.024
51.92	1.99	-1.89	80.11	2.803	5	61	66	0.076
52.28	1.68	-2.17	80.96	3.995	75	116	191	0.393
52.76	1.78	-2.16	81.20	2.894	44	92	136	0.324
53.07	1.85	-2.11	84.27	2.653	138	51	189	0.730
53.46	1.85	-2.13	85.42	4.271	60	21	81	0.741
53.73	2.00	-1.91	84.61	2.966	63	103	166	0.380
54.14	1.24	-2.14	27.78	2.119	2	49	51	0.039
54.32	1.08	-2.26	21.11	1.703	2	9	11	0.182
54.32	1.45	-1.95	21.12	1.799	3	28	31	0.097
54.51	2.19	-1.81	7.33	2.480	0	17	17	0.000
54.58	1.98	-2.04	9.18	1.798	1	12	13	0.077
54.97	2.65	-1.21	50.06	2.500	3	15	18	0.167
55.38	3.10	-0.98	68.47	3.623	11	127	138	0.080
55.65	2.98	-0.79	79.10	3.044	3	112	115	0.026
55.97	3.02	-0.74	75.77	2.369	9	92	101	0.089
56.30	3.22	-0.62	62.45	3.080	19	195	214	0.089
56.70	3.43	-0.64	51.64	2.696	14	140	154	0.091
57.17	3.09	-1.24	54.42	3.061	19	244	263	0.072
57.50	3.20	-1.45	79.69	3.595	87	240	327	0.266
57.90	3.13	-1.38	80.30	2.799	25	319	344	0.073
58.27	3.31	-1.32	73.70	2.805	24	127	151	0.159
58.77	3.18	-1.44	73.84	5.000	45	333	378	0.119
59.10	3.05	-1.69	73.33	2.751	19	247	266	0.071

Table B.1 – (Continued) Carbon and oxygen isotopes, carbonate content, sample dry weight, and foraminifera counts at ODP Site 1215A.

Depth	Radiolar..	Fish Teeth	Other Fossils	Chert	Iron	Ostrac.	Total Counts
mbsf	#	#	#	#	#	#	#
20.30		4					4
20.79		2					2
21.17		1					1
21.51		2					2
21.88		1					1
22.33		1					1
22.74		0					0
23.07		0					0
23.33		0					0
23.63		0					0
24.05	3	6					10
24.48		0					0
24.87	0	0					0
25.28		0					0
25.73	0	0					1
26.12	1	1					27
26.29	0	2					29
26.61							0
26.85	0	1					21
27.19							37
27.56	0	0					2
27.79	0	1					24
28.06		1					70
28.38							46
28.42							0
28.48							0
28.56							0
28.61							0
28.65	3						24
28.72	4	1		1			23
28.95	1	2					31
29.25		1					124
29.51		2					97
29.75		3					32
29.80	0	2		64			80
29.90	0	9		61	7	0	108
30.00	0	4		4			21
30.37		15			17		743
30.62	1	3					26
30.79		1			1		97

Table B.2 – Counts of other microfossils and mineral grains at ODP Site 1215A.

Depth	Radiolar..	Fish Teeth	Other Fossils	Chert	Iron	Ostrac..	Total Counts
mbsf	#	#	#	#	#	#	#
31.06		1					106
31.41							50
31.89		2					394
32.24							70
32.59							141
32.81				1			400
33.07		2		4			267
33.38		1					187
33.76	1			2			216
33.90				38			286
34.01		2		41			148
34.22	4			12			72
34.27	2	2		32	1		99
34.32				19			41
34.38	2			4			24
34.48	8	1		7			67
34.61		2		11			28
35.02		1		2			53
35.31		1		1			34
35.89		1		4			68
36.32				1			26
36.81	2						46
37.11							50
37.50							43
37.97		3					51
38.20	11				75	2	158
38.50	16			4	57		121
38.88	1				0		74
39.50		2			17		65
39.87							62
40.16					7		66
40.61		1			21		93
40.82					4		70
40.97							23
41.32		1					65
41.97	2			1			94
42.08	1	4					83
42.31							55
42.61							49

Table B.2 – (Continued) Counts of other microfossils and mineral grains at ODP

Site 1215A.

Depth	Radiolar.	Fish Teeth	Other Fossils.	Chert	Iron	Ostrac.	Total Counts
mbsf	#	#	#	#	#	#	#
43.12		1					30
43.49			1		3		210
43.99		1					44
44.38							101
44.76		3					91
45.01		1					131
45.31							14
45.62		1					166
46.12		2					72
46.47							354
46.93		3					69
50.70				4	0		5
50.99				4	1		12
51.29							38
51.58							41
51.92							66
52.28		3					194
52.76	2						138
53.07		1					190
53.46		1					82
53.73		3		4			173
54.14		3		35			89
54.32				8			19
54.32		1		23			55
54.51	1	2		11			31
54.58		4		7	1		25
54.97							18
55.38	1	1	1		4		145
55.65	2				5		122
55.97	1	6					108
56.30	1	0					215
56.70		7					161
57.17	2	4					269
57.50	2	6			0		335
57.90	1	7					352
58.27	1	5					157
58.77	1	7	4				390
59.10	1	2	1				270

Table B.2 – (Continued) Counts of other microfossils and mineral grains at ODP

Site 1215A.

Depth	Fragments	whole	(FRAG/8)/	Fragments
mbsf	#	tests	((FRAG/8)+WHOLE)	%
20.30	0	0	∞	∞
20.79	0	0	∞	∞
21.17	0	0	∞	∞
21.51	0	0	∞	∞
21.88	0	0	∞	∞
22.33	0	0	∞	∞
22.74	0	0	∞	∞
23.07	0	0	∞	∞
23.33	0	0	∞	∞
23.63	0	0	∞	∞
24.05	2	0	1.000	100.0
24.48	0	0	∞	∞
24.87	0	0	∞	∞
25.28	0	0	∞	∞
25.73	1	0	1.000	100.0
26.12	0	0	∞	∞
26.29	1	0	1.000	100.0
26.61	0	0	∞	∞
26.85	2	3	0.077	7.7
27.19	3	5	0.070	7.0
27.56	0	0	∞	∞
27.79	1	0	1.000	100.0
28.06	6	10	0.070	7.0
28.38	4	6	0.077	7.7
28.42	0	0	∞	∞
28.48	0	0	∞	∞
28.56	0	0	∞	∞
28.61	0	0	∞	∞
28.65	2	1	0.200	20.0
28.72	1	1	0.111	11.1
28.95	7	14	0.059	5.9
29.25	3	14	0.026	2.6
29.51	4	32	0.015	1.5
29.75	3	8	0.045	4.5
29.80	4	2	0.200	20.0
29.90	7	5	0.149	14.9
30.00	7	0	1.000	100.0
30.37	50	214	0.028	2.8
30.62	6	7	0.097	9.7
30.79	2	26	0.010	1.0

Table B.3 – Counts of planktic foraminifera fragments and whole test, and fragmentation percentage at ODP Site 1215A.

Depth	Fragments	whole	(FRAG/8)/	Fragments
mbsf	#	tests	((FRAG/8)+WHOLE)	%
31.06	5	62	0.010	1.0
31.41	15	35	0.051	5.1
31.89	22	309	0.009	0.9
32.24	6	43	0.017	1.7
32.59	4	108	0.005	0.5
32.81	8	306	0.003	0.3
33.07	24	198	0.015	1.5
33.38	16	119	0.017	1.7
33.76	13	121	0.013	1.3
33.90	74	187	0.047	4.7
34.01	7	52	0.017	1.7
34.22	11	35	0.038	3.8
34.27	10	30	0.040	4.0
34.32		9	0.000	0.0
34.38	3	6	0.059	5.9
34.48	1	27	0.005	0.5
34.61		5	0.000	0.0
35.02		10	0.000	0.0
35.31	2	5	0.048	4.8
35.89	2	45	0.006	0.6
36.32		1	0.000	0.0
36.81		16	0.000	0.0
37.11		9	0.000	0.0
37.50		2	0.000	0.0
37.97		1	0.000	0.0
38.20	13	29	0.053	5.3
38.50	12	4	0.273	27.3
38.88	9	2	0.360	36.0
39.50	2	8	0.030	3.0
39.87		2	0.000	0.0
40.16	2	15	0.016	1.6
40.61	4	8	0.059	5.9
40.82	2	15	0.016	1.6
40.97	2	3	0.077	7.7
41.32	2	0	1.000	100.0
41.97	4	19	0.026	2.6
42.08	20	32	0.072	7.2
42.31	27	28	0.108	10.8
42.61	3	15	0.024	2.4

Table B.3 – (Continued) Counts of planktic foraminifera fragments and whole test, and fragmentation percentage at ODP Site 1215A.

Depth	Fragments	whole	(FRAG/8)/	Fragments
mbsf	#	tests	((FRAG/8)+WHOLE)	%
43.12	1	8	0.015	1.5
43.49	4	20	0.024	2.4
43.99		8	0.000	0.0
44.38	7	5	0.149	14.9
44.76	2	3	0.077	7.7
45.01		3	0.000	0.0
45.31	2	7	0.034	3.4
45.62	6	73	0.010	1.0
46.12	7	31	0.027	2.7
46.47	23	307	0.009	0.9
46.93	13	46	0.034	3.4
50.70		0	∞	∞
50.99		1	0.000	0.0
51.29	1	1	0.111	11.1
51.58		1	0.000	0.0
51.92	2	5	0.048	4.8
52.28	18	75	0.029	2.9
52.76	27	44	0.071	7.1
53.07	34	138	0.030	3.0
53.46	12	60	0.024	2.4
53.73	26	63	0.049	4.9
54.14	2	2	0.111	11.1
54.32	1	2	0.059	5.9
54.32	2	3	0.077	7.7
54.51	0	0	∞	∞
54.58	2	1	0.200	20.0
54.97	2	3	0.077	7.7
55.38	2	11	0.022	2.2
55.65	2	3	0.077	7.7
55.97	3	9	0.040	4.0
56.30	4	19	0.026	2.6
56.70	7	14	0.059	5.9
57.17	20	19	0.116	11.6
57.50	29	87	0.040	4.0
57.90	10	25	0.048	4.8
58.27	14	24	0.068	6.8
58.77	17	45	0.045	4.5
59.10	23	19	0.131	13.1

Table B.3 – (Continued) Counts of planktic foraminifera fragments and whole test, and fragmentation percentage at ODP Site 1215A.

Depth (msbf)	CCSF (m)	Acarina (%)	Morozovella (%)	Subbotina (%)	Globanomalina (%)	Praetenuitella (%)	Igorina (%)	Chilloguembelina (%)	$\delta^{13}C$	$\delta^{18}O$
20.30	20.74	0.00	0.00	0.00	0.00	0.00	0.00	0.00		
20.79	22.71	0.00	0.00	0.00	0.00	0.00	0.00	0.00		
21.17	23.06	0.00	0.00	0.00	0.00	0.00	0.00	0.00		
21.51	23.37	0.00	0.00	0.00	0.00	0.00	0.00	0.00		
21.88	23.72	0.00	0.00	0.00	0.00	0.00	0.00	0.00		
22.33	24.14	0.00	0.00	0.00	0.00	0.00	0.00	0.00		
22.74	24.51	0.00	0.00	0.00	0.00	0.00	0.00	0.00		
23.07	24.82	0.00	0.00	0.00	0.00	0.00	0.00	0.00		
23.33	25.04	0.00	0.00	0.00	0.00	0.00	0.00	0.00		
23.63	25.32	0.00	0.00	0.00	0.00	0.00	0.00	0.00		
24.05	25.72	0.00	0.00	0.00	0.00	0.00	0.00	0.00		
24.48	26.11	0.00	0.00	0.00	0.00	0.00	0.00	0.00		
24.87	26.46	0.00	0.00	0.00	0.00	0.00	0.00	0.00		
25.28	26.85	0.00	0.00	0.00	0.00	0.00	0.00	0.00	1.44	-2.06
25.73	27.25	0.00	0.00	0.00	0.00	0.00	0.00	0.00		
26.12	27.60	0.00	0.00	0.00	0.00	0.00	0.00	0.00	1.90	-1.61
26.29	27.78	0.00	0.00	0.00	0.00	0.00	0.00	0.00	1.84	-1.85
26.61	28.06	0.00	0.00	0.00	0.00	0.00	0.00	0.00	1.71	-1.86
26.85	28.30	100.00	0.00	0.00	0.00	0.00	0.00	0.00	1.79	-1.62
27.19	28.61	80.00	0.00	0.00	0.00	0.00	0.00	20.00	1.82	-1.49
27.56	28.94	0.00	0.00	0.00	0.00	0.00	0.00	0.00	1.66	-1.76
27.79	29.16	0.00	0.00	0.00	0.00	0.00	0.00	0.00	1.65	-1.74
28.06	29.40	53.33	0.00	13.33	0.00	20.00	13.33	0.00	1.92	-1.39
28.38	29.70	66.67	16.67	0.00	0.00	16.67	0.00	0.00	1.72	-1.40
28.42	29.73	0.00	0.00	0.00	0.00	0.00	0.00	0.00	1.60	-1.41
28.48	29.79	0.00	0.00	0.00	0.00	0.00	0.00	0.00	1.15	-1.73
28.56	29.86	0.00	0.00	0.00	0.00	0.00	0.00	0.00	1.10	-2.06
28.61	29.90	0.00	0.00	0.00	0.00	0.00	0.00	0.00	1.02	-2.23
28.65	29.94	0.00	100.00	0.00	0.00	0.00	0.00	0.00	1.96	-1.48
28.72	30.01	0.00	0.00	0.00	0.00	100.00	0.00	0.00	1.98	-1.40
28.95	30.21	21.43	42.86	0.00	0.00	35.71	0.00	0.00	2.00	-1.38
29.25	30.51	42.86	0.00	0.00	0.00	57.14	0.00	0.00	1.87	-1.57
29.51	30.73	65.63	3.13	0.00	0.00	28.13	0.00	3.13	1.90	-1.50
29.75	30.97	62.50	0.00	0.00	0.00	37.50	0.00	0.00	1.86	-1.61
29.80	31.30	0.00	0.00	0.00	0.00	100.00	0.00	0.00	1.73	-1.73

Table B.4 – Relative abundances of selected planktonic foraminiferal genera at ODP Site 1215A.

Depth (msbf)	CCSF (m)	Acarinina (%)	Morozovella (%)	Subbotina (%)	Globanomalina (%)	Praetenuitella (%)	Igorina (%)	Chiloumbelina (%)	$\delta^{13}C$	$\delta^{18}O$
29.90	31.39	0.00	0.00	0.00	0.00	100.00	0.00	0.00	1.67	-1.73
30.00	31.48	0.00	0.00	0.00	0.00	0.00	0.00	0.00	1.68	-1.61
30.37	31.83	21.43	1.30	0.00	0.00	74.68	0.00	2.60	1.81	-1.46
30.62	32.05	66.67	6.67	0.00	0.00	26.67	0.00	0.00	1.76	-1.51
30.79	32.22	76.92	11.54	0.00	0.00	7.69	0.00	3.85	1.90	-1.44
31.06	32.46	66.13	19.36	1.61	0.00	12.90	0.00	0.00	1.86	-1.54
31.41	32.77	50.00	11.77	0.00	0.00	23.53	2.94	11.77	1.61	-1.43
31.89	33.23	59.87	5.83	0.65	0.00	25.24	0.97	7.44	1.70	-1.45
32.24	33.54	86.05	2.33	0.00	0.00	6.98	2.33	2.33	1.81	-1.57
32.59	33.87	85.19	3.70	0.93	0.00	4.63	0.93	4.63	1.69	-1.44
32.81	34.06	71.24	4.25	0.33	0.33	18.63	0.00	5.23	1.66	-1.47
33.07	34.24	70.71	6.57	0.00	0.00	16.16	1.01	5.56	1.67	-1.46
33.38	34.59	76.47	8.40	0.84	0.00	10.92	1.68	1.68	1.66	-1.48
33.76	34.94	69.42	10.74	2.48	0.00	12.40	0.00	4.96	1.62	-1.51
33.90	35.07	74.87	3.74	0.00	0.00	12.30	0.00	9.09	1.66	-1.47
34.01	35.16	78.85	1.92	0.00	0.00	11.54	0.00	7.69	1.52	-1.54
34.22	35.40	88.57	0.00	0.00	0.00	5.71	0.00	5.71	1.42	-1.67
34.27	35.42	80.00	0.00	0.00	3.33	16.67	0.00	0.00	1.46	-1.62
34.32	35.46	100.00	0.00	0.00	0.00	0.00	0.00	0.00	1.42	-1.63
34.38	35.51	100.00	0.00	0.00	0.00	0.00	0.00	0.00	1.43	-1.70
34.48	35.60	77.78	0.00	0.00	0.00	11.11	0.00	11.11	1.72	-1.57
34.61	35.71	100.00	0.00	0.00	0.00	0.00	0.00	0.00	1.81	-1.60
35.02	36.08	100.00	0.00	0.00	0.00	0.00	0.00	0.00	1.80	-1.65
35.31	36.38	100.00	0.00	0.00	0.00	0.00	0.00	0.00	1.86	-1.59
35.89	36.89	22.22	0.00	2.22	0.00	75.56	0.00	0.00	1.89	-1.45
36.32	37.30	95.65	4.35	0.00	0.00	0.00	0.00	0.00	1.87	-1.66
36.81	37.76	100.00	0.00	0.00	0.00	0.00	0.00	0.00	1.93	-1.67
37.11	38.01	92.86	0.00	7.14	0.00	0.00	0.00	0.00	2.03	-1.52
37.50	38.38	50.00	0.00	0.00	0.00	0.00	0.00	50.00	1.91	-1.55
37.97	38.82	0.00	0.00	0.00	0.00	100.00	0.00	0.00	1.84	-1.60
38.20	39.03	79.31	3.45	3.45	0.00	13.79	0.00	0.00	1.90	-1.52
38.50	39.30	66.67	22.22	0.00	0.00	11.11	0.00	0.00	1.92	-1.50
38.88	39.65	100.00	0.00	0.00	0.00	0.00	0.00	0.00	1.85	-1.49
39.50	40.22	87.50	0.00	0.00	12.50	0.00	0.00	0.00	1.85	-1.65
39.87	41.14	50.00	0.00	0.00	0.00	50.00	0.00	0.00	2.10	-1.80

Table B.4 – (Continued) Relative abundance of selected planktonic foraminiferal genera at ODP Site 1215A.

Depth (msbf)	CCSF (m)	Acarinina (%)	Morozovella (%)	Subbotina (%)	Globanomalina (%)	Praetenuitella (%)	Igorina (%)	Chiliguembelina (%)	$\delta^{13}C$	$\delta^{18}O$
40.16	41.40	93.33	6.67	0.00	0.00	0.00	0.00	0.00	2.13	-1.71
40.61	41.80	62.50	0.00	0.00	37.50	0.00	0.00	0.00	2.20	-1.63
40.82	42.01	93.33	6.67	0.00	0.00	0.00	0.00	0.00	2.22	-1.53
40.97	42.15	100.00	0.00	0.00	0.00	0.00	0.00	0.00	2.10	-1.66
41.32	42.50	0.00	0.00	0.00	0.00	0.00	0.00	0.00	2.19	-1.67
41.97	43.07	94.74	5.26	0.00	0.00	0.00	0.00	0.00	2.11	-1.60
42.08	43.17	90.63	0.00	0.00	0.00	9.38	0.00	0.00	2.07	-1.65
42.31	43.37	53.57	3.57	0.00	0.00	42.86	0.00	0.00	2.24	-1.57
42.61	43.66	100.00	0.00	0.00	0.00	0.00	0.00	0.00	2.15	-1.48
43.12	44.10	88.89	11.11	0.00	0.00	0.00	0.00	0.00	2.23	-1.52
43.49	44.45	35.00	5.00	0.00	0.00	60.00	0.00	0.00	2.32	-1.65
43.99	44.93	87.50	12.50	0.00	0.00	0.00	0.00	0.00	2.39	-1.63
44.38	45.28	60.00	20.00	0.00	20.00	0.00	0.00	0.00	2.35	-1.85
44.76	45.63	100.00	0.00	0.00	0.00	0.00	0.00	0.00	2.36	-1.83
45.01	45.87	33.33	0.00	0.00	0.00	66.67	0.00	0.00	2.41	-1.70
45.31	46.13	85.71	0.00	0.00	0.00	14.29	0.00	0.00	2.25	-1.70
45.62	46.42	64.38	23.29	0.00	1.37	10.96	0.00	0.00	2.27	-1.69
46.12	46.88	74.19	9.68	6.45	0.00	9.68	0.00	0.00	2.19	-1.80
46.47	47.20	76.87	14.66	2.93	0.00	3.91	0.65	0.98	2.11	-1.89
46.93	47.62	82.61	10.87	0.00	0.00	6.52	0.00	0.00	2.29	-1.80
50.70	50.18	0.00	0.00	0.00	0.00	0.00	0.00	0.00	2.26	-1.96
50.99	50.45	100.00	0.00	0.00	0.00	0.00	0.00	0.00	2.23	-1.82
51.29	50.71	100.00	0.00	0.00	0.00	0.00	0.00	0.00	2.02	-1.99
51.58	50.99	33.33	33.33	0.00	33.33	0.00	0.00	0.00	2.07	-1.67
51.92	51.30	40.00	0.00	20.00	0.00	40.00	0.00	0.00	1.99	-1.89
52.28	51.63	58.67	1.33	1.33	0.00	38.67	0.00	0.00	1.68	-2.17
52.76	52.07	84.09	6.82	0.00	0.00	9.09	0.00	0.00	1.78	-2.16
53.07	52.35	86.23	9.42	0.00	1.45	2.90	0.00	0.00	1.85	-2.11
53.46	52.72	70.00	8.33	0.00	0.00	21.67	0.00	0.00	1.85	-2.13
53.73	52.96	85.71	7.94	0.00	1.59	4.76	0.00	0.00	2.00	-1.91
54.14	53.34	100.00	0.00	0.00	0.00	0.00	0.00	0.00	1.24	-2.14
54.32	53.51	100.00	0.00	0.00	0.00	0.00	0.00	0.00	1.08	-2.26
54.32	53.51	66.67	0.00	0.00	0.00	33.33	0.00	0.00	1.45	-1.95
54.51	53.69	0.00	0.00	0.00	0.00	0.00	0.00	0.00	2.19	-1.81
54.58	53.75	100.00	0.00	0.00	0.00	0.00	0.00	0.00	1.98	-2.04

Table B.4 – (Continued) Relative abundance of selected planktonic foraminiferal genera at ODP Site 1215A.

Depth (msbf)	CCSF (m)	Acarina (%)	Morozovella (%)	Subbotina (%)	Globanomalina (%)	Praetenuitella (%)	Igorina (%)	Chiloguembelina (%)	$\delta^{13}\text{C}$	$\delta^{18}\text{O}$
54.97	54.11	0.00	0.00	33.33	33.33	33.33	0.00	0.00	2.65	-1.21
55.38	54.48	0.00	0.00	63.64	18.18	18.18	0.00	0.00	3.10	-0.98
55.65	54.72	33.33	0.00	0.00	66.67	0.00	0.00	0.00	2.98	-0.79
55.97	55.03	0.00	0.00	0.00	46.15	53.85	0.00	0.00	3.02	-0.74
56.30	55.33	0.00	0.00	0.00	52.63	47.37	0.00	0.00	3.22	-0.62
56.70	55.70	0.00	0.00	0.00	28.57	71.43	0.00	0.00	3.43	-0.64
57.17	56.14	0.00	0.00	50.00	0.00	50.00	0.00	0.00	3.09	-1.24
57.50	56.43	5.80	1.45	0.00	60.87	23.19	8.70	0.00	3.20	-1.45
57.90	56.80	4.00	0.00	0.00	64.00	32.00	0.00	0.00	3.13	-1.38
58.27	57.15	0.00	0.00	0.00	79.17	20.83	0.00	0.00	3.31	-1.32
58.77	57.61	0.00	0.00	0.00	70.00	30.00	0.00	0.00	3.18	-1.44
59.10	57.81	5.26	0.00	0.00	78.95	15.79	0.00	0.00	3.05	-1.69

Table B.4 – (Continued) Relative abundance of selected planktonic foraminiferal genera at ODP Site 1215A.